2014

ANALYSIS AND MODELING OF THE ROLES OF ACTIN-MYOSIN INTERACTIONS IN BLADDER SMOOTH MUSCLE BIOMECHANICS

Seyed Omid komariza
Virginia Commonwealth University

ANALYSIS AND MODELING OF THE ROLES OF ACTIN-MYOSIN INTERACTIONS IN BLADDER SMOOTH MUSCLE BIOMECHANICS

A Dissertation submitted in partial fulfillment of the requirements for the degree of Doctor of Philosophy in Engineering at Virginia Commonwealth University.

by

SEYED OMID KOMARI ZADEH ASL

Master of Science in Mechanical Engineering, California State University, 2011

Bachelor of Science in Mechanical Engineering, Iran Azad University, 2006

Director: JOHN E. SPEICH, PhD
Associate Professor and Associate Chair,
Department of Mechanical and Nuclear Engineering

Virginia Commonwealth University
Richmond, Virginia
December, 2014

Acknowledgements

This work would not have been possible without the contributions of a few special people. Research often benefits significantly from guidance, discussions and debates courtesy of one's colleagues and teachers. I, too, have received valuable insights from some of fine minds. First, I would like to uniquely express my thanks to my research advisor, Dr. John Speich for supporting me during these past three years. Dr. Speich has changed my way of looking at things in this life and has been supportive and has given me the freedom to pursue various projects without objection. I am also very grateful to Dr. Speich for his scientific advice and knowledge and many insightful discussions and suggestions. He has been a tremendous mentor for me. His advice on both research as well as on my career have been invaluable.

I would like also to extend my thanks to Dr. Paul Ratz, first, for serving on my committee, and second, for opening his laboratory for me to be able to conduct my research and for the nice work environment. I would like also express my sincere thanks to the members of my committee Dr. Rebecca Heise, Dr. Charles Cartin, and Dr. Woon-Hong Yeo. I would like to thank my colleagues at the smooth muscle laboratory, especially Amy Miner. I would like to especially thank Patrick Headley for providing me with some of his experimental data that I utilized for my research. A special thanks to School of Engineering Mechanical Engineering Department represented by the head of the department Dr. Gary Tepper for the constant financial support provided during the period of my study.

I could not end my acknowledgements without thanking my parents, Mostafa Komarizadeh and Zahra Loghavi, my brother, Aria Komarizadeh, and my girlfriend who have, individually and collectively, kept me on the path to success in both my academic and personal

lives by offering me an invaluable amount of motivation, support and guidance, even in times when I was at my lowest. I truly cannot thank them enough for all that they have done for me.

Dedication

To my father, Mostafa Komarizadeh, and to my mother, Zahra Loghavi,

who waited so long for this moment

Table of Contents

Page

List of Tables

Page

List of Figures

Page

Abstract

ANALYSIS AND MODELING OF THE ROLES OF ACTIN-MYOSIN INTERACTIONS IN BLADDER SMOOTH MUSCLE BIOMECHANICS

By SEYED OMID KOMARI ZADEH ASL, PhD

A Dissertation submitted in partial fulfillment of the requirements for the degree of Doctor of Philosophy in Engineering at Virginia Commonwealth University.

Virginia Commonwealth University, 2014

Major Director: JOHN E. SPEICH, PhD
Associate Professor and Associate Chair,
Department of Mechanical and Nuclear Engineering

Muscle mechanical behavior potentially plays an important role in some of the most common bladder disorders. These include overactive bladder, which can involve involuntary contractions during bladder filling, and impaired contractility or underactive bladder, which may involve weak or incomplete contractions during voiding. Actin-myosin cross-bridges in detrusor smooth muscle (DSM) are responsible for contracting and emptying the bladder. The total tension produced by muscle is the sum of its preload and active tensions. Studies suggest that

actin-myosin cross-links are involved in adjustable preload stiffness (APS), which is characterized by a preload tension curve that can be shifted along the length axis as a function of strain history and activation history. DSM also exhibits length adaptation in which the active tension curve can exhibit a similar shift. Actin-myosin cross-bridges are also responsible for myogenic contractions in response to quick stretch of DSM strips and spontaneous rhythmic contractions (SRC) that may occur during bladder filling. Studies show that SRC may participate in the mechanical regulation of both APS and length adaptation. However, the mechanical mechanisms by which actin-myosin interactions enable this interrelated combination of behaviors remain to be determined and were the primary focus of this dissertation. The objectives of this study were to: 1) provide evidence to support the hypothesis that a common mechanism is responsible for SRC and myogenic contraction, 2) develop a sensor-based mechanical model to demonstrate that SRC in one cell is sufficient to trigger stretch-induced myogenic contraction in surrounding cells and propagate the contraction, and 3) develop a conceptual model with actin-myosin cross-bridges and cross-links that produces the coupled mechanical behaviors of APS, SRC, and length adaptation in DSM. Improved understanding of bladder biomechanics may enable the identification of specific targets for the development of new treatments for overactive and underactive bladder.

CHAPTER 1 INTRODUCTION AND BACKGROUND

1.1.Motivation

Two common bladder disorders are overactive bladder (OAB), which is ranked above diabetes among the top chronic disorders in U.S., and impaired contractility or underactive bladder. OAB affects approximately 17% of adult population worldwide (Mullins, 2009). It involves increased voiding frequency and may involve involuntary spontaneous contractions during bladder filling. Underactive (UAB) bladder may involve weak, difficult or incomplete contractions during voiding. Both OAB and UAB can have a significant impact on the quality of life, activities, and finances of those individuals who suffer from one of these two disorders. Therefore, it is worthy to investigate potential causes of OAB and impaired contractility because this research could lead to improved treatment options. Currently the treatments that are used for overactive bladder are not specific to the smooth muscle in the bladder, and therefore can affect smooth muscles in other parts of the body (K.-E. Andersson, Nomiya, Sawada, & Yamaguchi, 2014). The next step in targeting these disorders is to identify aspects of contraction regulation unique to detrusor smooth muscle (DSM) in the bladder. This dissertation is focused on the mechanical functions of DSM and their sensitivity to stretch.

The following introduction highlights some background information about muscle types, smooth muscle structures, and contraction with an emphasis on bladder smooth muscle. Furthermore, some important mechanical characteristics such as length-tension relationships (preload, active and total tension), spontaneous rhythmic contractions, quick-stretch induced

myogenic contractions, and the role of actin-myosin interactions in these characteristics are discussed.

1.2.Muscles Types

Muscles are the contractile tissues of the body. They are classified as skeletal, cardiac, and smooth muscles. Their function is to produce force and cause motion. Skeletal muscle tissue is named for its location, attached to bones. It is striated, which means that the cells contain alternating light and dark bands that are perpendicular to the long axes of the fibers (Fung, 1993; Guyton, Hall, 2000). Skeletal muscle tissues are designed to contract or relax voluntarily. Cardiac muscle tissue forms the bulk of the wall of the heart which is striated much like skeletal muscle tissue. Unlike skeletal muscle, its contraction is involuntary. Muscles in which striations cannot be seen are called smooth muscles. These muscles contract involuntary.

1.3. Smooth Muscles

Smooth muscles are located in the walls of hollow internal structures such as blood vessels, airways, the stomach, intestines, and the urinary bladder (Fung, 1993; Pollard, Earnshaw, & Lippincott-Schwartz, 2007). Smooth muscle cells are generally long, spindle shaped cells, and therefore they are wide in the middle and narrow to almost a point at both ends (Garfield and Somlo 1985). Smooth muscle cells have a single centrally located nucleus. The cells range in size from 5 to 10 μm in diameter in the center of the cell and from 300 to 600 μm

in length (Garfield and Somlo 1985). The size of smooth muscle cells varies between different tissues and species. Smooth muscle cells contain the same contractile proteins as skeletal and cardiac muscles; however, these proteins are laid out in a different pattern (Fung, 1993). One main feature among all muscles are the contractile proteins actin and myosin (Fung, 1993). Smooth muscle in the bladder is called detrusor smooth muscle (DSM), and is the main focus in this dissertation.

1.4.The Bladder and Its Function

The bladder is a hollow, muscular, and elastic organ. The main functions of the bladder are storage of urine and emptying the urine produced by the kidneys. Each kidney has its own ureter through which urine travels to the bladder (Andersson & Arner, 2004). The empty human bladder is about the size of a tennis ball, and shaped somewhat like a pear. The bladder is composed of two main parts, the body, which is the major part of the bladder in which the urine collects, and the neck, which is the funnel-shaped extension of the body (Andersson & Arner, 2004). The bladder neck is 2-3 cm long, and its wall composed of detrusor muscle interlaced with a large amount of elastic tissue. The muscle in this area is called the internal sphincter. Its natural tone normally keeps the bladder neck empty of urine and therefore, prevents emptying of the bladder. Beyond the bladder neck, the urethra passes through the urogenital diaphragm, which contains a layer of muscle called the external sphincter of the bladder. This muscle is a voluntary skeletal muscle, in contrast to the muscle of the bladder body and bladder neck, which contains only involuntary detrusor smooth muscle. The external sphincter muscle is under voluntary control of the nervous system and can be used to consciously prevent urination even

when involuntary controls are attempting to empty the bladder (Costanzo, 2002; Guyton & Hall, 1961). Once the stretch-receptors in the trigone, which is a triangular space between the two ureters and the bottom opening of the bladder, get stretched by a certain degree of bladder filling, the brain receives a signal that the bladder is full and should be emptied (Guyton & Hall, 1961).

During the voiding phase, the ring shaped muscle sphincter is relaxed, and the detrusor contracts to release the urine. The bladder flattens and changes shape as contraction occurs. If the signal to void is ignored, the bladder keeps filling, but eventually the bladder will empty itself (Guyton & Hall, 1961).

1.5.Bladder disorders

A large population of men and women around the world struggles with incontinence, bladder pain and other bladder disorders. Various organs and parts in the body, including the brain, nerves, and the urothelium that lines the bladder, may be involved in bladder disorders, but two well-known disorders that may be related to the mechanical properties of bladder smooth muscle are overactive bladder and impaired contractility or underactive bladder.

1.5.1. Overactive bladder

Affecting over 17% of the worldwide population , OAB is a common disorder (Mullins, 2009). The viscoelastic behavior of the bladder and urethra depend on both neuromuscular and mechanical properties. Mechanical properties are extremely sensitive to tissue structure and

composition. Increased wall tension activates bladder afferent nerves that lead to the sensation of bladder filling and may cause involuntary bladder contractions. Conversely, a decrease in compliance or efferent neural input can alter wall tension, cause afferent firing, and thereby change bladder sensations and the volume threshold for voiding (Brading, 1997; Wein, 2007). One aspect of the present study was to examine the quantity of change in compliance due to muscle activity.

1.5.2. Impaired contractility (underactive bladder)

Another common bladder disorder in which the mechanical properties of muscle may play an important role is impaired contractility or underactive bladder (UAB). Unlike OAB, UAB is defined by urinary symptoms including hesitancy, straining, and difficulty in voiding that causes incomplete bladder emptying. Patients with UAB can sometimes hold large amounts of urine without feeling urgency (Wein, 2007). As in OAB disorder, the number of muscle cells, motor proteins or nerves, as well as their orientation and degree of activation, are potentially involved in causing impaired contractility disorder. Therefore, studies of the mechanical behavior of bladder muscle could lead to a better understanding of bladder function and improve the treatment options for these disorders.

1.6. Smooth Muscles Contractile Proteins Actin and Myosin

Actin is one of two proteins responsible for contraction of muscle cells. Actin occurs as a monomer; G-actin, a globular protein; and in muscle cells as a polymer, F-actin, which resembles two strings of beads twisted around each other into thin filaments (Fung, 1993; Pollard

et al., 2007). Each actin filament is about 1 μm long. The filaments occur in regular structures, alternated and interwoven with thick filaments that contain myosin, the other major muscle protein. Myosins are a large family of proteins found in muscle cells (Fung, 1993). Myosin is made up of 200 or more individual myosin molecules. Each myosin molecule consists of tail and two heads (Guyton & Hall, 1961). The total length of each myosin filament is almost 1.6 μm. Actin is attached to dense bodies throughout cells and is also attached to the cell membrane in numerous areas.

1.7. Smooth Muscle Contraction

Contraction of the detrusor muscle is a major step for emptying the bladder. It was first believed that detrusor smooth muscle cells fuse with one another so that low resistance electrical pathways exist from one muscle cell to the other. Therefore, an action potential could spread throughout the detrusor muscle, from one muscle cell to the next, to cause contraction of the entire bladder at once (Guyton and Hall 1961). However, later studies indicated that all smooth muscle cells are not electrically coupled well, and therefore, mechanical propagation could be a potential mechanism for a uniform contraction (Elbadawi, 1995). The present study investigates the mechanical coupling hypothesis and provides a mechanical model to demonstrate a potential propagation mechanism.

It is widely known that the principal physiological events underlying the contraction of smooth muscle are similar to those of skeletal and cardiac muscles (Webb, 2003). Contractions in smooth muscles are initiated by action potentials that occur in the smooth muscle cell membrane. The depolarization of the action potential opens calcium channels in the membrane. Stimulation of smooth muscle results in an elevation in intracellular calcium, which binds to the

protein calmodulin. The calcium-calmodulin complex then activates the enzyme myosin light chain kinase, when myosin light chain kinase is activated it attaches with a phosphate group to (i.e., phosphorylates) myosin. When myosin is phosphorylated, it can cyclically bind to actin to form a cross-bridge, move through a power stroke to develop force, release from actin, and return to its original orientation to begin the next cycle, as illustrated in Figure 1.1. When the intracellular calcium concentration decreases, myosin is dephosphorylated by the enzyme myosin light chain phosphatase. In this case, myosin can still interact with actin, but the attachments are called latch-bridges (Richard A Murphy & Rembold, 2005). The latch-bridges do not detach, or they detach slowly; thus maintaining a tonic level of tension in the smooth muscle with little consumption of ATP. When the intracellular calcium concentration decreases below the level necessary to form a calcium-calmodulin complex, relaxation of the muscle occurs (Andersson & Arner, 2004; Costanzo, 2002; Fung, 1993; Webb, 2003).

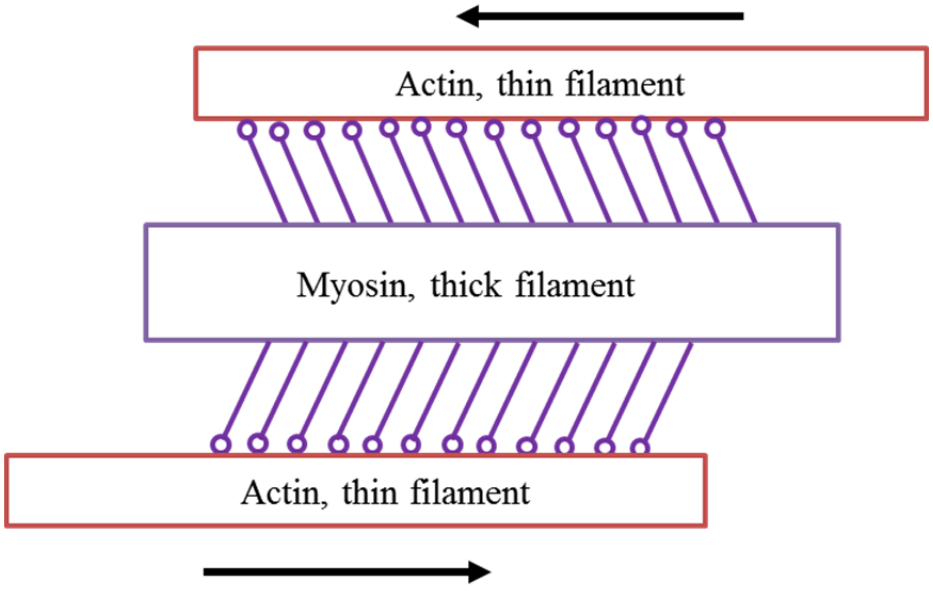

Figure 1.1 Illustration of actin and myosin sliding to contract a muscle

1.8.Mechanical Cycling of Actin-Myosin Cross-Bridges

As mentioned in the previous section, when calcium ions are present, the binding sites of actin myofilaments get uncovered and exposed to myosin heads. Myosin heads attach to actin filaments in the presence of ADP and phosphate from the previous cycle. Phosphate releases and the energy from this reaction makes myosin heads pivot. This step is also known as power stroke. This movement causes the actin filament to slide past the myosin filament. As myosin heads relocate, the ADP is released. Another molecule of ATP is attached to myosin head as ADP is released and the bond between actin and myosin is broken. The ATP is broken down into ADP and phosphate where the energy of this chemical reaction is stored in myosin heads for the next cycle. Myosin head molecules return back to their upright position (Figure 1.2). This dissertation includes the development of a combination of viscoelastic models to investigate the potential contribution of actin-myosin cross-bridges to muscle mechanical properties. These models may be useful for understanding the mechanical role of actin-myosin interactions in muscles.

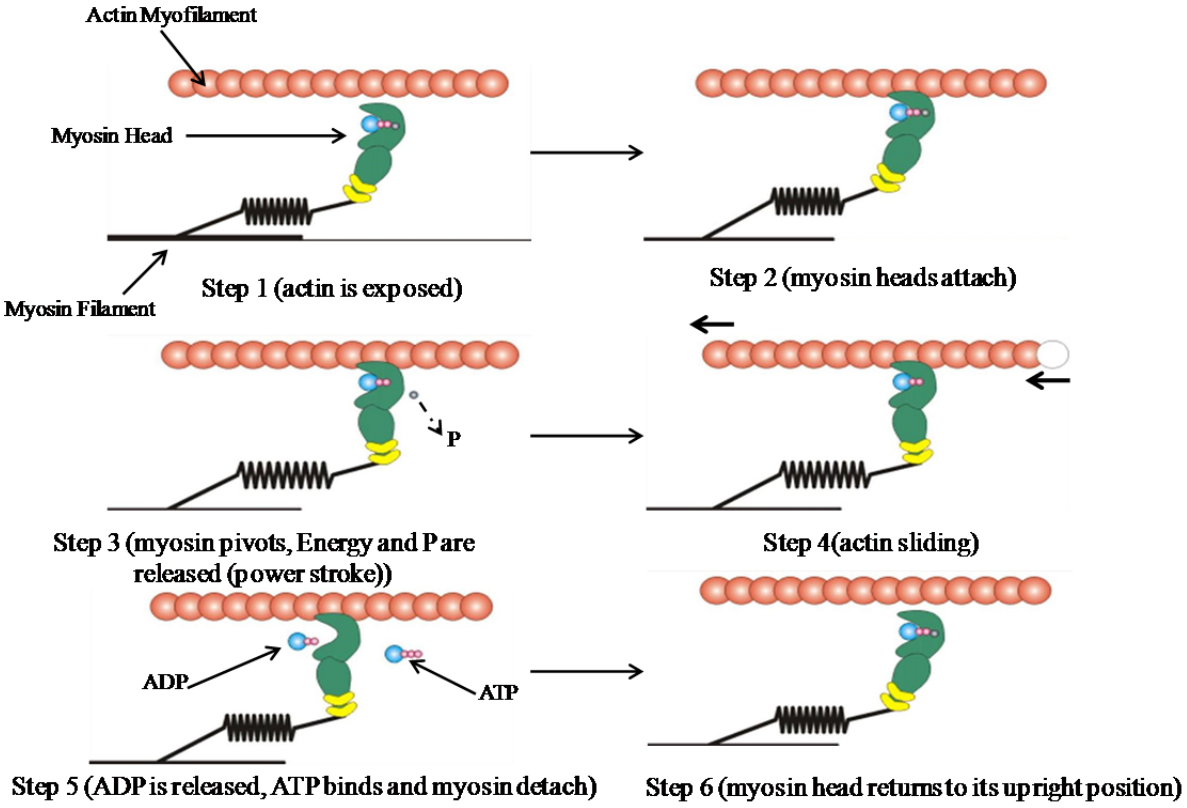

Figure 1.2 A schematic of actin-myosin cycling (Geeves & Holmes, 1999)

1.9.Preload Force

In smooth muscles, force has both preload and active components as shown in Figure 1.3. Preload force is the force exerted by the muscle as it is stretched when it is not stimulated to cause rapid cross-bridge cycling and muscle shortening (Speich et al., 2006). Preload is due to the elastic elements in the fibers and those surrounding the fibers, which are primarily connective tissue. Like an elastic object, a rubber band for example, the preload force is very small below a certain length and as the muscle is stretched beyond this length, the preload force rises. The rise becomes steeper as the muscle is stretched to greater lengths (i.e., the same length change gives greater changes in preload force at longer muscle lengths). The length-preload tension curve, as

seen in Figure 1.3, is an increasing, somewhat exponential curve. In smooth muscles the preload tension can be a significant fraction of the total tension especially at long lengths, which makes smooth muscles different from striated muscles (Seow, Pratusevich, & Ford, 2000). In smooth muscles, there are many candidate structures that contribute to preload force. Elastin, an extracellular protein, and collagen, the basic structural protein in the living tissues, are the most likely candidates especially at long lengths (ROACH & BURTON, 1957; Siegman, Butler, Mooers, & Davies, 1976). In striated muscles, the protein titin plays a role in preload force. There is a similar protein in smooth muscles called smitin (Kim & Keller, 2002), which may contribute to preload force. There are other possible intracellular candidates, including any protein associated with transmission of the force, as well as actin-myosin cross-bridges and actin-myosin cross-linking proteins like filamin (Speich, Borgsmiller, Call, Mohr, & Ratz, 2005). This dissertation presents a model for the mechanical role of actin-myosin cross-bridges and cross-links in shifting preload force at different muscle lengths, known as adjustable preload stiffness or adjustable preload stiffness (Speich et al., 2007), and couples this behavior with length adaptation which will be described in a later section.

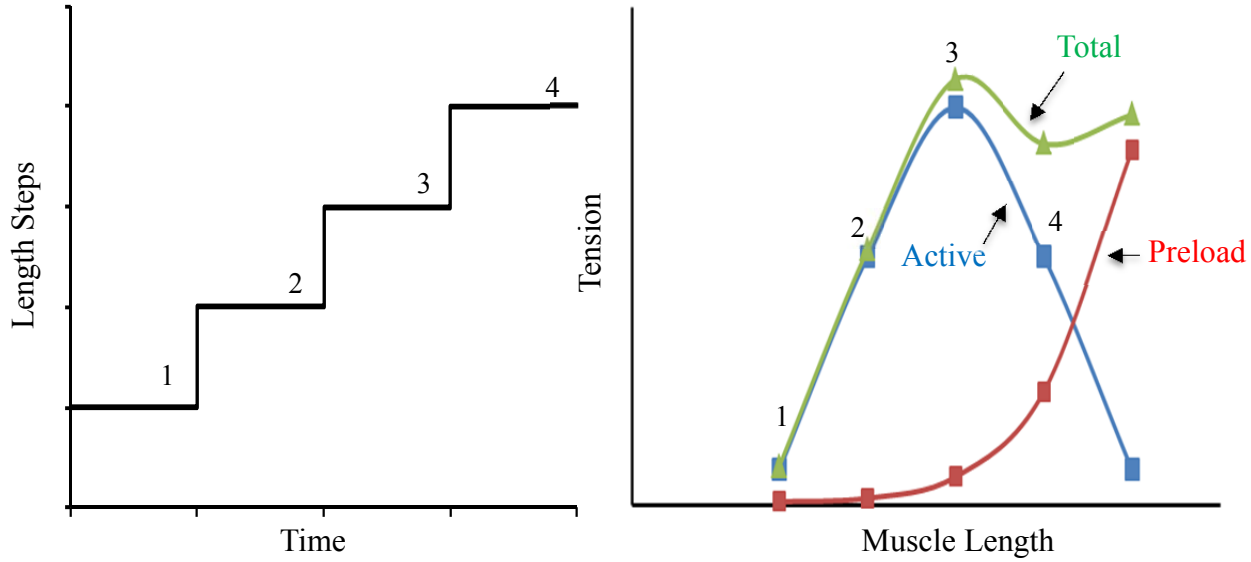

Figure 1.3 A schematic diagram that shows total, active and preload tension due to the multiple step-stretches.

1.10. Active Force

Active force is the additional force (above the preload force) observed when muscle is stimulated in living tissues. The active force is due to the interaction between actin-myosin cross-bridges. The "rowing" action of the actin-myosin cross-bridges causes relative sliding of actin and myosin filaments, which shortens the cells and develops force. The level of active tension produced is dependent on the number of active cross-bridges producing positive work, which is dependent on muscle length. Figure 1.4 shows a length-active tension curve for smooth muscle. The active curve is somewhat parabolic with ascending and descending limbs with a plateau region in which the muscle can produce approximately the same amount of active force, not as in striated muscles where the active force has a maximum value at essentially single length (Seow, Pratusevich, & Ford, 2000).

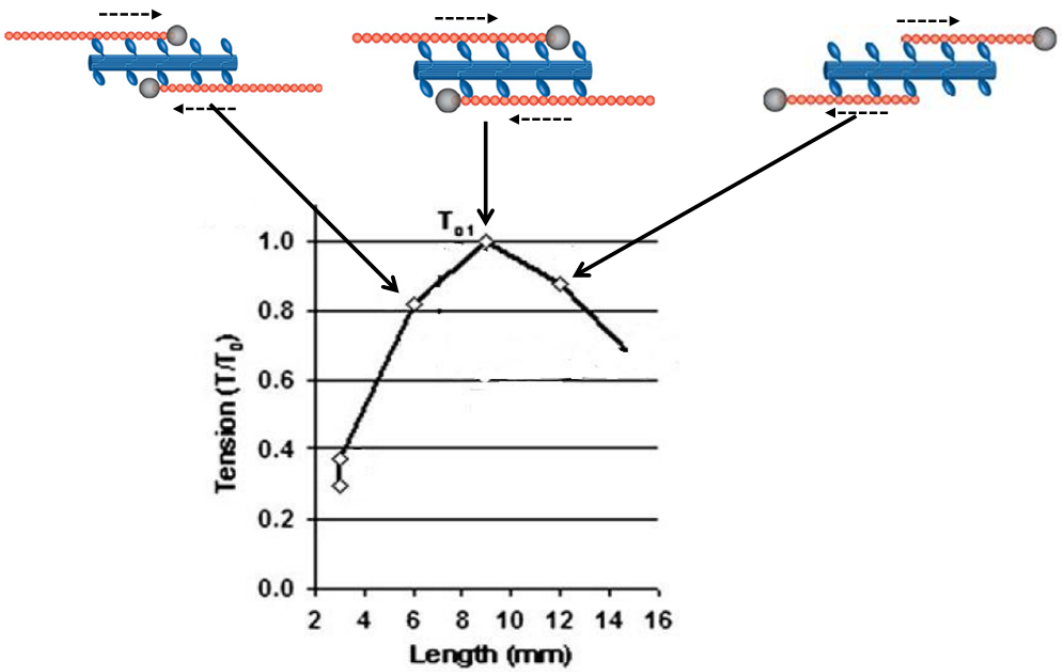

Figure 1.4 Sample data illustrating a parabolic active tension and a conceptual schematic showing corresponding cross-bridge positions (A. M. Almasri, Ratz, & Speich, 2010a).

Smooth muscles are capable of generating at least as much active force as striated muscles. In striated muscles, the active force developed is in direct proportion to the degree of overlap of the actin and myosin filaments. In smooth muscles, the relationship of myosin with actin appears to be less organized (Battistella-Patterson, Wang, & Wright, 1997; Wang, Paré, & Seow, 2001), and the contractile unit has never been clearly understood. Mechanically speaking, the "unit cell" has never been identified in smooth muscles relative to striated muscles in which the "unit cell" is well organized and well understood. Smooth muscle contraction theories are based on mimicking the striated muscle contractile unit cells, or "sarcomeres". It has been recognized for a long time that smooth muscles can function over a long length range because of the large volume changes required by some hollow organs. Detrusor smooth muscle tissues are

subjected to large changes in volume during bladder filling and voiding. The detrusor smooth muscle is continuously changing mechanical conditions during normal physiological bladder cycles. As bladder volume increases and decreases with each cycle, the detrusor smooth muscle is stretched and retracted. The urinary bladder can decrease its volume several hundred-fold over a time span of seconds, and it has been shown that bladder muscle cells develop active force over a 7-fold length range (Bengt Uvelius, 1976). This is much greater than the 3-fold total range of filament sliding over which force is generated in skeletal muscle (A. M. Gordon, Huxley, & Julian, 1966). Therefore, active force plays an important role in the mechanical properties of bladder smooth muscle. This dissertation describes the development of models for different bladder smooth muscle phenomena during the filling and voiding phases, such as spontaneous rhythmic contractions, stretch-induced myogenic contractions, acute muscle length adaptation, and adjustable preload stiffness which will be described in following sections. The goal in developing these models was to achieve a better understanding of bladder smooth muscle properties.

In the following sections, some bladder activities contributing to preload and active tension during the filling and voiding phases will be briefly described. Portions of the following sections that describe spontaneous rhythmic contraction and quick-stretch-induced myogenic contractions have been previously published by the author (Komari, Headley, Klausner, Ratz, & Speich, 2013).

1.11. Spontaneous Rhythmic Contraction (SRC)

Spontaneous contraction is a phenomenon common to many muscular organs (Fung, 1993). Detrusor smooth muscle tension is not totally preload during the filling phase (Gillespie, 2004). Instead, detrusor smooth muscle can produce localized rhythmic contractions during filling, with less amplitude (~10%) than during a voiding contraction (Collins et al., 2009). Thus, active contraction is not only responsible for voiding, but it also may be involved during the filling phase (Figure 1.5). SRC has been identified in detrusor in a range of mammalian species, including rabbits (Shenfeld, McCammon, Blackmore, & Ratz, 1999), rats (Kanai et al., 2007), and humans (Biers, Reynard, Doore, & Brading, 2006). This phenomena has seen in other muscles, including gastrointestinal (Huizinga, Robinson, & Thomsen, 2000) and vascular smooth muscle (Griffith, 1996). SRC is elevated in detrusor strips from patients with overactive bladder (Kinder & Mundy, 1987), and SRC is likely responsible for micromotion observed during filling of human bladders, which is also elevated in patients with overactive bladder (M. Drake & Harvey, 2005). SRC was investigated in the present study because it may be important to understanding OAB.

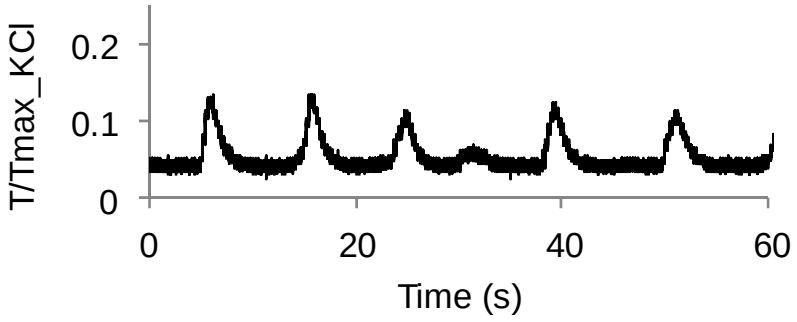

Figure 1.5 Example of spontaneous rhythmic contractions (Komari et al., 2013)

1.12. Quick Stretch-Induced Myogenic Contraction

When subjected to a quick stretch (QS) or hypo-osmotic solutions, human (Masters, Neal, & Gillespie, 1999), rabbit (BURNSTOCK & PROSSER, 1960), and mouse (Ji, Barsotti, Feldman, & Kotlikoff, 2002) detrusor can exhibit a phasic myogenic contraction independent of neural input. Figure 1.7 shows an example of a QS-induced contraction in DSM. The myogenic contraction has been studied extensively in vascular smooth muscle, where it has an important role in blood flow regulation (Davis & Hill, 1999). Rapid volume increase can produce myogenic bladder pressure transients (S. Andersson, Kronström, & Teien, 1988). In rabbit detrusor, there are several similarities between SRC and myogenic contractions. Both types of contraction have small amplitudes, with SRC producing an estimated 5-12% of peak active tension (Ratz & Miner, 2003) and QS-induced myogenic contraction producing an estimated 4-13% of peak active tension (Poley, Dosier, Speich, Miner, & Ratz, 2008). In addition, the amplitudes of both types of contraction are muscle length dependent, with SRC amplitude increasing at longer muscle lengths (Byrne et al., 2013) and the myogenic contraction amplitude increasing with the length of the QS (Poley et al., 2008). Both types of contraction are also phasic. In rabbit detrusor, SRC appears as a somewhat sinusoidal tension wave, or a combination of waves, with varying amplitude(s) and a frequency or frequencies ranging from an estimated 2-11 cycles/min (~5-30 sec between peaks) (Byrne et al., 2013). The myogenic contractile response to QS exhibits a refractory period of 10-30 seconds, with a QS repeated after 10 seconds inducing a significantly smaller contraction and a QS repeated after 30 seconds inducing only a slightly smaller contraction (Poley et al., 2008). Thus, the refractory period between

myogenic contractions due to QS and the timing of SRC are similar, suggesting a common oscillatory regulation system (Komari et al., 2013).

As described in Chapter 3, a major objective of this study was designed to test the hypothesis that a common contractile mechanism is responsible for SRC and the myogenic contractile response following a QS in detrusor. This hypothesis was tested using a mechanical protocol during which QSs were imposed randomly throughout the rhythm cycle to determine whether: 1) the myogenic response would be relatively large when tension in the rhythm cycle was small, suggesting that the common mechanism was primarily "off" at that point in the rhythm cycle, leaving a substantial fraction that was "turned on" by the QS, and 2) the myogenic response would be relatively small at a point when tension in the rhythm cycle was large, suggesting that the common mechanism was mostly "on" and only a small fraction remained to be "turned on" by the QS. The hypothesis was also tested using a pharmacological protocol to determine whether Rho kinase (ROCK), cyclooxygenase-1 (COX-1) and cyclooxygenase-2 (COX-2) inhibitors (H-1152, SC-560 and NS-398, respectively) affected SRC and the myogenic contractile response due to QS to the same degree.

Uniform tissue contractions seen during SRC or a QS-induced contraction require cell-to-cell synchronization of contraction. Not every smooth muscle cell of a detrusor muscle bundle is innervated by a post-ganglionic parasympathetic fiber (Elbadawi, 1995), suggesting that cell-to-cell coupling is necessary to synchronize contraction. Detrusor cells are poorly coupled electrically (Bramich & Brading, 1996), and therefore, mechanical coupling may be responsible for synchronization. Elbadawi (Elbadawi, 1995) and Ji (Ji et al., 2002) have proposed a mechanical coupling model in which rapid contraction of one muscle cell stimulates surrounding cells by rapidly stretching them to propagate contraction throughout a bundle of cells. The

present study tested the hypothesis that a common contractile mechanism is responsible for both SRC and QS-induced contraction, which is consistent with a model in which cell stretch is a stimulus to propagate SRC throughout a bundle or bundles of detrusor cells. The results of this study are presented in Chapter 3.

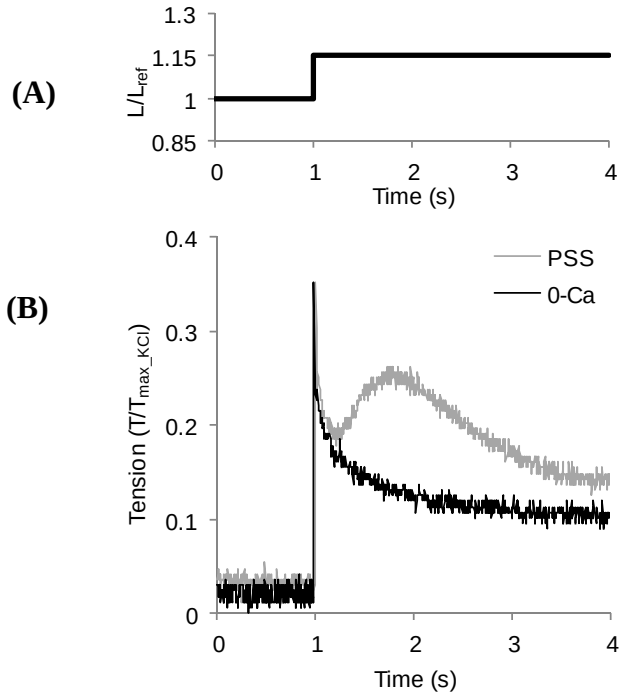

Figure 1.6 Quick stretch protocol from a reference length, L_{ref} to 1.15 L_{ref} in 10 ms (**A**) and the corresponding rise in preload tension, subsequent stress relaxation and subsequent myogenic contraction (**B**). Tension data are normalized to the maximum KCl induced tension. The myogenic contraction is present for a stretch in physiological salt solution (PSS) but not in a calcium-free solution (0-Ca). (Komari et al., 2013)

1.13. Dynamic Length-Preload Tension Curve

Until 1990s, the preload and the active length-tension relationships for smooth muscles were believed to be static, with a single preload tension value and a single maximum active tension value for each muscle length. However, DSM preload exhibits both viscoelastic softening that is reversible within a short period of time (~ 10 min), and strain softening that is irreversible with time alone (Speich et al., 2005). Strain softening is revealed by a shift to the right in the length-preload tension curve as shown in Figure 1.7. Previous studies showed that strain softening in DSM is irreversible unless the tissue is contracted either by exposure to KCl or Carbachol (Speich et al., 2007). It was found that a 3 min contraction was enough to regain the stiffness. Therefore, DSM has a preload stiffness that can be regained by contraction, and maintained unless the tissue is stretched. Thus, preload tension is dynamic and can be adapted to different lengths as a function of activation and stretch, as shown in Figure 1.8. Since the preload stiffness can be adjusted, this characteristic was labeled adjustable passive stiffness (APS) (Speich et al., 2007). It is more appropriate to use the term adjustable preload stiffness (Southern et al., 2012). Even though both terms are used in this dissertation, they refer to the same concept. There is a reversible stain softening in DSM that can be regenerated by a contraction at short muscle lengths.

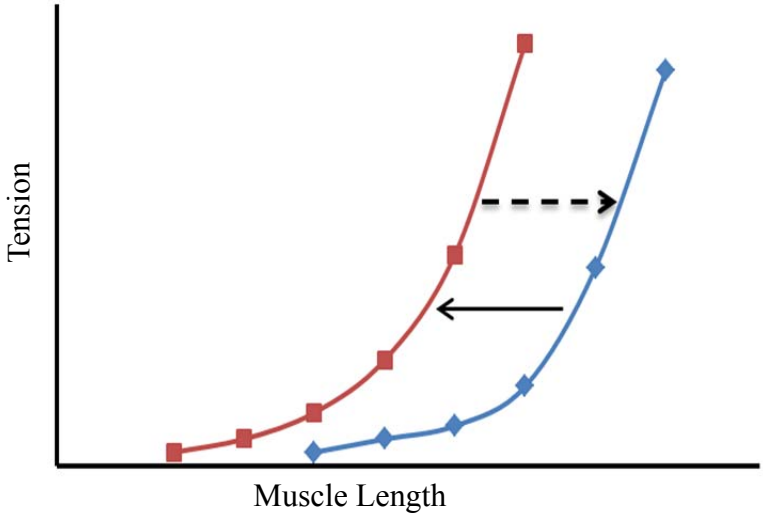

Figure 1.7 Illustration of a shifting length-preload tension curve. Solid arrow shows the direction of a preload tension curve shifting due to strain softening to longer length and the dashed arrow shows the direction of preload tension curve shifting due to pre-contracting at a shorter muscle length to reverse strain softening.

A study by Seow (Seow, Pratusevich, Ford, Chun, & Lincoln, 2000) showed that the length-preload tension of vascular smooth muscle is time dependent and therefore not static. Seow obtained two different preload curves at two minutes and at twenty-seven minutes after a length change (see Figure 1.8, preload force). Therefore, preload tension in vascular smooth muscle is also dynamic and can be adapted to different lengths.

1.14. Dynamic Length-Active Tension Curve

The length-tension relationships in airway and vascular smooth muscles have been the focus of intensive research. Previous studies (Herlihy & Murphy, 1973; Mulvany & Warshaw, 1979; Stephens, Kroeger, & Mehta, 1969) on the length-active tension curves of different smooth muscles have shown relationships that were assumed to be static, but more recent studies (Fust &

Stephens, 2005; King, Paré, & Seow, 1999; Pratusevich, Seow, & Ford, 1995; Seow, Pratusevich, Ford, et al., 2000; XU, GILLIS, & CRAIG, 1997) showed that the length-active tension relationship is dynamic, and that the muscle has the ability to accommodate large length changes without compromising the ability to generate tension (see Figure 1.8.).

One of the earliest studies to demonstrate that smooth muscle active force is dynamic focused on airway smooth muscle (Whitney et al., 1995). In 1995, Pratusevich, Seow (Pratusevich et al., 1995) showed that active force in airway smooth muscle is dynamic, with multiple optimum lengths, which is different than striated muscles in which there is a single maximum active value with a unique optimum length range. That study also showed that the muscle can adapt at different lengths, and this dynamic behavior was explained by the dynamic nature of the subcellular structures in airway smooth muscle. Therefore, the airway smooth muscle length-active tension curve is dynamic. In 2000, Seow (Seow, Pratusevich, Ford, et al., 2000) demonstrated that the length-active tension curve in vascular smooth muscles (VSM) is also dynamic. This behavior is termed length adaptation. Strong evidence from a previous study supports the theory of similar dynamic length-active tension in detrusor smooth muscle (Speich, Almasri, Bhatia, Klausner, & Ratz, 2009).

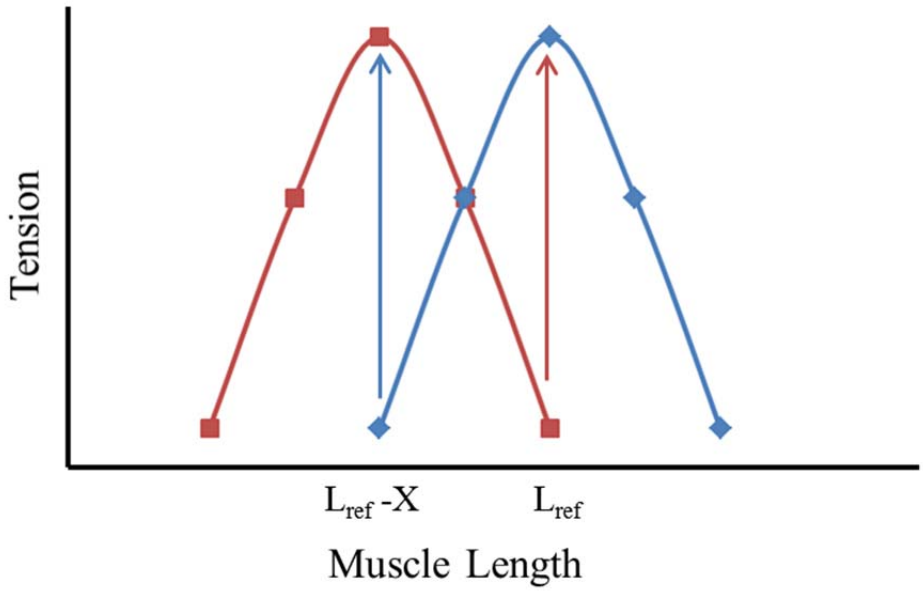

Figure 1.8 The schematic dynamic length-active tension curve, with multiple curves produced by the same tissue strips. Active tension increases at L_{ref} (red arrow) and decreases at shorter length $L_{ref} - X$, (blue arrow) due to contraction.

1.15. Active and Preload Adaptation Mechanisms

Several mechanisms for length adaptation of smooth muscle and the dynamic active-preload length-tension relationship in smooth muscle have been proposed and investigated primarily in ASM (Figure 1.9). These mechanisms include the addition of contractile filaments in series (Pratusevich et al., 1995) or parallel, (Seow, Pratusevich, & Ford, 2000) or lengthening of myosin (Ford, Seow, & Pratusevich, 1994); parallel-to-series transitioning of contractile units (Dulin et al., 2003); actin polymerization or shifting of the sites where actin filaments connect to dense bodies (Gunst, Meiss, Wu, & Rowe, 1995); and cytoskeletal deformation and re-organization; (Gunst & Zhang, 2008; Silveira, Butler, & Fredberg, 2005).

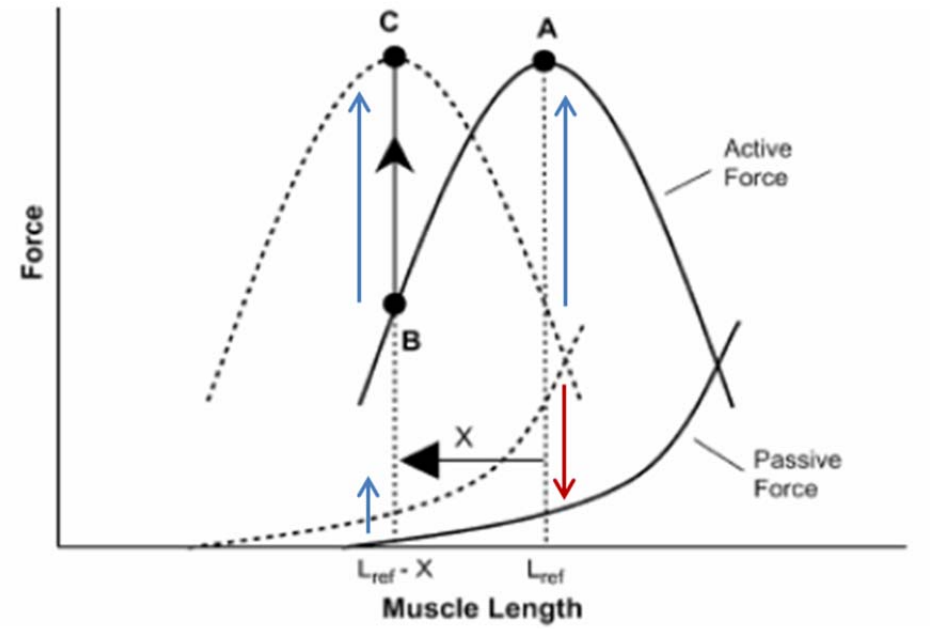

Figure 1.9 Conceptual schematic showing dynamic length-active tension and length-preload tension curves (Bossé, Sobieszek, Paré, & Seow, 2008) with arrows added to highlight the curve shifts. Repeated contractions at a length on the ascending limb of the original length-active tension curve (solid lines) increase both the preload (passive) and active tension (blue arrows and B to C) at that shorter length to shift the curves to the left (dotted lines). Subsequent repeated contractions on the descending limb of the shifted curve, increase active tension (red arrow) and decrease preload tension (blue arrow) to shift the curve back to the original length range (dotted lines shift to solid lines).

Several mechanisms for length adaptation of smooth muscle have been proposed and investigated primarily in ASM. These mechanisms include the addition of contractile filaments in series (Pratusevich et al., 1995) or parallel, (Seow, Pratusevich, & Ford, 2000) or lengthening of myosin (Ford et al., 1994) (reviewed by (Bossé et al., 2008) and (Ford, 2005)); parallel-to-series transitioning of contractile units (Dulin et al., 2003); actin polymerization or shifting of the

sites where actin filaments connect to dense bodies (Gunst et al., 1995) ; and cytoskeletal deformation and re-organization; (Gunst & Zhang, 2008; Silveira et al., 2005).

Speich et al. previously proposed that APS could be due to cross-linked cross-bridges (latch-bridges) (Speich et al., 2005). Later, Almasri demonstrated that adaptation of T_p, i.e., changes in APS, can occur while a DSM strip is isometric (Speich et al., 2009). Thus, the isometric increase in T_p (purple arrow) following a contraction on the ascending limb of the L–Ta curve (Figure1.10., A&B points 14–19) could be due to latch-bridges that are formed during internal shortening due to the contraction and revealed as the latch-bridges are loaded upon internal lengthening during relaxation. Furthermore, the isometric decrease in T_p (red arrow) following a contraction at L_o or on the descending limb of the L–T_a curve (Figures.1.10, points 8–13) could be due to the breakage or regulated release of these latch-bridges. If APS is due to latch-bridges, then the decrease in T_p corresponding to the increase in Ta (blue arrow) during adaptation on the descending limb (Figure1.10, points 8–13) suggests that the increase in T_a may be due to the conversion of latch-bridges responsible for T_p into actively cycling cross-bridges. The increase in both Ta (green arrow) and T_p (purple arrow) during adaptation on the ascending limb (Figure1.10., points 14–19) also supports this hypothesis if a fraction of the actively cycling cross-bridges were latched to increase T_p, which subsequently maintained a more efficient arrangement of thick and thin filaments while increased the number of active cross-bridges to produce greater T_a (A. M. Almasri, Ratz, & Speich, 2010a). One objective of this dissertation was to develop a conceptual model that supports this cross-link hypothesis.

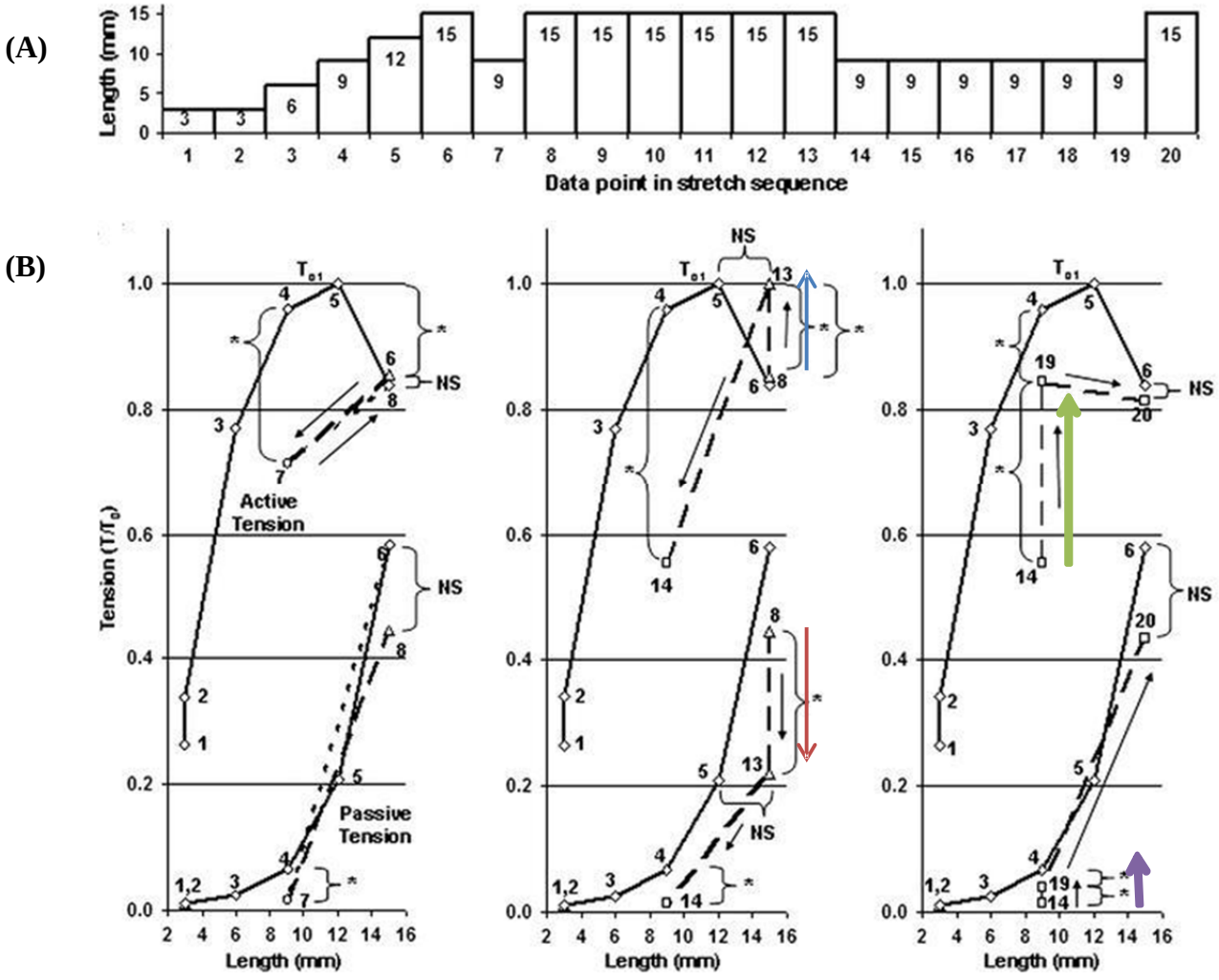

Figure 1.10 (**A**) L–T curve protocol consisting of 20 contraction cycles. (**B**) dynamic L–Ta and L–T_p curves (A. M. Almasri, Ratz, & Speich, 2010a).

1.16. Literature summary

Table 1.1 presents a summary of some of the most relevant literature regarding length adaptation and adjustable preload stiffness in smooth muscle. Several previous studies about DSM were focused on using experimental protocols to identify DSM dynamic characteristics

such as length adaptation and adjustable preload stiffness at different muscle lengths. Some mathematical models were developed with a focus on DSM cross-bridges and their roles in producing active and preload tension. Some labs have developed conceptual models that proposed theories about the roles of cross-bridges in length adaptation.

Table 1.1 Relevant Smooth Muscle Studies in the Literature

Behavior	Author	Year	Tissue	Mechanism	Model Type
Adaptation	Pratusevich, Seow, & Ford	1995	DSM	additional of contractile filaments in series	Hill Hyperbola
Adaptation	Seow, Pratusevich, & Ford	2000	ASM	additional of contractile filaments in parallel	Monoexponential Function
Adaptation	Ford, Seow, & Pratusevich	1994	ASM	lengthening of myosin	Experimental Study
Adaptation	Seow	2000	ASM	parallel-to-series transitioning of contractile units	Conceptual Model
Adaptation	Solway, Dulin	2003	ASM	parallel-to-series transitioning of contractile units	Mathematical Model
Adaptation	Seow, Lambert	2004	ASM/ DSM	parallel-to-series transitioning of contractile units	Mathematical Model Mass/Spring Model
Adaptation	Bossé, Sobieszek, Paré, Seow	2008	ASM	Phosphorylation	Conceptual Model (Assembly, Disassembly)
Adaptation	Gunst, Meiss, Wu, & Rowe	1995	ASM	actin polymerization or shifting of the sites where actin filaments connect to dense bodies	Conceptual Model
Adaptation	Gust, Zhang	2008		cytoskeletal deformation and re-organization	Integrated Model

Adaptation	Silveira, Butler, & Fredberg	2005	ASM	cytoskeletal deformation and re-organization	Mass/Spring Model
APS	Speich and Ratz	2006	DSM	crosslink breakage due to strain softening and crosslink reformation upon contraction	lumped-parameter mechanical model; springs, dashpots and crosslink elements
APS	Campbell, Patel	2003	Myocardial	Cross-bridges	Statistical Model
Strain Softening	Bergstrom JS, Boyce MC.	1998	Chloroprene rubber	Filler content and Crosslink density	Lamped parameter Model Mathematical Model
Strain Softening	Mullins	1969	Elastomeric material	Structural reorganization and soft/hard deformation	Mathematical Model
Preload Tension	MeissRA, Pidaparti RM	2003	ASM	Tensegrity-like structure made up of connective tissue and cross-bridges detachment	Mass/Spring Model
Preload Tension	Speich, Ratz	2012	DSM	Myosin Phosphorylation	Experimental Study
SRC	Byrne	2013	DSM	Cross-bridges cycling	Fast Fourier Transform Model
Quick-Stretch Myogenic Response	Poley, Ratz	2008	DSM	Membrane Depolarization	Experimental Study
Quick-Stretch Myogenic Response	Burnstock, Prosser	1960	SM	Membrane Depolarization	Experimental Study

This review of the smooth muscle literature indicates that a biomechanical model that combines the behaviors of SRC, length adaptation and adjustable preload stiffness, and defines the role of actin and myosin in producing those characteristics in a single model has not been proposed before this dissertation. In addition a novel mechanical-sensor-based lumped-parameter

model for SRC and stretched-induced myogenic contractions is proposed in this dissertation. Finally, previous models ignored the effects of SRC on other behaviors, and this will be incorporated into the models developed in this dissertation. This dissertation will build upon existing models by combining DSM behaviors and showing interactions between them at different lengths, with a focus on the mechanical role of actin-myosin interactions in these DSM functions.

1.17. Dissertation Objectives

This dissertation focused on the following objectives:

1. Analyze experimental data to test the hypothesis that the same population of actin-myosin cross-bridges is responsible for SRC and QS-induced contraction (Chapter 3).
2. Develop a lumped parameter biomechanical model of myogenic stretch-induced contraction that exhibits characteristics from the literature, including contraction amplitude that is stretch-rate dependent, stretch-length dependent and refractory period dependent (Chapter 4).
3. Incorporate spontaneous rhythmic contraction into the lumped element model for myogenic contraction (Chapter 4).
4. Develop a quantitative biomechanical network model to test the hypothesis that contraction rapidly stretches DSM cells to initiate a myogenic contraction to propagate the contraction throughout a bundle of cells (Chapter 4).
5. Develop a conceptual biomechanical model for the multiple interrelated actin-myosin functions of spontaneous rhythmic contraction, adjustable preload stiffness and length adaptation (Chapter 5).

6. Incorporate the rhythmic contraction into the multiple interrelated actin-myosin functions and exhibit the role of spontaneous rhythmic contraction in DSM dynamic length tension relationship (Chapter 5).

1.18. Contribution of the Dissertation

Previous studies have shown that the preload length-tension relationship in rabbit detrusor smooth muscle is dynamic and the muscle exhibits adjustable preload stiffness characterized by a length-preload tension curve that can shift along the length axis as a function of strain history and activation history (Speich et al., 2007). This activity, in addition to quick-stretch-induced myogenic response and spontaneous rhythmic contraction, involve cross-bridges either cycling to produce active tension or operating as cross-links to produce preload tension. To the best of my knowledge, this is the first study to develop a purely biomechanical model using mechanical elements to explain the multiple interrelated actin-myosin roles in muscle contraction. Bladders of all known mammalian species, including humans, display spontaneous rhythmic contractile activity, but this activity has largely been ignored and the physiological function of the rhythm has yet to be identified. To the best of my knowledge, this is the first study to model the role of rhythmic contraction and its mechanical role in the dynamic active and preload length-tension relationship in detrusor smooth muscle. Furthermore, previous studies showed that DSM cells are independent of neural input and they are poorly coupled electrically (Ji et al., 2002; Poley et al., 2008). To the best of my knowledge, this is the first study to demonstrate that rapid contraction of one muscle cell can stimulate surrounding cells by rapidly stretching them to propagate contraction throughout a bundle of cells.

This study presents a better understanding of multiple interrelated mechanical characteristics of detrusor smooth muscle, which may be helpful in understanding overactive or underactive bladder disorders, and may be useful in developing drugs to treat these disorders. Since low-grade rhythmic contractions occur in human bladder and elevated levels of SRC have been shown in patients with OAB disorder (M. Drake & Harvey, 2005), a better understanding SRC may be essential to understanding a potential mechanism for OAB. Lastly, the results this study could be useful in future research to develop artificial bladder patches or artificial muscles.

1.19. Dissertation Organization

This study of the mechanical behavior of bladder smooth muscle consists of five chapters. This chapter has provided background information, a review of previous studies from the relevant literature, a list of the main objectives, and a description of the expected contributions of this dissertation. Chapter 2 discusses the experimental methods utilized within this study. Chapter 3 presents an analysis of experimental data to compare the spontaneous rhythmic contraction and quick-stretch-induced myogenic response mechanisms. Chapter 4 presents a sensor-based mechanical model for myogenic contraction and spontaneous rhythmic contraction. Chapter 5 focuses on the role of actin and myosin interactions in spontaneous rhythmic contraction, length adaption and adjustable preload stiffness in DSM. Chapter 6 presents some primary experimental data about the effect of age on adjustable preload stiffness. Finally, Chapter 7 provides conclusions and recommendations for future research.

CHAPTER 2 METHODS AND MATERIALS

2.1. Choice of Animal Model

Rats, rabbits, mice, and pigs have been the main focus of numerous studies in various biological scientific research disciplines. Although there are differences in bladder size,, compliance, and physiology, bladders from these species still have many common characteristics with humans. The detrusor muscle of the bladder wall consists of layers of fibers. In human detrusor, bundles of the muscle cells are surrounded by connective tissue rich in collagen (Andersson & Arner, 2004). Within the bundles, the smooth muscles cells may exist in groups of small functional units. The orientation and interaction between the smooth muscle cells in the bladder are important, since this will determine activity, shape, pressure, and physical behavioral characteristics of the overall system. For small animals such as rabbits, the muscle bundles are less complex and the patterns of the arrangement are more simple than in the human bladder (Andersson & Arner, 2004). Both rabbits and humans the muscle consists of three layers of smooth muscle fibers and most of the fibers are arranged longitudinally (Andersson & Arner, 2004; Guyton & Hall, 1961).

In this study New Zealand White Rabbits were used for a number of reasons. First, the detrusor consists of three layers of smooth muscle fibers and most of the bundles are arranged longitudinally, as in humans. Second, it is relatively easy to cut strips from the rabbit bladder since the bundles are clearly visible. Third, unlike mice, the size of the rabbit bladder is large enough to provide the number of tissue strips necessary for some experiments that require

control and multiple test strips. Fourth, the cost is reasonable when compared to larger animals such as pigs. Fifth, there are extensive studies published about rabbit bladder, which will allow the results from this study to be compared to the literature. Finally, this dissertation builds upon prior studies from our laboratory which used New Zealand White rabbits (A. M.- Almasri, 2009).

In addition, bladders from two groups of male C57BL6 mice 8 weeks (adult) and 20 months (old) were used to test the effect of age on adjustable preload stiffness (Chapter 6). The number of mice in each group was 15.

2.2. Tissue Preparation

All experiments involving animals were conducted within the appropriate animal welfare guidelines and regulations with additional approval by the VCU Institutional Animal Care and Use Committee. Whole bladders were removed from adult female New Zealand White rabbits (2-4 kg) sacrificed by an overdose of anesthesia. Bladders were washed with modified physiologic salt solution, cleaned of adhering serosa and fat, and stored in cold (0–4 ^{o}C) modified physiologic salt solution. Thin strips (~0.2 mm thick) of longitudinal DSM, without mucosa, were dissected from the bladder wall close to the dome and following the natural bundling (Ratz & Miner, 2003). Whole bladders were removed from old and adult male mice and dissected for the study in Chapter 6.

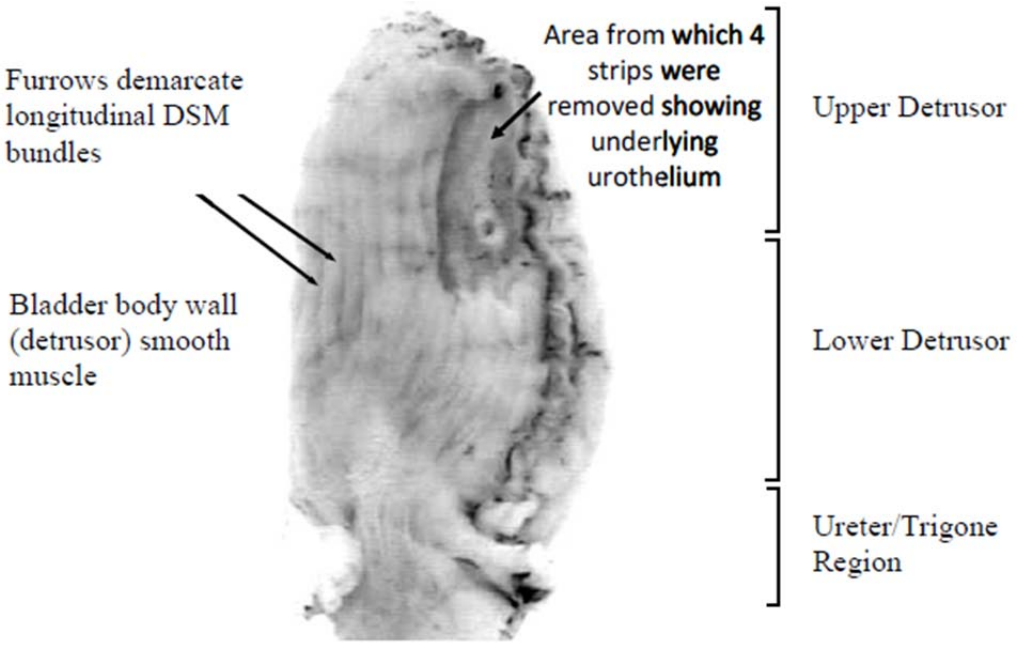

Figure 2.1 A photograph showing the posterior surface of a female New Zealand White rabbit bladder (A. M.- Almasri, 2009).

2.3. Solutions and drugs

Modified physiological salt solution (**PSS**) was composed of NaCl, 140 mM; KCl, 4.7 mM; $MgSO_4$, 1.2 mM; $CaCl_2$, 1.6 mM; Na_2HPO_4, 1.2 mM; morpholinopropanesulfonic acid, 2.0 mM (adjusted to pH 7.4 at either 0 or 37^oC, as appropriate); Na_2 ethylenediamine tetraacetic acid, 0.02 mM; and dextrose, 5.6 mM. Modified PSS, in which 110 mM KCl was substituted isosmotically for NaCl, (**KPSS**) was used to induce muscle contractions, and a Ca^{2+}-free solution (**0-Ca**), composed of PSS without $CaCl_2$, was used to abolish rapid crossbridge cycling for preload tension measurements (Shenfeld et al., 1999). ROCK inhibitor 0.3 μM H-1152 (Toronto Research Chemicals), COX-1 inhibitor 0.1 μM SC-560 (Cayman Chemical) and COX-2 inhibitor 0.1 μM NS-398 (Cayman Chemical) were used to inhibit detrusor contractions(Collins

et al., 2009; Teixeira, Jin, Priviero, Ying, & Webb, 2007). Drugs were dissolved in dimethyl sulfoxide (**DMSO**), which was added at a final concentration of 0.1%. At this percentage, the DMSO does not affect the myogenic response (Poley et al., 2008).

2.4. Apparatus, muscle strip setup and reference length determination

Significant portions of this section have been previously published by the author (Komari et al., 2013). One end of each detrusor strip was clamped to a rigid post connected to a micrometer for manual length adjustments, and the other end was clamped in a small aluminum foil tube which was connected to a computer-controlled lever (model 300H, Aurora Scientific) to record tension and to induce time-controlled changes in muscle length. Tension and length signals were digitized (PCI-6024E, National Instruments) and stored electronically for analysis. Each strip was secured with a cold, zero-preload length of ~4 mm and then equilibrated in aerated physiological salt solution at 37°C. The mechanical and pharmacological protocols in this study were performed based on a reference length (L_{ref}) for each tissue. To determine L_{ref}, the detrusor strips were equilibrated at 4 mm in physiological salt solution for 10 minutes and stretched to 5mm for another 10 minutes. Next, the tissues were stretched to a load of 0.5 grams and permitted to stress relax for 30 minutes. Then, the strips were stretched to a load of 1.0 gram and permitted to isometrically stress relax for another 30 minutes. At the end of each experiment, tissues were contracted isometrically to determine the (T_{max_KCl}) at that muscle length which was subsequently used as L_{ref}. To reduce tissue-to-tissue variability, tension produced by myogenic contraction or rhythmic contraction (RC) was reported as a fraction maximum KCl-induced tension.

2.5. Statistics and Curve Fitting

Analyses were performed using Excel (2007, Microsoft) or Prism (5.0, GraphPad Software). The *n* value for each experiment refers to the number of animals. To determine significant differences a Student's *t*-test was used when comparing two groups, and when comparing more than two groups, a Student's t-test with the Bonferroni correction or a one-way ANOVA with the post-hoc Student-Newman-Keuls test was utilized. The null hypothesis was rejected at $p<0.05$.

2.6. Computational Simulation

The models were simulated using MATLAB Simulink. The equations used in the simulations are provided in the Appendices A & B and were solved using the ode45 solver in Simulink 6.0. The model parameters are listed in Tables A.1 and B.1. These parameters were selected to qualitatively demonstrate the observed muscle behaviors.

CHAPTER 3 EVIDENCE FOR A COMMON MECHANISM FOR SPONTANEOUS RHYTHMIC CONTRACTION AND MYOGENIC CONTRACTION INDUCED BY QUICK STRETCH IN DETRUSOR SMOOTH MUSCLE

Significant portions of this chapter have been previously published by the author (Komari et al., 2013). Detrusor smooth muscle exhibits myogenic contraction in response to a quick stretch (QS) as well as spontaneous rhythmic contraction (SRC). However, whether the same population of actomyosin cross-bridges with a common regulatory mechanism is responsible for these two types of contraction has not yet been determined. Detrusor strips from New Zealand White rabbit bladders were allowed to develop SRC at a reference muscle length ($\mathbf{L_{ref}}$) or rhythmic contraction (RC) was induced with tetraethylammonium (TEA). Multiple 10ms stretches of 15% L_{ref} were then imposed at L_{ref} randomly during the rhythmic cycle, and the nadir-to-peak (NTP) tension amplitude of the resulting myogenic contraction was measured. The amplitude and period of the rhythm cycle were measured prior to each QS. NTP was larger when a QS was imposed during a portion of the cycle when tension was smaller (n=3 each SRC and TEA-induced RC). These data suggest that when the rhythmic mechanism was mostly inactive and tension was near a minimum, a larger portion of a shared population of cross-bridges was available to produce a myogenic response to a QS. Rho kinase, cyclooxygenase-1, and cyclooxygenase-2 inhibitors (H-1152, SC-560 and NS-398) affected both SRC amplitude and NTP amplitude following a QS to the same degree (n=3 each drug), providing additional evidence to support the hypothesis that a common mechanism is responsible for SRC and

myogenic contraction due to QS. If a common mechanism exists, QS is a potential mechanical probe to study SRC regulation and its alteration affect in overactive bladder.

3.1. QS protocol

Quick Stretches were from L_{ref} to 115% L_{ref} with a stretch duration of 10 ms (Figure 3.1.A) as previously described(Poley et al., 2008). At the end of each QS, tissues were held isometrically at 115% L_{ref} for 10 s and then returned to L_{ref}. Tissues responded to QS with an immediate increase in tension followed by rapid stress relaxation (Figure 3.1.B). Following a brief latency period, tissues in PSS ceased to stress-relax and produced a phasic myogenic contraction. However, in 0-Ca solution stress relaxation continued toward a steady-state tension value (Figure 3.1.B). Nadir-to- peak (NTP) tension of the myogenic contraction was measured from the minimum stress relaxed value before the contraction to the peak of the contraction (Figure 3.1.B). The peak myogenic response (PMR) was calculated as the tension difference between the peak of the myogenic contraction and the stress relaxed value in 0-Ca at the same time from the QS (Figure 3.1.B). The PMR tension induced by a QS has been shown to rise with increased stretch amplitude and increased stretch rate (Poley et al., 2008). The stretch magnitude (15% L_{ref}) and rate (10 ms) (Figure 3.1.A) were selected to induce a near maximal myogenic contraction.

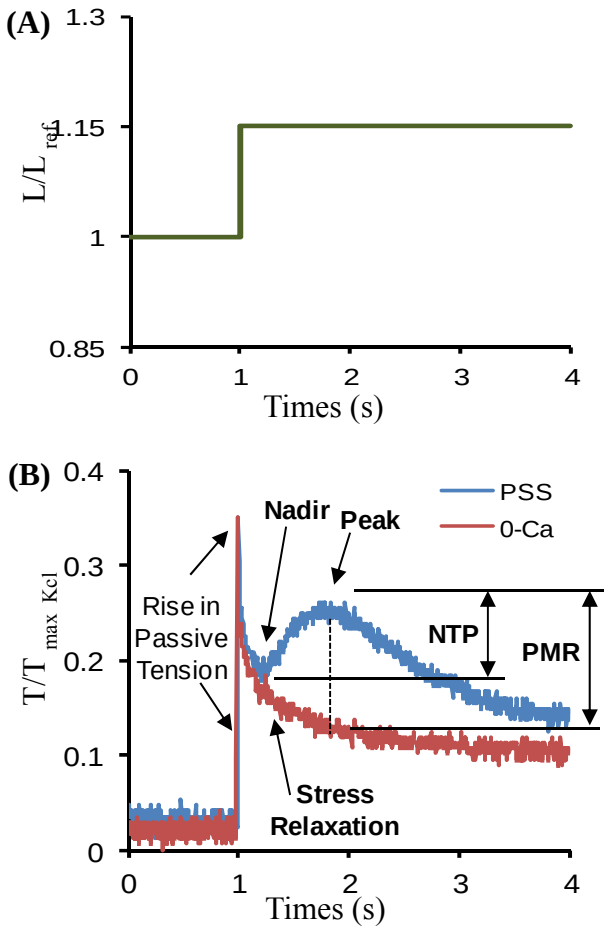

Figure 3.1 (**A**) Quick stretch protocol from L_{ref} to 1.15 L_{ref} in 10 ms & (**B**) the corresponding rise in preload tension, subsequent stress relaxation and subsequent myogenic contraction or lack of contraction from a DSM strip incubated in normal (PSS) or Ca^{2++}-free (0-Ca) physiological salt solution. Tension (T) was normalized to the maximum KCl-induced tension at 1.15 L_{ref} (T_{max_KCl}). PMR tension was calculated as the difference between the 0-Ca and PSS curves at the peak of the myogenic contraction and NTP tension was calculated as the difference between the nadir and subsequent peak of the PSS tension curve.

3.2. Quantification of RC

In one group of detrusor strips, SRC was allowed to spontaneously develop at L_{ref} (Figure 3.2.A). To increase the frequency of RCs in another group of tissues, the potassium channel blocker tetraethylammonium (TEA), which depolarizes the plasma membrane by reducing

potassium conductance (Wellner & Isenberg, 1994), was added at a concentration of 2 mM (Figure 3.2.B). TEA was utilized since it typically induces rhythmic contractions with a more consistent frequency (Figure 3.2.B). Tension amplitudes were measured for 19 or more cycles, and average tension amplitudes for SRC and 2 mM TEA-induced transient contractions were not significantly different (Figure 3.2.C). Rhythm cycle duration was measured from tension peak (0%) to tension peak (100%) for the cycle (Figure 3.3).

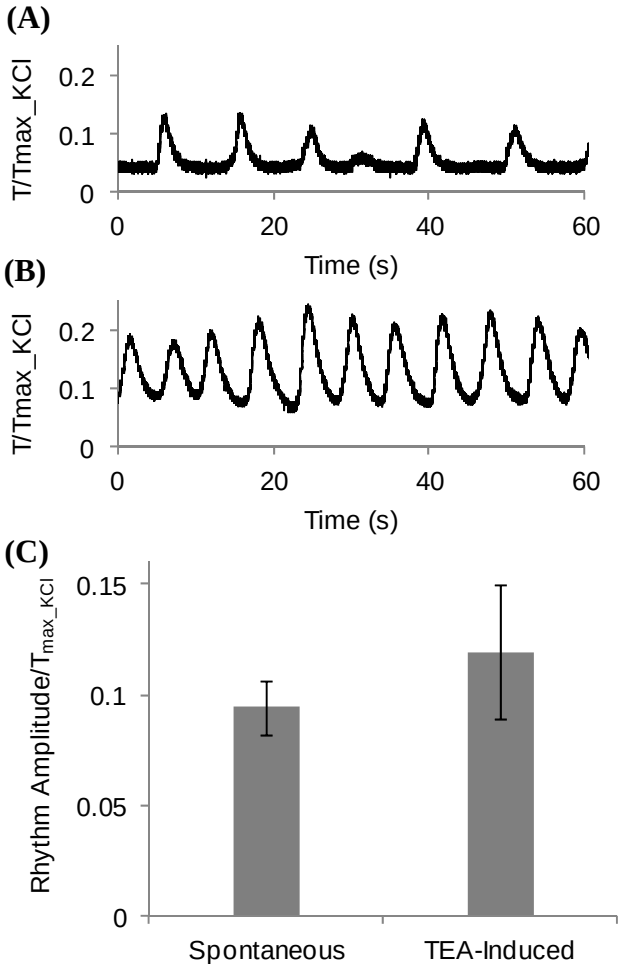

Figure 3.2 Examples of spontaneous (**A**) and 2 mmol/L tetraethylammonium (TEA)-induced (**B**) rhythmic contraction. (**C**) TEA-induced rhythmic amplitude was not significantly different from spontaneous rhythmic amplitude ($P > 0.05$, $n = 3$).

3.3. QS and rhythm synchronization

To test the hypothesis that the myogenic contraction following QS would be relatively large (or relatively small) at a point in the rhythm cycle when tension was relatively small (or relatively large), multiple QSs (19-23 per strip) were imposed on detrusor strips randomly throughout the SRC or TEA-induced rhythm cycle. The tension amplitude and duration from peak (0%) to peak (100%) of the rhythm cycle were measured immediately prior to each QS, and the NTP tension of the myogenic contraction was measured following each QS (Figure 3.3). The duration of the rhythm cycle was assumed to be the same as the previous cycle and used to estimate the percentage of the cycle at which the QS was imposed. Figures 3.3.A and 3.3.B show tension levels produced by myogenic contractions induced by QS at ~91% (near the peak) and ~58% (near the trough), respectively, of the TEA-induced RC cycle.

3.4. QS following pharmacological inhibition of SRC

Previous studies indicate that ROCK activity is required for QS-induced myogenic contraction (Poley et al., 2008), and that both prostaglandins produced by COX isoforms (Collins et al., 2009; Klausner et al., 2011) and ROCK (Ratz & Miner, 2003) participate in the regulation of SRC. To test the hypothesis that a common regulatory mechanism is responsible for SRC and QS-induced myogenic contraction, the effects of ROCK and COX inhibitors on each type of contraction were quantified and compared. More specifically, the tension produced by each type of contraction was measured before and during the presence of a ROCK, COX-1 or COX-2 inhibitor, 0.3 μM H-1152, 0.1 μM SC-560 or 0.1 μM NS-398, respectively. SRC amplitude was

measured at the end of a 20 minutes period prior to addition of an inhibitor (control), and at the end of a 20 minutes exposure to one of the three inhibitors. Average SRC amplitude was calculated as the average amplitude of 5 consecutive rhythm cycles near the end of each 20 min period. Tissues were also subjected to two QSs at the trough of a SRC cycle, with one at the end of the 20 min period before exposure to the inhibitor and one at the end of the 20 min period in the presence of the inhibitor. As with SRC amplitudes, QS-induced NTP myogenic tension values were measured prior to addition of an inhibitor (control), and during the presence of each inhibitor. The effects of the inhibitors on contraction amplitude values were reported as normalized to the control, pre-drug amplitude values.

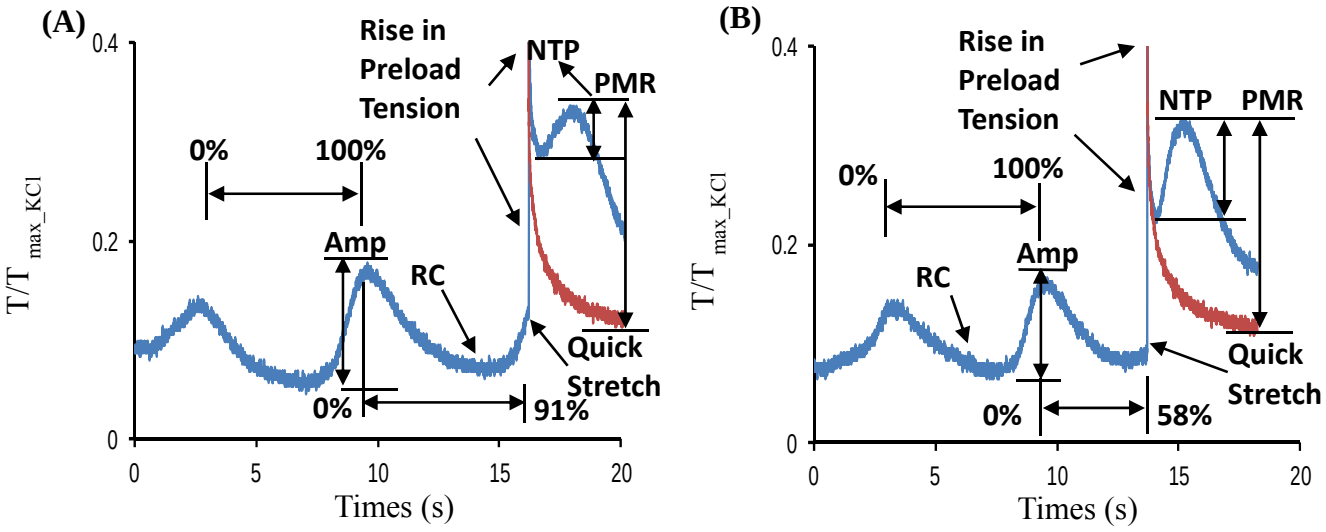

Figure 3.3 Examples of myogenic response due to quick stretch imposed during spontaneous rhythmic contraction. The amplitude (AMP) and duration from peak (0%) to peak (100%) of the rhythm cycle were measured immediately prior to each stretch. Nadir-to-Peak (NPT) myogenic responses for stretches imposed at 58% (**A**) and 91% (**B**) of the rhythm cycle. Tension (T) was normalized to the maximum KCl-induced tension at 1.15 Lref (T_{max_KCl}).

3.5. Effect of QS and rhythm synchronization

NTP tension values for typical detrusor strips were plotted as a function of the percentage of the SRC cycle (Figure 3.4.**A**) or the TEA-induced RC cycle (Figure 3.4.**B**) at which each QS was initiated, and a 2nd order polynomial (parabolic) curve was fit to each data set (Figure 3.4.**A-B**). Data for all tissues were divided into five 20% incremental groups according to the percentage of the SRC or TEA-induced rhythm cycle at which each QS was imposed (Figure 3.4.**C-D**, 0−20, 20−40, 40−60, 60−80, 80−100%), and parabolic curves were fit to each group. Both groups showed parabolic relationships, with tissues in the SRC group producing significantly higher NTP tension in the 40-60% and 60-80% ranges of the rhythm cycle. Additionally tissues in the TEA-induced RC group produced higher NTP tension in the 20-40%, 40-60% and 60-80% ranges when the tension amplitude in the RC was relatively low (i.e., during the trough between sequential RCs; Figure 3.4.**C-D**).

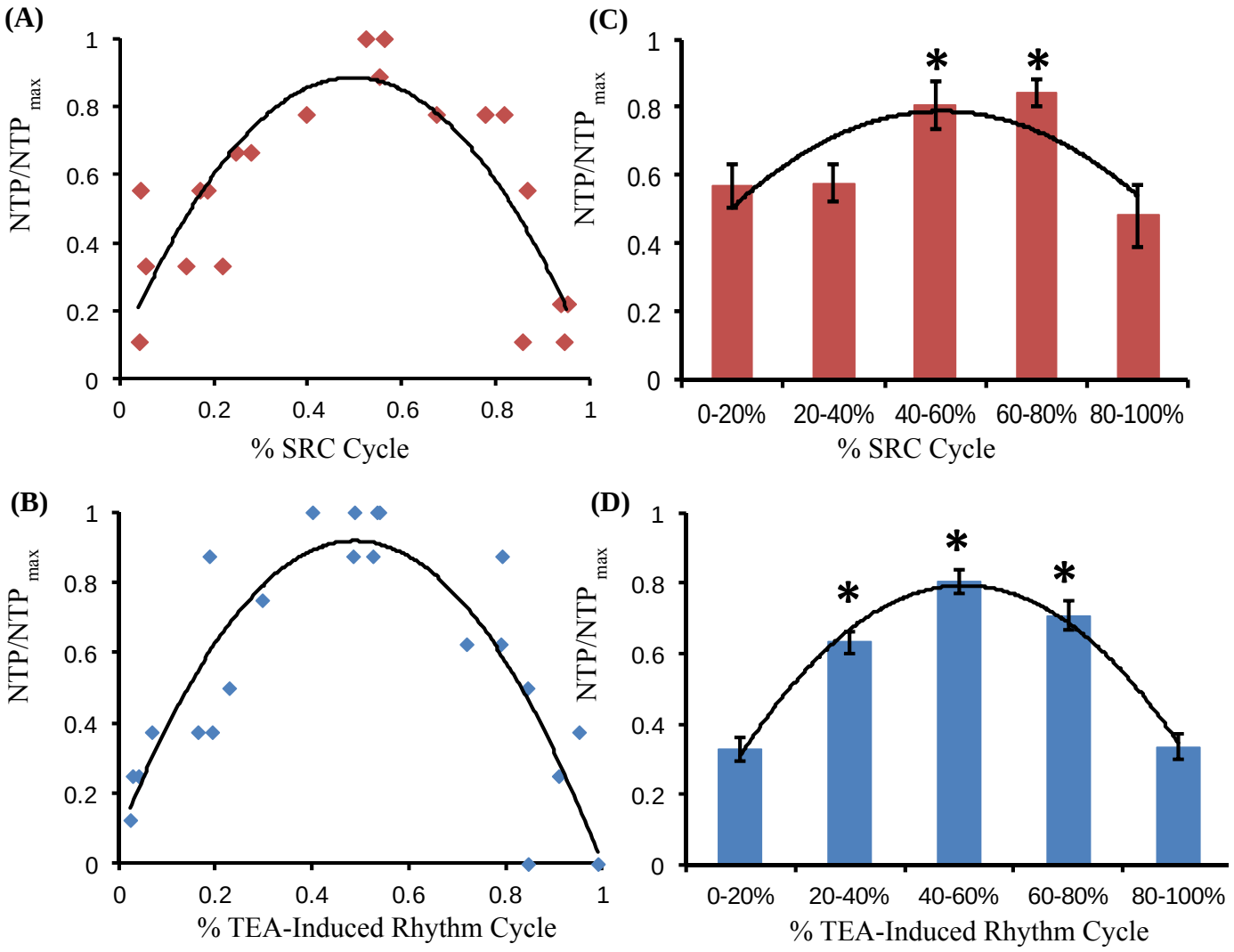

Figure 3.4 Examples of nadir-to-peak (NTP) myogenic contractions at points throughout spontaneous rhythmic contraction (SRC) (**A**) and tetraethylammonium (TEA)-induced rhythmic contraction (RC) (**B**) cycles with second-order polynomial fits ($R^2 = 0.63$ and 0.75, respectively). Average NTP values for stretches in the ranges of 0–20% 20–40% 40–60% 60–80, and 80–100% of the rhythm cycle (as defined in Figure 3.3) for SRC (**C**) and TEA-induced RC (**D**) with second-order polynomial fits ($R^2 = 0.62$ and 0.99, respectively). NTP values for each tissue were normalized to the maximum NTP value for that tissue (NTP_{max}). Average NTP values indicated with the * symbol were significantly different from values without the symbol (analysis of variance [ANOVA], $P < 0.05$, n = 3 animals, 19–23 stretches per tissue, 9–17 stretches in each cycle range).

PMR tension values for typical detrusor strips, the same strips as illustrated in Figure 3.4.**A**-**B**, were also plotted as a function of the percentage of the SRC cycle (Figure 3.5.**A**) or the TEA-induced RC cycle (Figure 3.5.**B**) at which each QS was initiated (Figure 3.5.**A**-**B**). As with the NTP contraction data, average PMR tension data for all tissues were divided into five groups according to the percentage of the SRC or TEA-induced rhythm cycle at which each QS was imposed (Figure 3.4.**C**-**D**). Average PMR tension for each of the cycle percentage ranges (0-20%, 20-40%, 40-60%, 60-80% and 80-100%) was not different from that of any of the other cycle ranges for either SRC (Figure 3.5.**C**) or TEA-induced rhythm (Figure 3.5.**D**). Thus, PMR tension, in contrast to NTP tension, was independent of the percentage of the rhythm cycle at which the QS was imposed.

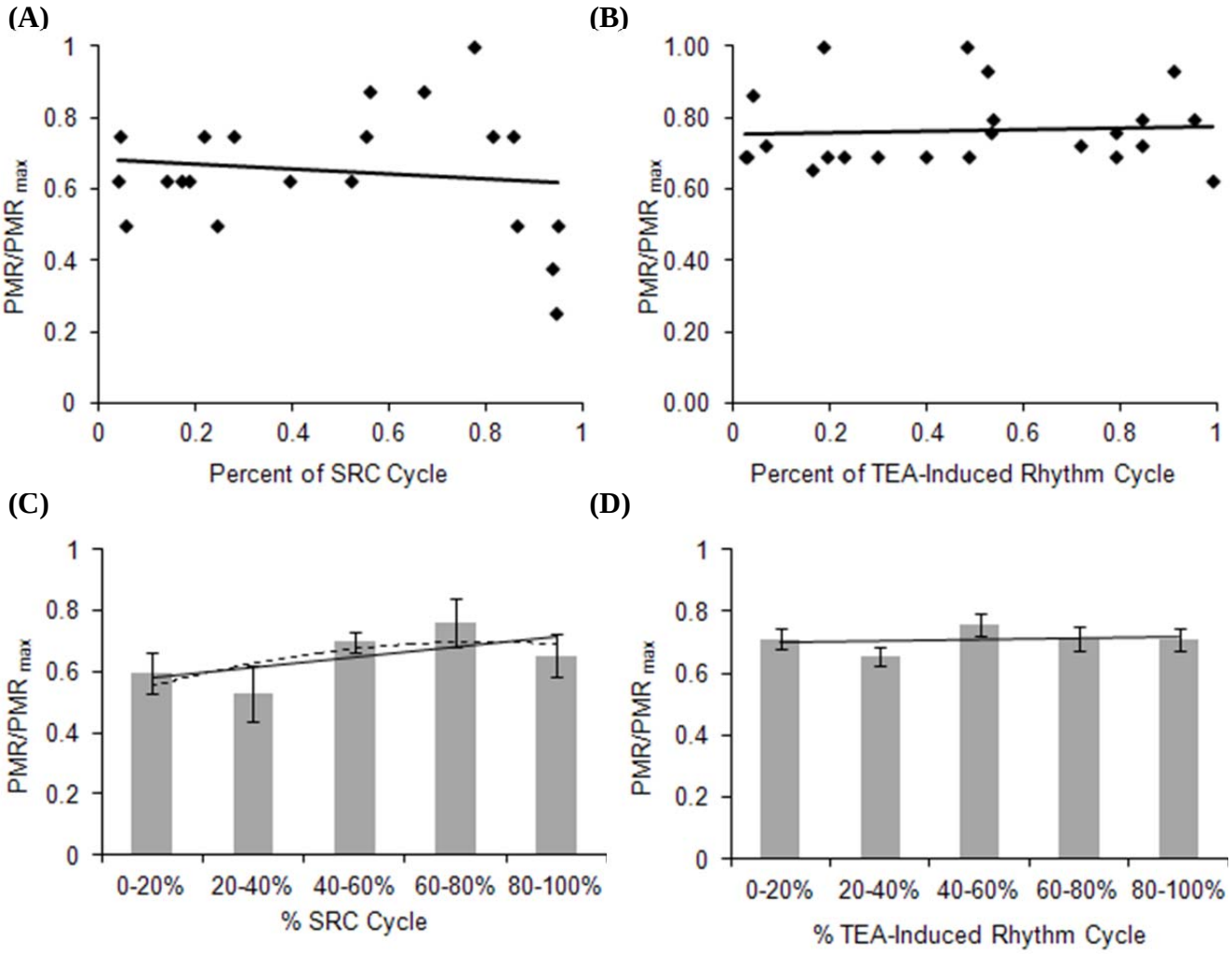

Figure 3.5 Examples of peak myogenic response (PMR) tension (defined in Figure. 3.1) at points throughout SRC (**A**) and tetraethylammonium (TEA)-induced rhythmic contraction (RC) (**B**) cycles (same detrusor strips as in Figure. 3.4A-B). PMR values for each tissue were normalized to the maximum PMR value for that tissue (PMR_{max}). Average PMR tension for stretches in the ranges of 0–20, 20–40, 40–60, 60–80, and 80–100% of the rhythm cycle (defined in Figure. 3.3) for SRC (**C**) and TEA-induced RC (**D**). Average PMR tension for each of the cycle percentage ranges (0–20, 20–40, 40–60, 60–80, and 80–100%) was not different from that of any of the other cycle ranges for either SRC (**C**) or TEA-induced rhythm (**D**) (analyses of variance [ANOVA], $P > 0.05$, n = 3 animals, 19–23 stretches per tissue, 9–17 stretches in each cycle range). Second-order polynomial fits (R^2 = 0.45 (**C**) & 0.08 (**D**)) produced relatively flat curves compared to the NTP tension data in Figure. 3.4.

3.6. Pharmacological Inhibition of SRC and NTP following QS

The ROCK (0.3 µM H-1152), COX-1 (0.1 µM SC-560) and COX-2 inhibitors (0.1 µM NS-398), each inhibited NTP myogenic tension following the QS and SRC amplitude by approximately 30-40% (Figure 3.6, *). Furthermore, H-1152, NS-398 and SC-560 inhibited NTP myogenic tension and SRC amplitude by the same amount (Figure 6, NS). These data support the hypothesis that SRC and myogenic contraction are regulated by common mechanisms.

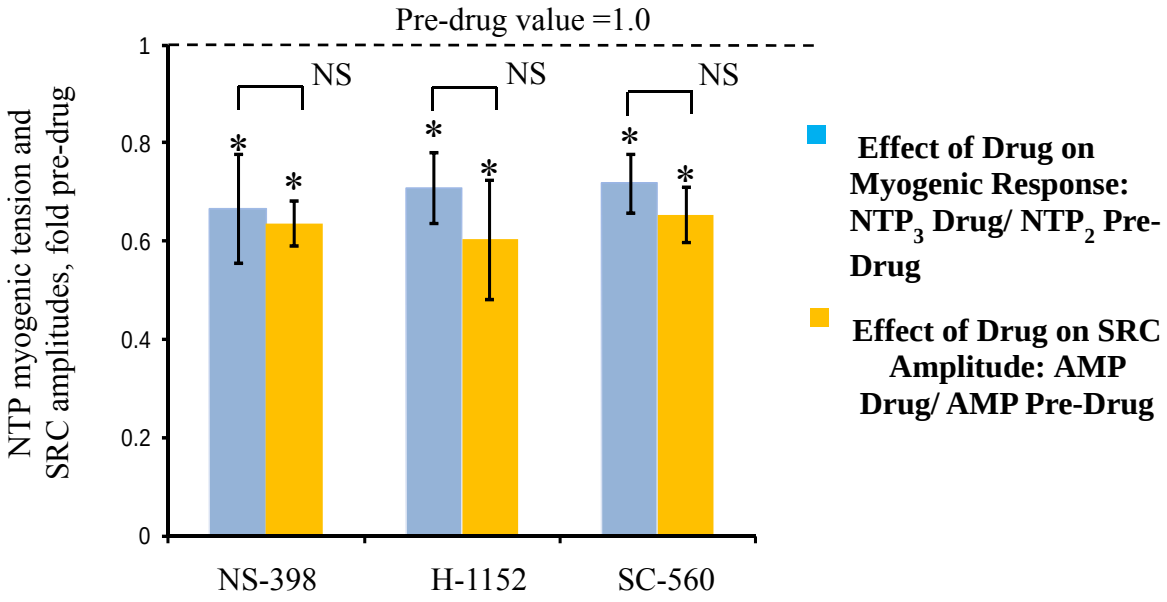

Figure 3.6 Both nadir-to-peak (NTP) myogenic tension amplitude following quick stretch (QS) and spontaneous rhythmic contraction (SRC) amplitude were inhibited approximately 30–40% by 0.3 lmol/L H-1152, 0.1 lmol/L SC-560, and 0.1 lmol/L NS-398 (NTP and SRC amplitudes were normalized to predrug values, *normalized value < 1.0, analysis of variance (ANOVA), $P < 0.05$, n = 3–4). The extent of inhibition was equivalent for both types of phasic contraction (NS, not statistically significant).

CHAPTER 4 MECHANICAL-SENSOR-BASED STRETCH-INDUCED MYOGENIC CONTRACTION

4.1 Introduction

Detrusor smooth muscle (DSM) can produce a spontaneous rhythmic contraction (SRC) that is observed as a procession of transient low-amplitude twitches. A quick-stretch (QS) can initiate a single myogenic twitch with a duration and amplitude that is similar to an isolated SRC twitch. In addition, spontaneous filling phase contractile activity has been shown to be resistant to both atropine and tetrodotoxin, suggesting that this process may be intrinsic to the DSM (Klausner et al., 2013). In addition, partial bladder outlet obstruction enhances the autonomous contractile activity in discreet bundles of DSM, and coordination of these contractions is enhanced by stretching the muscle (M. J. Drake, Harvey, & Gillespie, 2014), but the mechanism for these changes is not known. All DSM cells are not innervated, and it has been proposed that rapid shortening of innervated cells may myogenically activate non-innervated cells through mechanical coupling to produce a uniform DSM contraction. This concept was supported by a study by Ji et al. (Ji et al., 2002). Previous studies also show that phasic myogenic contractions of DSM cells are independent of neural input (Poley et al., 2008). Since DSM cells are poorly coupled electrically (Elbadawi, 1995), a mechanical coupling model has been proposed in which rapid contraction of one muscle cell stimulates surrounding cells by rapidly stretching them to propagate contraction throughout a bundle of cells (Komari et al., 2013). This model confirms

Golenhofen's hypothesis that mechanical coupling between smooth muscle units is responsible for synchronization (Golenhofen, 1970).

Researchers have studied the mechanotransduction mechanism and the process of converting mechanical inputs into biochemical signals in different types of smooth muscles and found that various types of protein (e.g. titin, smitin, etc.) (Kim & Keller, 2002)can behave as mechanical sensors. Gill and his colleagues reported that mechanical and chemical lipid sensing by the TRPC6 channel has a common molecular mechanism in vascular smooth muscles (VSM). The mechanosensing properties of TRPC6 channels are highly expressed in smooth muscle cells and are likely to play a key role in regulating myogenic tone in vascular tissue (Spassova, Hewavitharana, Xu, Soboloff, & Gill, 2006). In this dissertation, it is proposed that stretch triggers a mechanical sensor that provides feedback to the biochemical signaling system that initiates and regulates the myogenic contraction.

In the present study, a spring-dashpot model was implemented as mechanical sensor to initiate and regulate the amplitude of QS-induced contraction based on the stretch amplitude, stretch rate, and the delay time between quick stretches, as demonstrated in an earlier experimental study. A single population of cross-bridges was modeled to produce both SRC and QS-induced contraction. All of these cross-bridges were active at the peak and inactive at the trough of each SRC cycle. Additionally, a QS imposed during SRC was modeled to activate any remaining cross-bridges in this population. Model simulations were consistent with the previous experimental data described in Chapter 3 (Komari et al., 2013), which showed that QSs imposed throughout the SRC cycle produced a myogenic contraction with greater nadir-to-peak tension when the QS was imposed near the trough of the cycle, suggesting more cross-bridges were available to be activated. Furthermore, simulations demonstrated that stretch-induced myogenic

contraction in one cell was sufficient to trigger up to 24 in-series cells. QS in one cell was able to trigger SRC with amplitude of 10% T_{A_max} in up to 3 in-series cells (Figure 4.15.B) and propagate the contraction through the muscle.

The objectives of the study discussed in this chapter are as follows:

1) Develop a biomechanical model for DSM contraction that incorporates a single mechanism for SRC and QS-induced contraction.
2) Incorporate a simple mechanical sensor that regulates QS-induced contractions with amplitudes that are dependent on stretch magnitude and stretch rate (Poley et al., 2008).
3) Simulate previously completed experimental protocols to demonstrate whether the model can qualitatively reproduce the characteristics of QS-induced myogenic contraction observed in experimental studies (Poley et al., 2008).
4) Develop a network model to test the hypothesis that rapid stretching of one DSM cell initiates a myogenic contraction to propagate the contraction throughout a bundle of cells.

4.2. Sensor-Based Mechanical Model

Two simple mechanical models of smooth muscle are the Kelvin (standard linear) model and the Voigt model (Speich et al., 2006). Each of these viscoelastic models contains three elements:

1) A viscoelastic component (VC) that generates active force when the actomyosin cross bridges are attached and cycling (termed a contractile component), or acts as a dashpot when actomyosin cross bridges do not actively cycle through a power stroke to cause muscle contraction (i.e., when DSM is maintained under preload conditions).

2) A series elastic component (SEC) in series with the contractile component.

3) A parallel elastic component (PEC) in parallel with the contractile component.

In the Kelvin configuration, the nonlinear elastic component (PEC) is in parallel with both the elastic component (SEC) and the viscoelastic component(s) (VC_K) (Maxwell configuration) (Fung, 1993; R A Murphy, 2011), whereas, in the Voigt configuration (R A Murphy, 2011), the PEC is in parallel only with the VC (Speich et al., 2006).

In the present study, a mechanical sensor-based SRC and QS-induced contraction model (Figure 4.1.) was developed with four main segments:

1) A Kelvin model with a viscous component (dashpot, VC_K), with in-series and in-parallel elastic components (springs, SEC_K & PEC_K) used to represent the muscle preload tension and stress relaxation.
2) An adjustable preload stiffness model (Speich et al., 2006) to represent stretch-history-dependent and activation-history-dependent DSM preload tension in the tissue. This portion of the model consisted of a slow viscous component (VC_{slow}), a weak in-parallel elastic component (PEC_{Slow}), and a group of in-series crosslinking elastic components represented by a single element with an equivalent variable stiffness (SEC_{eq}).
3) A single population of cross-bridges was modeled as a linear motor which produced both SRC & QS-induced contraction transmitted via series elastic component (SEC_M).
4) A mechanical sensor was modeled as a viscous component (VC_S) with in-series and in-parallel elastic components (SEC_S & PEC_S).

For the model simulations performed in this study, all the crosslinking elastic components were modeled to be attached, so the system had maximum adjustable preload stiffness. Since the preload stiffness section is in parallel with other sections of the model, the stiffness of the cross-

links does not affect sensor or the myogenic response. It only shifts the total force-time graph as shown in Figure 4.2.

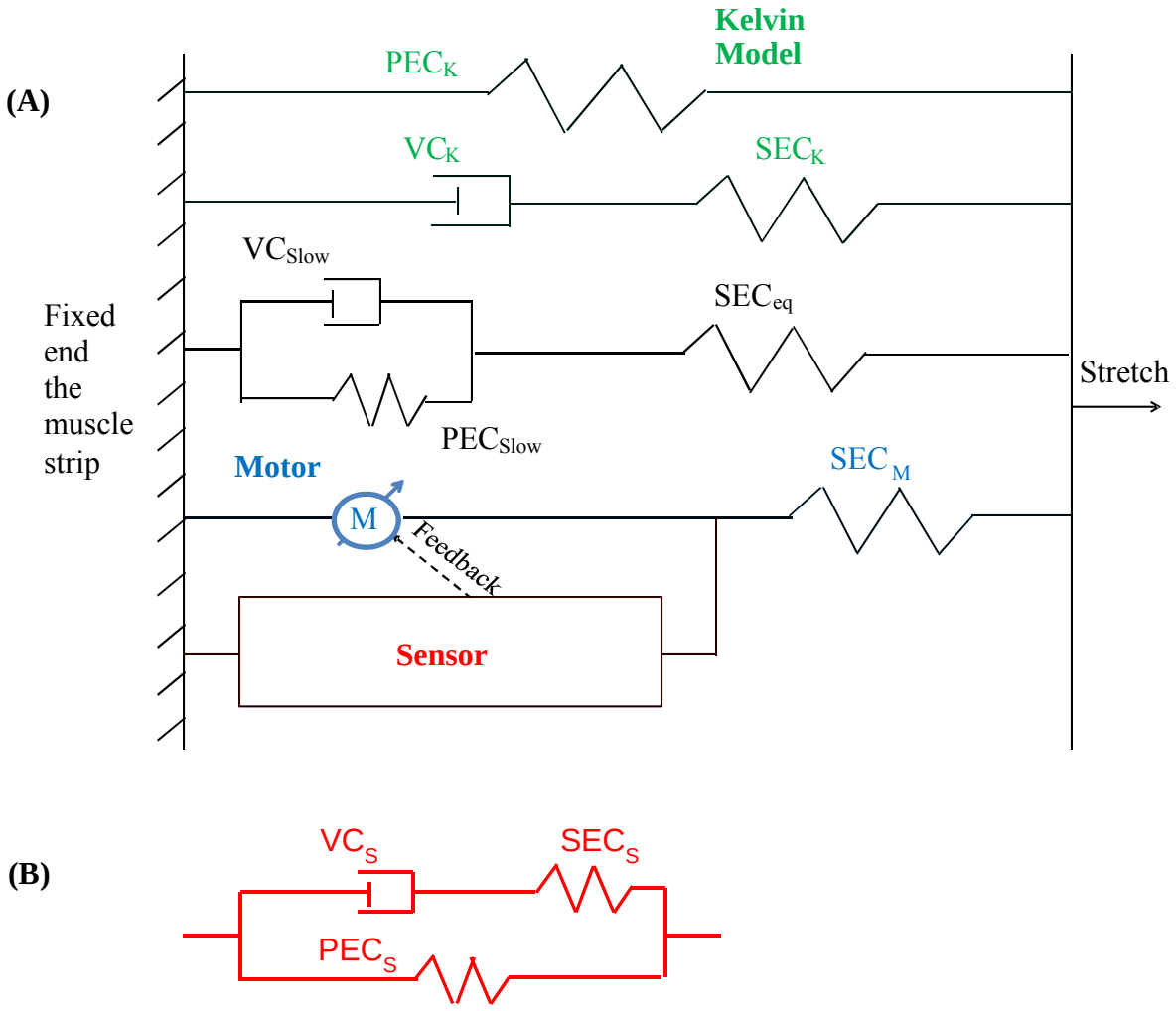

Figure 4.1 (**A**) A mechanical sensor-based SRC and QS-induced contraction model was developed with four main segments: 1) a Kelvin model with a viscous component (dashpot, VC_K), and in-series and in-parallel elastic components (springs, SEC_K & PEC_K) 2) an adjustable preload stiffness model consisting of slow viscous component (VC_{Slow}), an in-parallel elastic component (PEC_{Slow}) and a variable in-series elastic component (SEC_{eq}) 3) a linear motor (M) which produced both SRC & QS-induced contraction transmitted via series elastic component (SEC_M). (**B**) A mechanical sensor was modeled as a viscous component (VC_S) with in-series and in-parallel elastic components (SEC_S & PEC_S).

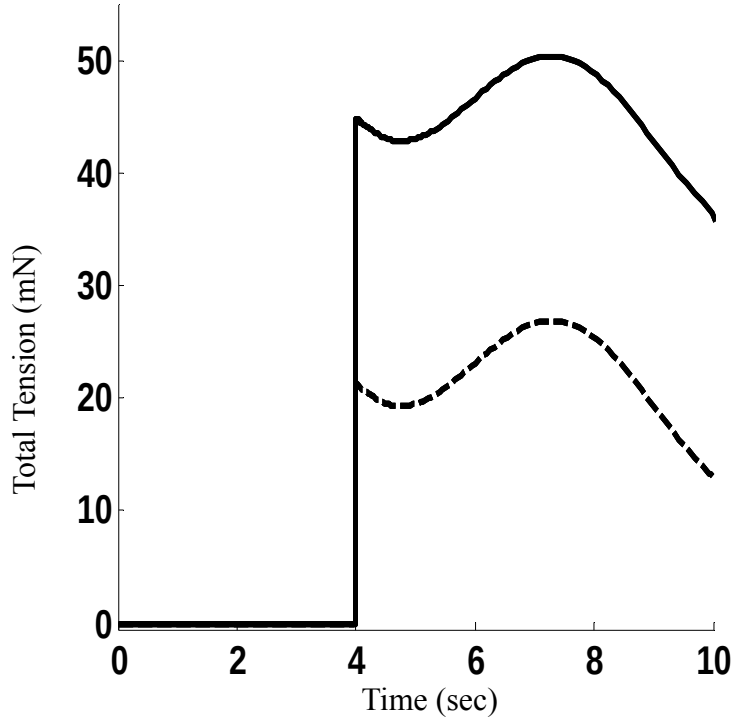

Figure 4.2 Example of myogenic model simulation comparing total tension output with all cross-links in APS model attached (solid line) and detached (dashed line).

The simulation output of each segment of the model when the system was subjected to a QS equal to 15% of the muscle reference length at stretch rate of 5 ms is shown in Figure 4.3. The tension in the SEC_S was used to trigger QS-induced contraction and regulate its amplitude. In the absence of SRC, a QS that produced a change in SEC_S (ΔSEC_S) greater than a threshold value was programmed to induce a myogenic contraction with a simplified tension-time relationship corresponding to one half of a sine wave (Figure 4.4B). The magnitude of the myogenic contraction was controlled by the ΔSEC_S produced by the QS, with a greater ΔSEC_S producing a stronger contraction.

During SRC, the motor output was sinusoidal tension that was simulated as having all cross-bridges active at the peak and all cross-bridges inactive at the trough of each SRC cycle

(see Figure 4.12A-B). A QS imposed during the SRC cycle triggered the mechanical sensor to activate any remaining cross-bridges by resetting the SRC cycle to begin at a trough with an amplitude equal to the tension generated by the remaining cross-bridges (Figure 4.12A-B). The sensor was designed to produce much less tension than the Kelvin viscoelastic portion of the model to provide a minimal direct contribution to the total tension produced by the simulated muscle.

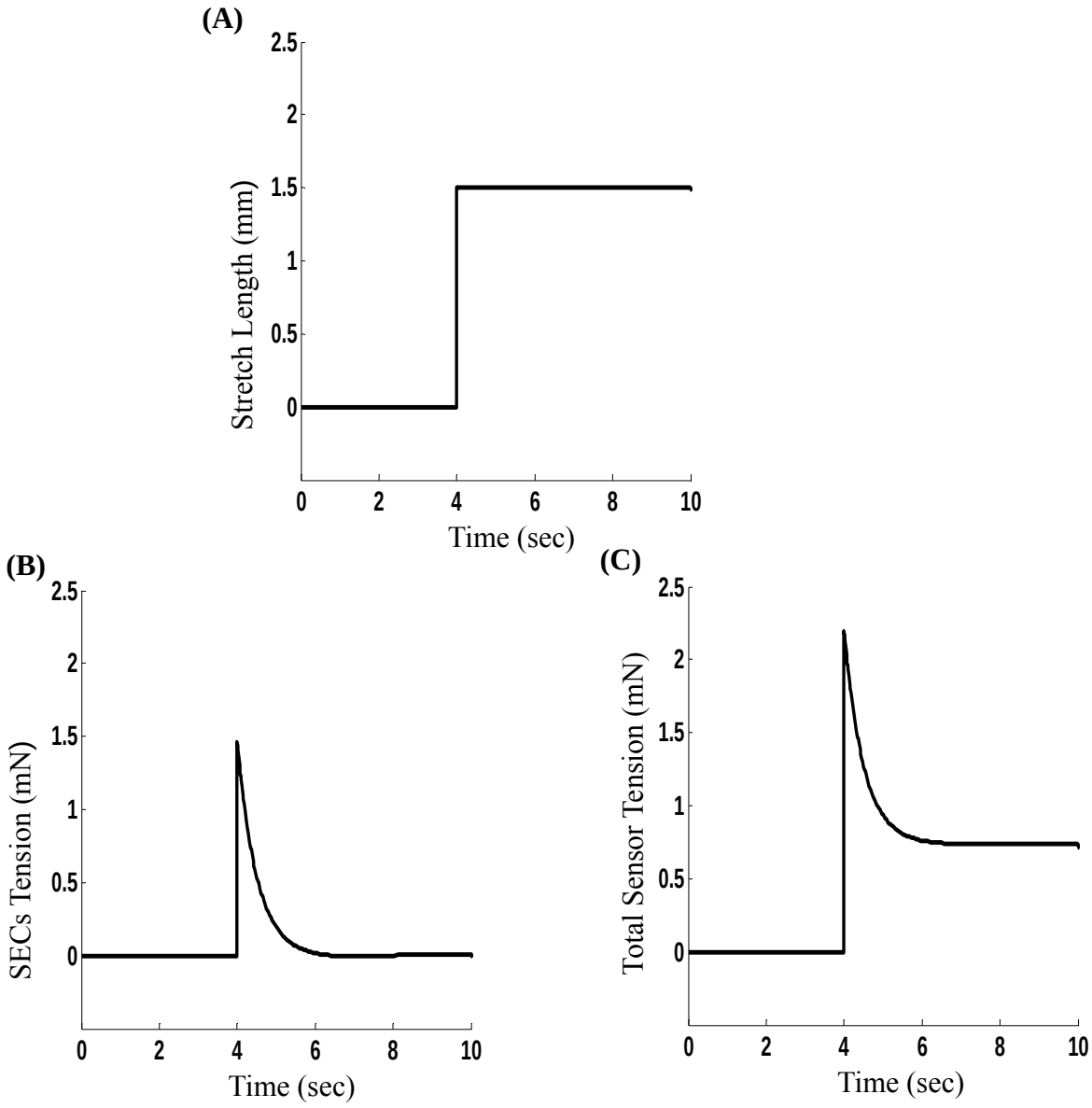

Figure 4.3 (**A**-**C**) Model simulation example. (**A**) Length-time graph for the quick-stretch protocol. (**B**) Tension in the series elastic component of the sensor (SEC_s) that triggers the rhythmic cross-bridges. (**C**) Total tension in sensor component (Figure4.1.B).

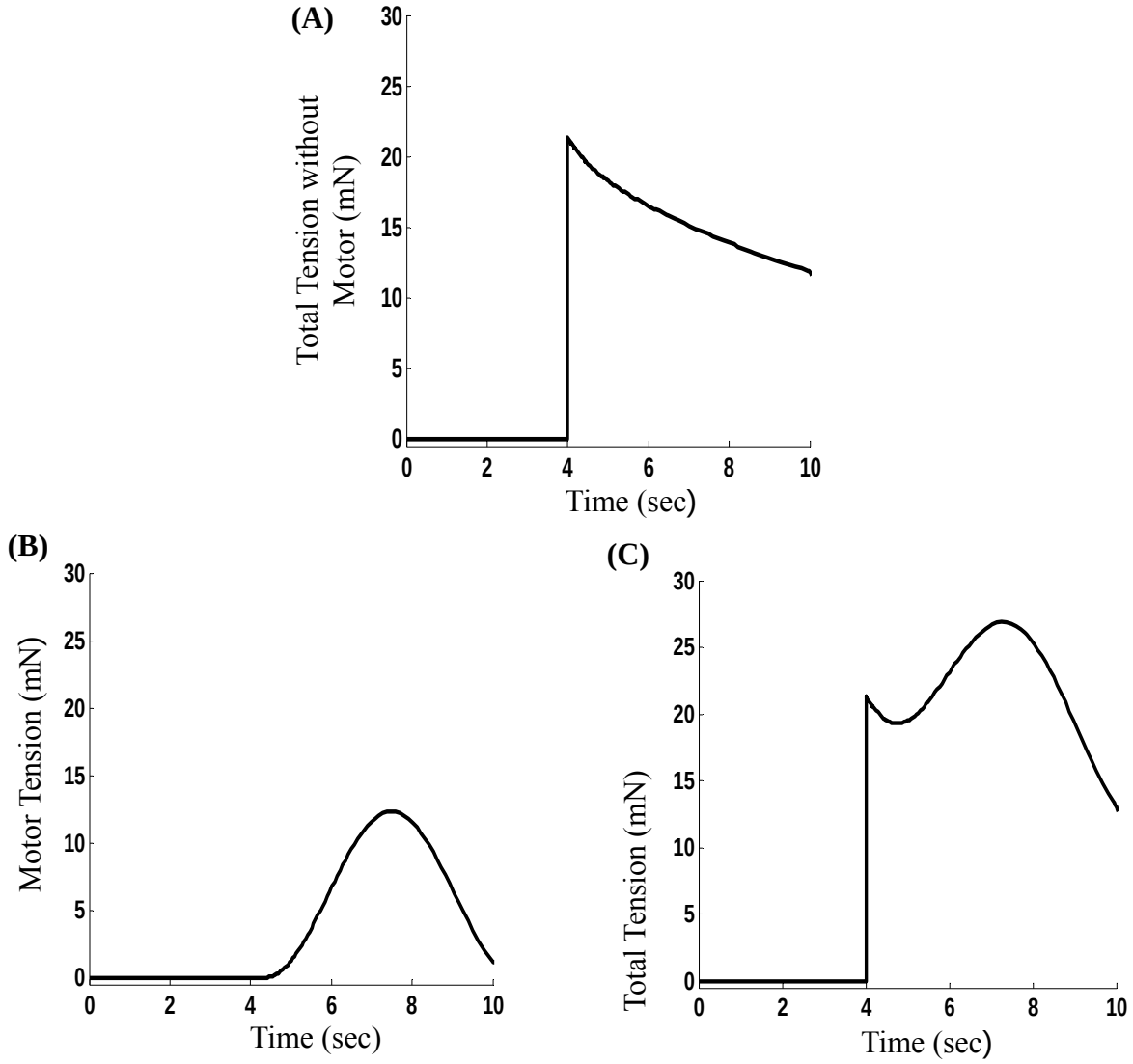

Figure 4.4 (**A**-**C**) (**A**) Total tension in model including the Kelvin model, the APS model, the SEC_m and the sensor elements when the motor was off. (**B**) Motor tension during a single rhythmic contraction cycle. (**C**) Total tension from all components produced by model (**A**+**B**).

The model was simulated using MATLAB Simulink. The equations used in the simulation are defined in APPENDIX 1 and were solved using the ode45 solver in Simulink 6.0. The parameters listed in Table A.1 were selected for the myogenic model simulations to qualitatively reproduce experimentally observed DSM characteristics. All of the model elements are linear, except for the PEC_K, which was assumed to model collagen and elastin. These elements provided the classic nonlinear preload length-tension curve for smooth muscle.

4.3. Sensor threshold tension values

Previously experimental data (Poley et al., 2008) was curve fitted to determine the threshold tension values for the sensor (SEC_s) in the model that activates the motor in response to a QS (Figure 4.5A-B). NTP data for the stretch magnitude dependency of the myogenic response correlated with a logarithmic curve and was extrapolated to predict the minimum percentage of the reference muscle length (Table 4.1) to which the tissue must be stretched to induce a myogenic contraction. Similarly, experimental data showing the rate dependency of the myogenic response were fit to an exponential curve and extrapolated to predict the slowest stretch rate that would induce a myogenic contraction (Table 4.1).

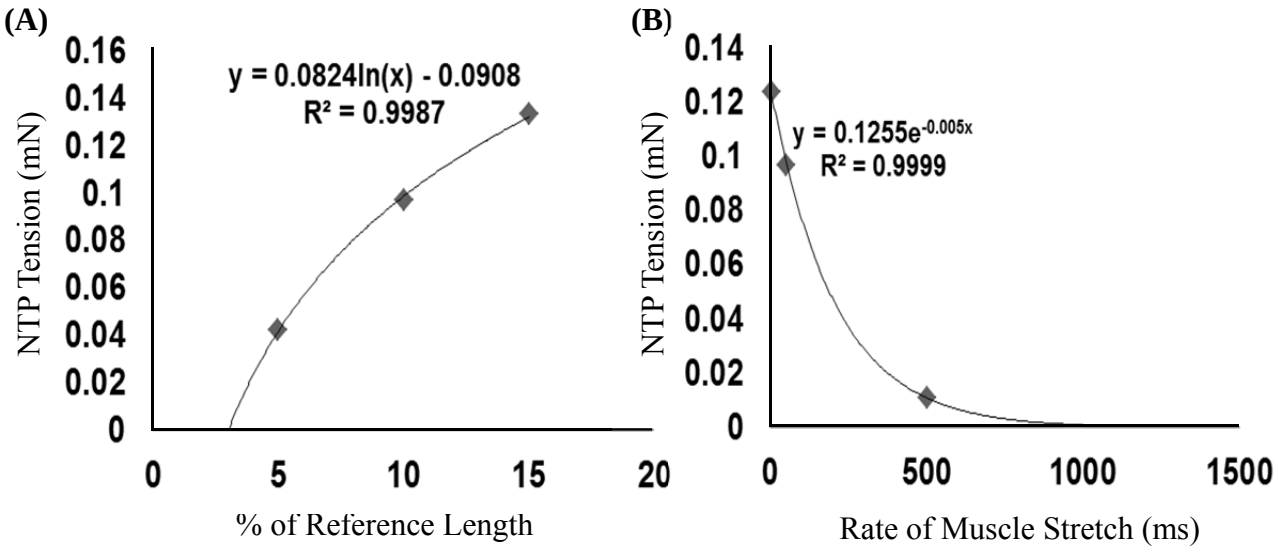

Figure 4.5 (**A**-**B**) Curve fits for NTP tension data from a previous experimental study (Poley et al., 2008). (**A**) A logarithmic curve was fit to the stretch length dependent data. (**B**) An exponential curve was fit to the stretch rate dependent data.

Minimum values for both length dependency and rate dependency were calculated based on the curve fits and applied to the sensor element of the model to set up the threshold that

triggered a contraction (Figure 4.5A-B). The minimum value of the reference length from Figure 4.5A was utilized in length dependency model simulation as the threshold for the sensor, while the sensor threshold for the rate dependency and refractory period model simulations was calculated from Figure 4.5B.

4.4. Stretch Magnitude, Rate and Refractory Period Dependency

Model simulations were performed to demonstrate the effect of QS magnitude, rate, and delay between stretches on the amplitude of the myogenic contraction. All of the stretches began at slack length where there was no preload tension. Each QS stretched the SEC_S, and consequently a QS with a greater magnitude produced a greater ΔSEC_S and greater feedback to the motor. As a result, larger amplitude QSs induced stronger myogenic contractions (Figures 4.6 & 4.7).

Tension in the VC_S is proportional to the rate at which it is stretched, so a faster stretch imposes greater tension on the SEC_S and therefore produces greater ΔSEC_S. As a result, simulation of faster QSs produced a greater ΔSEC_S, and therefore induced stronger myogenic contractions (Figures 4.8 & 4.9). Thus, the QS-induced myogenic tension produced by the model simulations was stretch magnitude and stretch rate dependent, corresponding to experimentally observed behaviors (Poley et al., 2008).

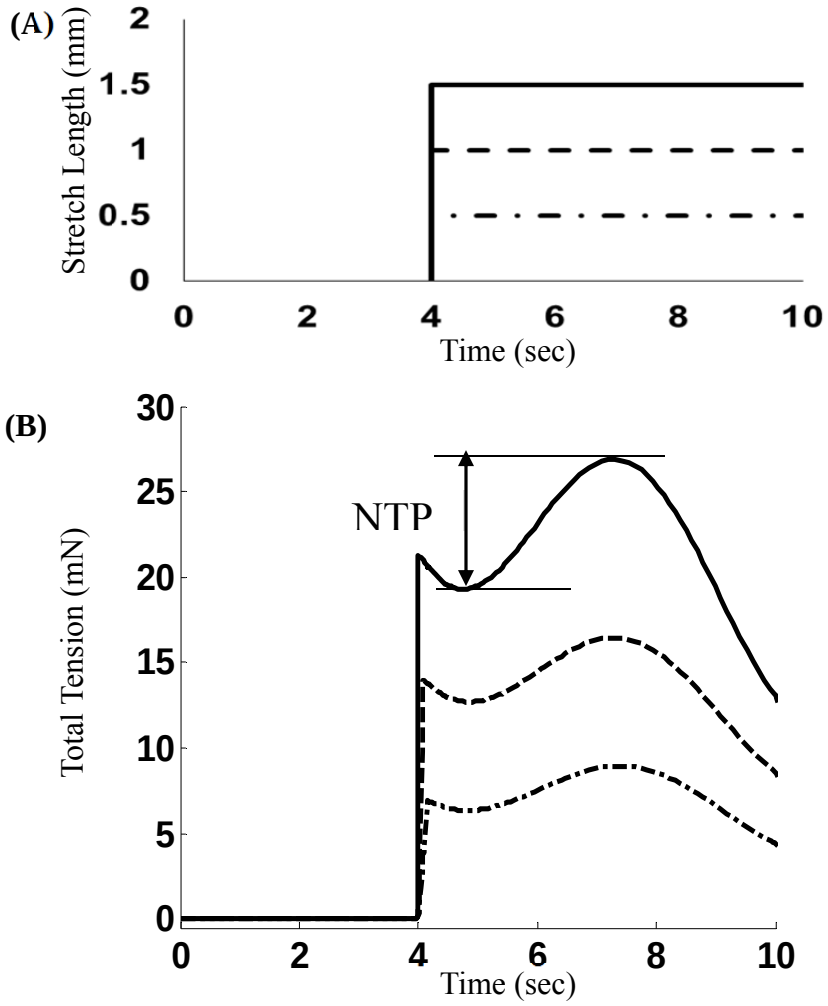

Figure 4.6 (**A**-**B**) Stretch magnitude dependency of the myogenic response (**A**) Length-time protocol in which the model was subjected to three stretches equaling to 5%, 10% and 15% of muscle reference length at stretch rate of 5ms. (**B**) Tension output of the model in correspondence to the 3 stretches. Upon QS, the sensor initiated a myogenic contraction as a single twitch of sinusoidal SRC with amplitude proportional to the length of SEC_S.

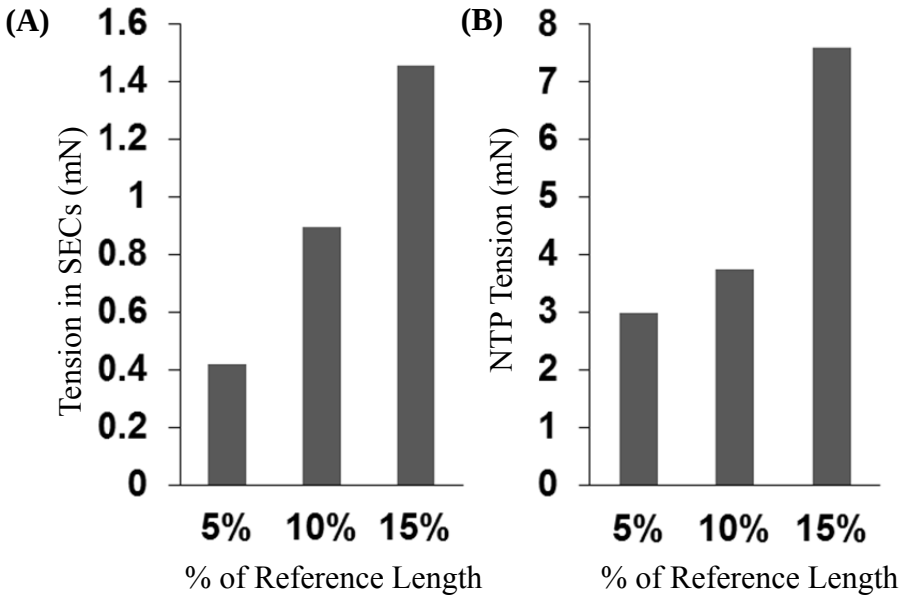

Figure 4.7 (**A**) Tension in series elastic component of the sensor (SEC_s) that triggers the motor and regulates the amplitude of the myogenic contraction. (**B**) Nadir-to-peak (NTP) tension increased with increasing stretch magnitude, as in the published experimental results (Poley et al., 2008).

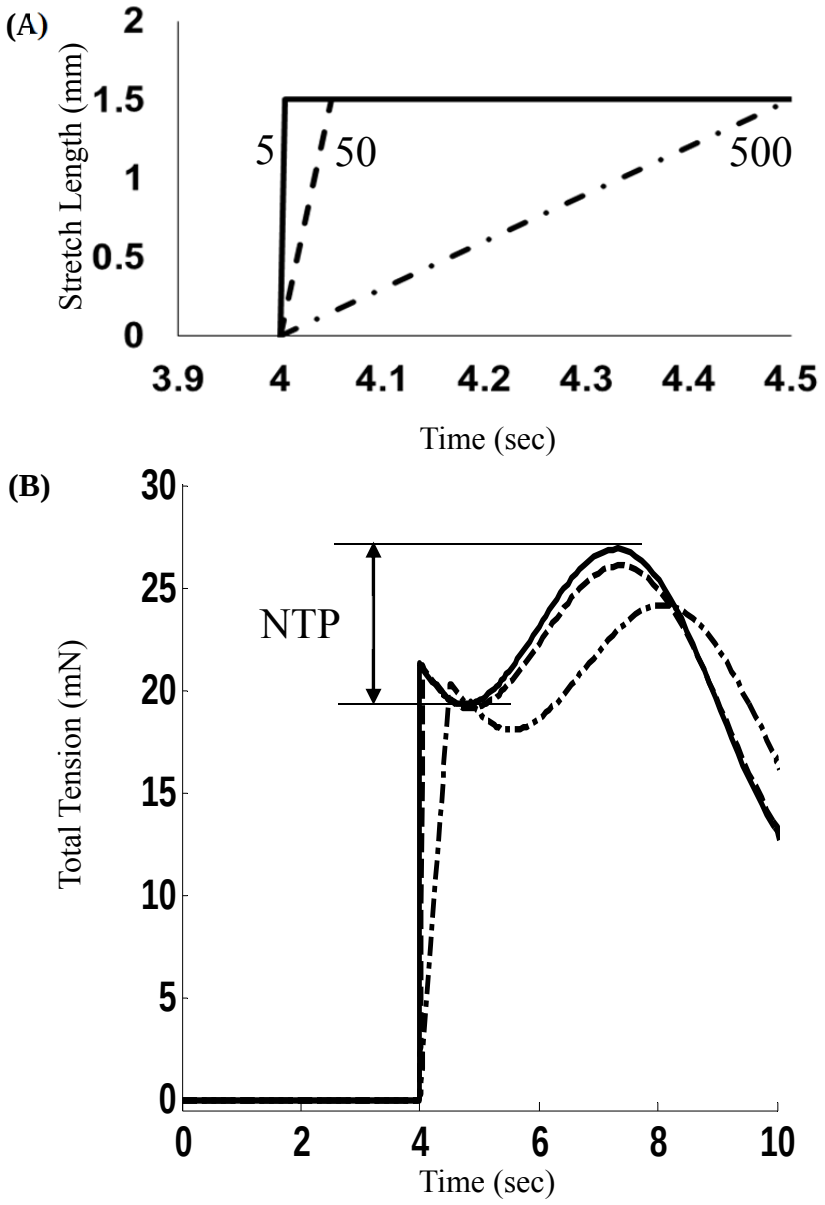

Figure 4.8 (**A**-**B**) Stretch rate dependency of the myogenic response. (**A**) Length-time protocol in which the model was subjected to stretches equaling to 15% of muscle reference length at 5ms (solid black line), 50ms (solid-dash black line) and 500ms (dash-dot line). (**B**) Tension output of the model simulations for corresponding the three QS rates.

.

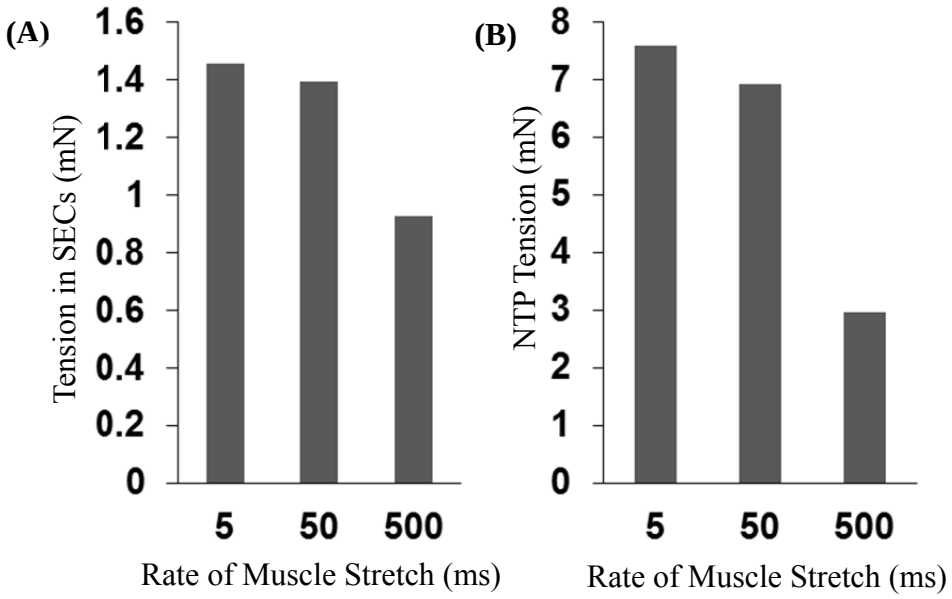

Figure 4.9 (**A**) Tension in the series elastic component of the sensor (SEC_s) that triggers the motor and increases with increasing stretch rate to induce a larger rhythmic contraction amplitude. (**B**) The myogenic contraction induced by the slower stretch (500 ms) had a smaller NTP (nadir-to-peak) tension amplitude compared to the 10-fold faster (50 ms) and 100-fold faster (5ms) stretches, corresponding to the trend observed in a published experimental study (Poley et al., 2008).

Due to the viscoelasticity of the sensor, when the tissue model was returned to its original length following a QS, a period of time was required for the SEC_S to return to its original length because it had to push the rate dependent VC_s back to its original length. When a second identical QS was imposed before the SEC_S had returned to its original length, then the ΔSEC_S for the second stretch was less than the ΔSEC_S for the first stretch. As a result, the magnitude of the myogenic response to the second QS was less than the magnitude of the response to the first QS (Figures 4.10. & 4.11).Thus, the simulation of a second QS produced a myogenic tension that was dependent on the delay time since the most recent QS, as observed in an experimental study (Poley et al., 2008).

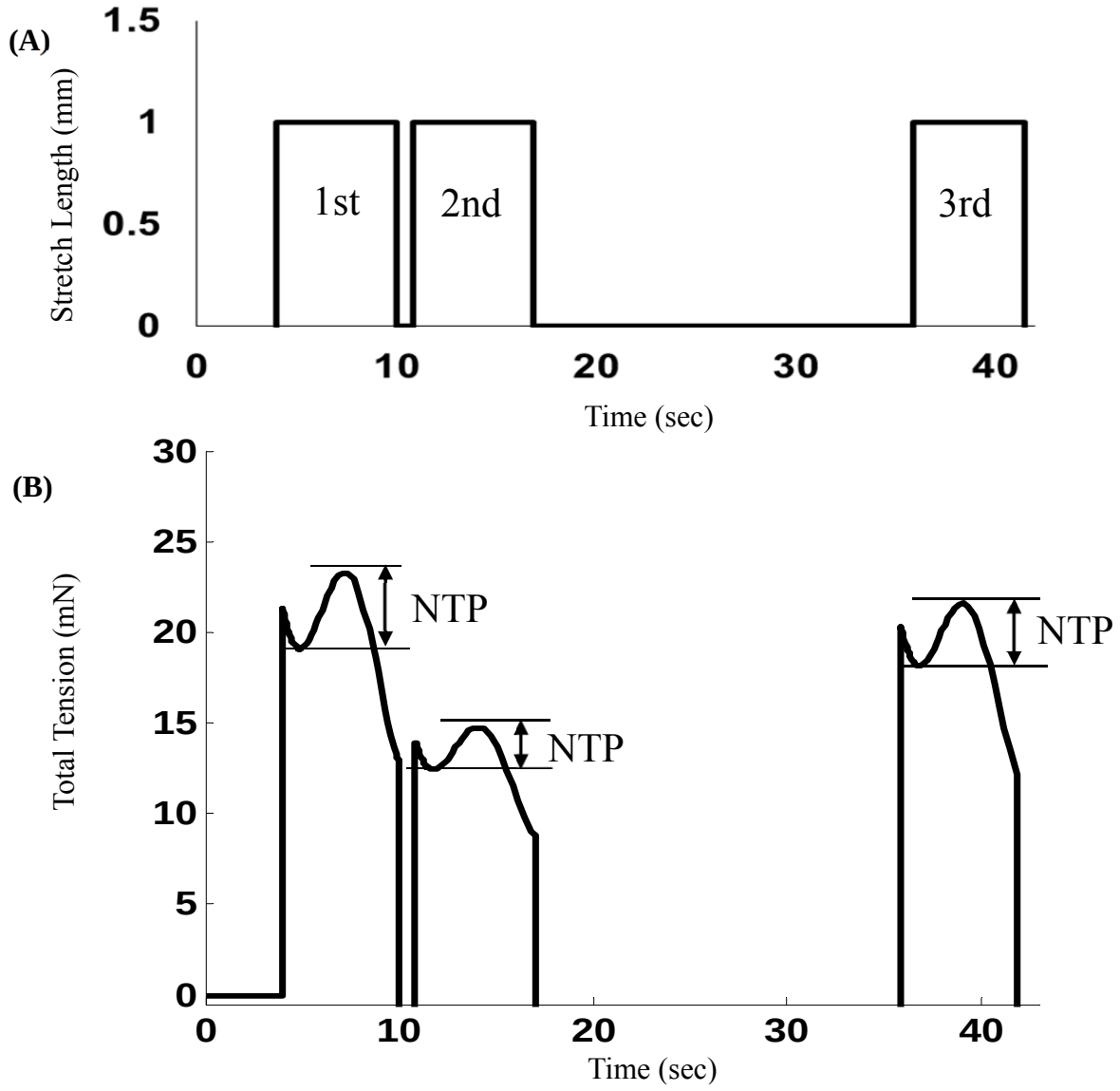

Figure 4.10 (**A-B**) Refractory period dependency of the myogenic response. (**A**) Length-time protocol for a series of three 5 ms stretches applied to the model with a shorter wait between the first and second stretches and a longer wait between the second and third stretches. (**B**) Tension output of the model corresponding to the three stretches.

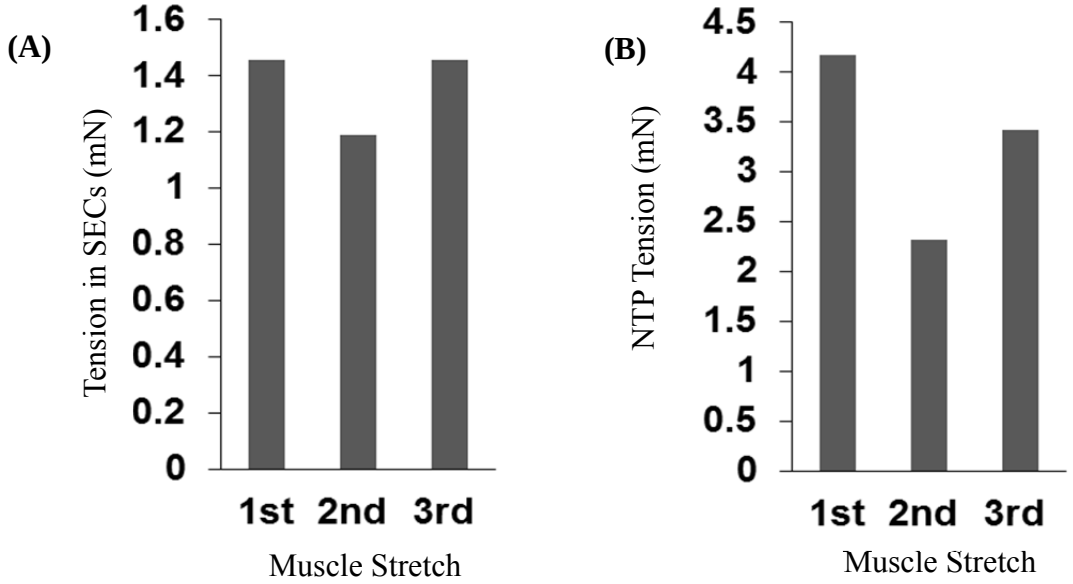

Figure 4.11 (**A**) Tension in series elastic component of the sensor (SEC_s) that triggers and regulates the motor increased with increasing delay between the stretches. (**B**) The myogenic contraction induced by the short refractory period had smaller NTP (nadir-to-peak) tension amplitude compared to the contraction following the longer refractory period.

4.5. SRC and Quick-Stretch-Induced Myogenic Response Due to the Same Mechanism

SRC was simulated to produce sinusoidal tension, and two identical QSs were imposed during SRC, one near the peak (Figure 4.12A) and one near the trough (Figure 4.12B) of the SRC cycle. These stretches triggered the mechanical sensor to activate any remaining cross-bridges by resetting the SRC cycle to begin at a trough with amplitude equal to the tension generated by the remaining cross-bridges. As a result, the nadir-to-peak (NTP) tension of the myogenic contraction was smaller when the QS was imposed at a point in the SRC cycle when tension was relatively high (Figure 4.12A). Conversely, NTP tension was greater when the QS was imposed at a point in the SRC cycle when tension was relatively low (Figure 4.12B). Furthermore, the total peak tension values for the myogenic contractions were identical because in both cases (Figure 4.12A-B) all cross-bridges responsible for SRC and QS-induced

contraction were active. These simulation results qualitatively correlate with the published experimental data in Figure 3.3. (Komari et al., 2013).

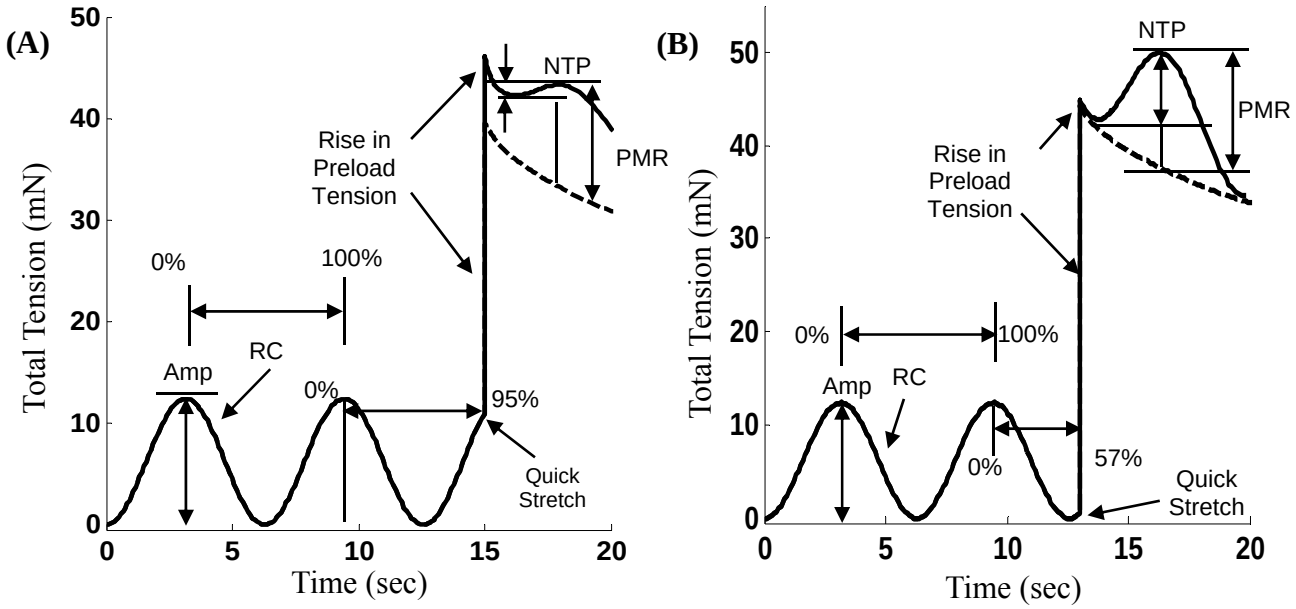

Figure 4.12 (**A-B**) Model simulations for a QS imposed at (A, 95% of the cycle) near the peak and (B, 57% of the cycle) near the trough during SRC cycle triggered the mechanical sensor to activate any remaining cross-bridges by resetting the SRC cycle to begin at a trough with an amplitude equal to the tension generated by the remaining cross-bridges. (**A**) When the QS was imposed near the peak of the SRC cycle, fewer cross-bridges were available to be activated, and therefore smaller nadir-to-peak tension was generated by the model. (**B**) When the QS was imposed near the trough of the SRC cycle, more cross-bridges were available to be activated, and therefore greater nadir-to-peak tension was generated by the model. Model results qualitatively correlate with the published experimental data (Komari et al., 2013).

4.6. Contraction Propagation Model

This section presents a model to test the hypothesis that rapid stretching of one DSM cell initiates a myogenic contraction to propagate the contraction throughout a bundle of cells. A simple double model was developed by placing two of the models from Figure 4.1. in series as illustrated in Figure 4.13. The cell on the right side was the initially activated cell; therefore, it did not require sensor feedback. The model was stretched from slack length to 200% slack length to approximate the optimum length for muscle contraction. The model was held isometrically at this length to permit complete stress relaxation. At this point, the Kelvin and APS portions of the model exhibited equal preload tension in both the left and right sides of the model. The motor on the right side of the double model was activated maximally to stretch the left side of the model. The stretch rate was calculated from Hill's equation (Hill, 1938) and utilizing Van Mastrigt's (R. van Mastrigt, 1979) constants for Hill's equation for bladder smooth muscle. These equations and parameters are presented in Appendix A. The contributions of the preload tension on the right side of the model were not considered when determining the stretch of the left side of the model. The motor in the right cell was conservatively assumed to produce all the force to stretch the left cell.

Active shortening of the cell on the right stretched the cell on the left, and therefore stretched the sensor segment of left cell. The degree of sensor stretch depended on the rate of shortening of the right cell which was calculated based on the Hill's equation (Hill, 1938) as shown in Figure 4.14A (solid line). Contraction of the right cell was sufficient to trigger the sensor and produce a myogenic contraction in the left cell (Figure 4.15A-B).

Simulations were performed in order to predict the number of in-series cells that could be triggered by contraction of the right cell. To accomplish this, the force-velocity relationship for the motor in the right side of the model was divided by the number of model units or cells on the left side. Stretching one cell with half the velocity produces the same stretch in each cell as stretching two cells with the full velocity. Likewise, stretching one cell with 1/24 the velocity would be equivalent to stretching 24 cells with the full velocity. This methodology was simpler to implement than implementing the equations for several cells in-series. Simulation results indicate that one activated cell can trigger the sensor element and cause a myogenic contraction in maximum 24 cells in the in-series configuration. The sensor stretch value for the 25^{th} cell in series was lower than the sensor threshold value (Figure 4.15A) that was calculated from the length dependency data in Figure 4.5A.

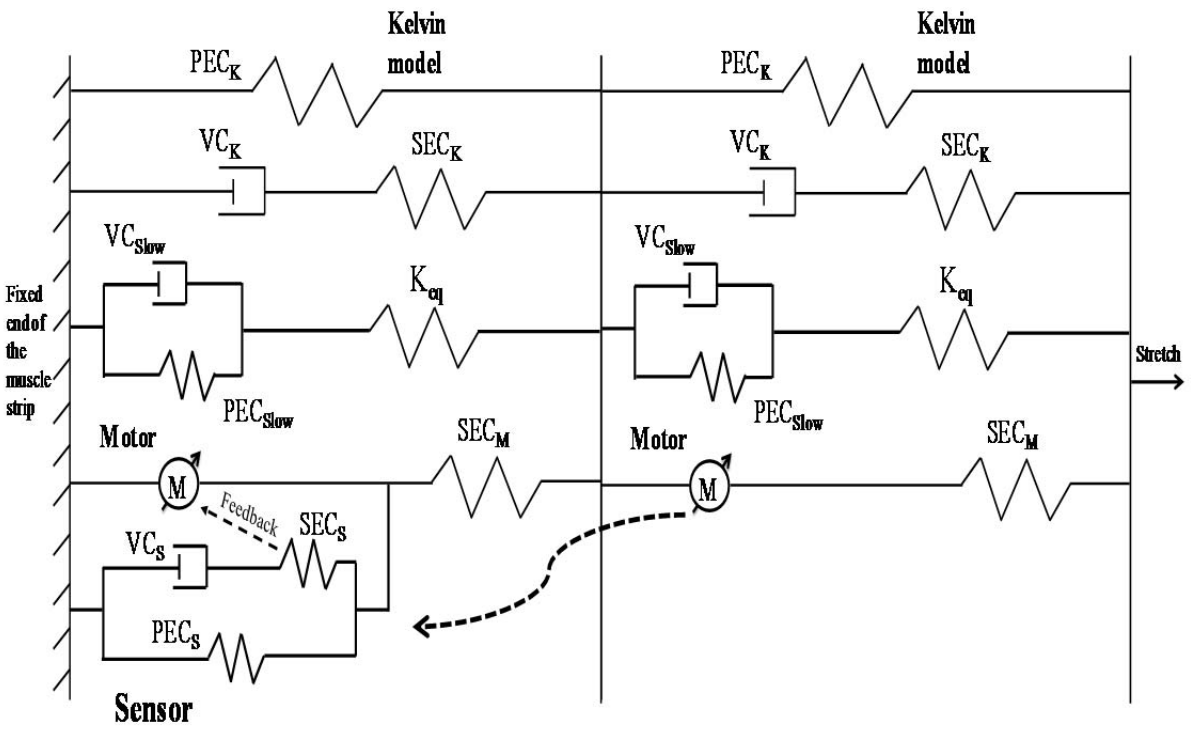

Figure 4.13 Two model units in an in-series configuration. The motor in the right cell is activated, and shortens to stretch the left cell, which potentially triggers the sensor to cause a myogenic contraction in the left cell to propagate the contraction throughout the model.

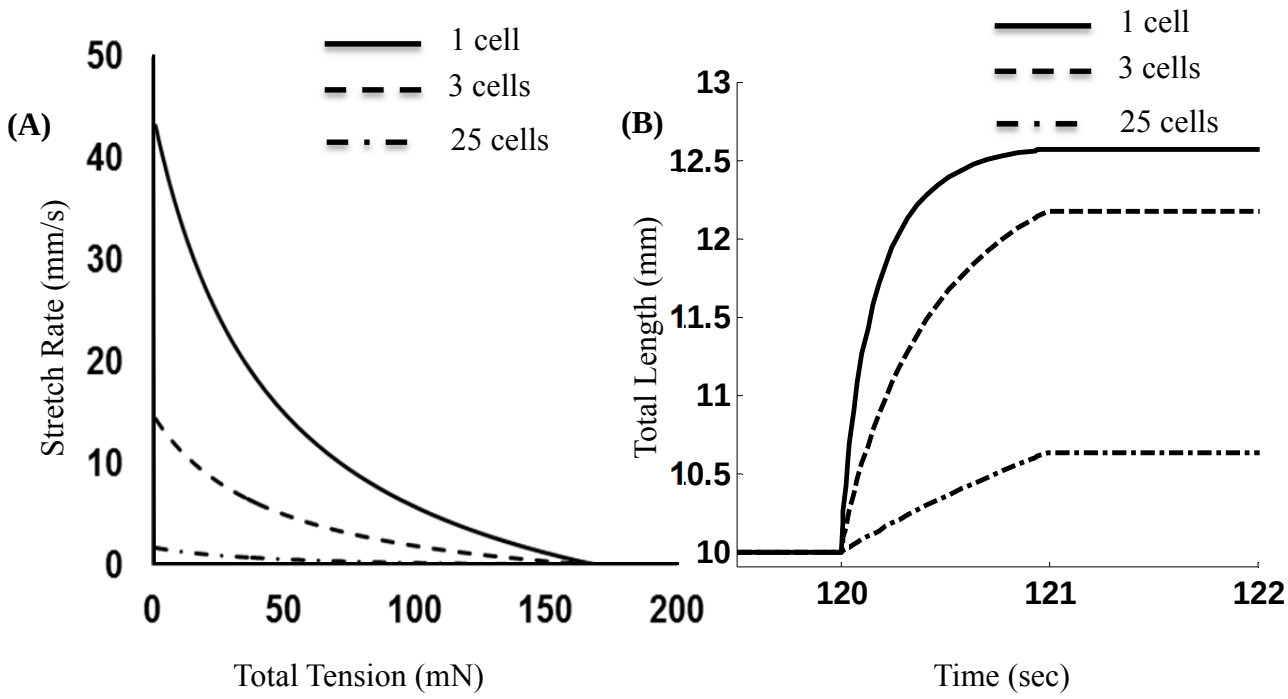

Figure 4.14 (A-B) Simulation results for one cell (solid line), 3 cells (dash line) and 25 cells (dash-dot line) in-series with one activated cell. (**A**) Force velocity curve for the activated cell. (**B**) Total length of the model.

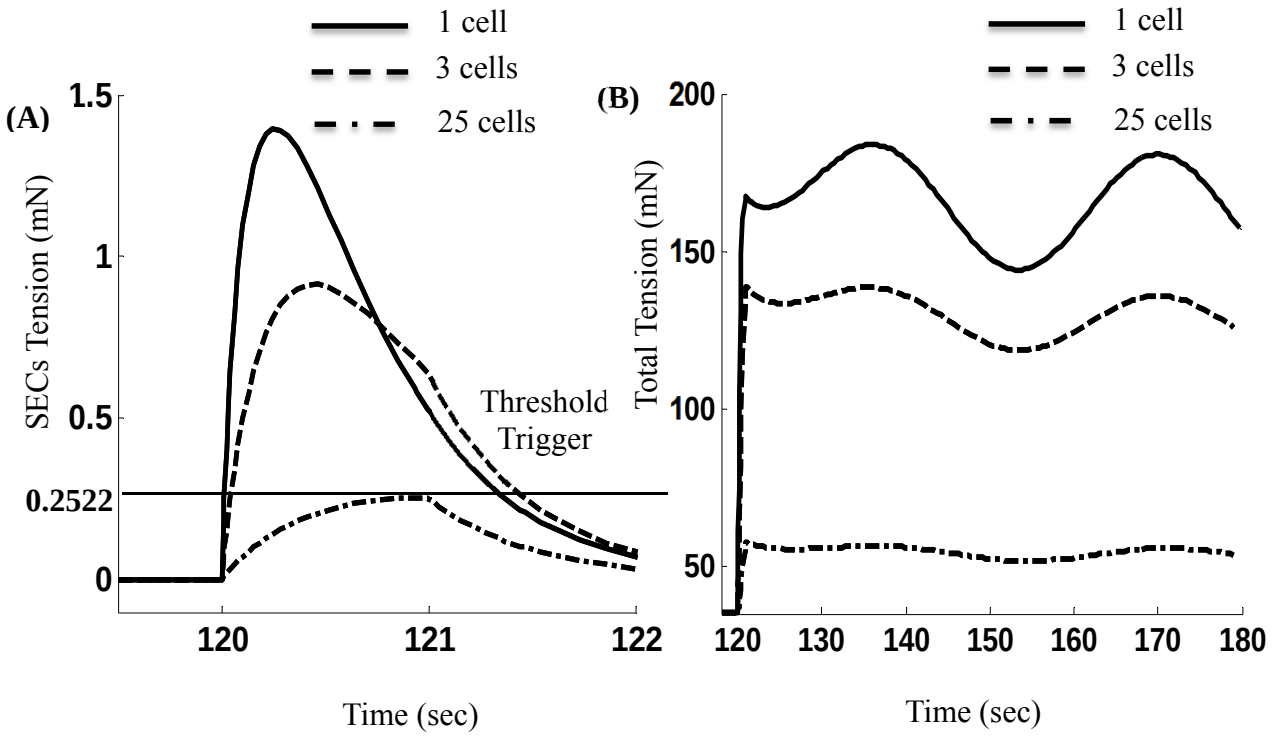

Figure 4.15 (**A-B**) Simulation results for one cell (solid line), 3 cells (dash line) and 25 cells (dash-dot line) in-series with one activated cell. (**A**) Tension output (mN) of sensor (**B**) Total tension output (mN) of the model. Contraction of the right cell triggered SRC equal to approximately 20% of the maximum tension produced by the motor in the right cell for a single in-series cell (solid line) and approximately 10% of the maximum tension in 3 in-series cells (dashed line).

CHAPTER 5 A MODEL FOR THE ROLES OF ACTIN AND MYOSIN IN ADJUSTABLE PRELOAD TENSION AND ACUTE LENGTH ADAPTATION

5.1. Introduction

In striated muscle the strength of active tension is determined by the number of attached cross-bridges additively generating positive force that is transmitted through intracellular and extracellular force-bearing structures in series with cross-bridges (McMahon, 1984). The macroscopic mechanical length-tension measurement accurately reflects the degree of molecular cross-bridge overlap within the fundamental muscle unit, the sarcomere (Huxley, 1995). Active length-tension curves generated by striated muscles display an ascending and descending limb arranged around a central and narrow length range for optimal contraction (L_o). For each striated muscle type, the active length-tension curve is acutely static, adapting only slowly after perturbations leading to alterations in gene transcription and translation that alter specific sarcomeric proteins (Willis, Schisler, Portbury, & Patterson, 2009). Geometry and structures linking cross-bridges to cytoskeletal and extracellular proteins determine the active tension generated by arterial smooth muscle. Although the sarcomere is not well defined in smooth compared with striated muscles, early mechanical studies (Somlyo & Somlyo, 1968; Speden, 1960) revealed a somewhat parabolic active length tension curves displaying ascending and descending limbs analogous to striated muscle. Biochemical studies on smooth muscle motor proteins, also provide support for the notion that smooth muscle contraction involves sliding filaments driven by actomyosin cross-bridge cycling (Somlyo & Somlyo, 1968; Speden, 1960).

An additional complexity is that actin-myosin cross-links other than cross-bridges may participate in bearing some of the load during active tension maintenance (Marston, Pinter, & Bennett, 1992; Rasmussen, Takuwa, & Park, 1987; Szymanski, 2004). However, several critical differences exist between smooth and striated muscles, including but not limited to, a longer working length range and a broader L_o length range (A. R. Gordon & Siegman, 1971; Speden, 1960; B Uvelius, 1976). Also, the likelihood that thick filaments in smooth muscles are arranged in a side polar rather than bipolar nature (Craig & Megerman, 1977), and the finding that changes in muscle length may lead to specific changes in the distribution of the components of the contractile apparatus within individual cells (Cooke & Fay, 1972) are other critical differences. In addition, extensive investigations (Bai et al., 2004; Naghshin, Wang, Pare, & Seow, 2003) over the last two decades on smooth muscles have revealed that smooth muscle length-tension curves may undergo acute length adaptation. That is, rather than being static, as in striated muscle, the active length-tension curve in certain smooth muscles can shift along the length axis due to accommodation of the muscle at different lengths (Bai et al., 2004).

Several models have gained some traction indicating that length adaptation involves contractile unit and cytoskeletal rearrangements and contractile apparatus reshaping (Ford, 2005; Gunst, Tang, & Opazo Saez, 2003; Herrera et al., 2005). However, the precise mechanism for length adaptation remains to be fully elucidated. One objective of the present study was to create a simple conceptual model that combines multiple previous hypotheses such as parallel-to-series transitioning of contractile units, additional of contractile filaments in series and cross-linked cross-bridges (latch-bridges), while incorporating the role of SRC in the regulation of dynamic length adaptation in bladder smooth muscle.

In smooth muscle, force has both active and preload components. The preload component is the portion of the total force remaining when cross bridges directly responsible for force development are not rapidly cycling to produce active force. In smooth and cardiac muscles, preload force contributes significantly to the total force produced at the optimum length for muscle contraction (Herlihy & Murphy, 1973; B Uvelius, 1976). Bladder smooth muscle cells can undergo a sevenfold length change during filling (B Uvelius, 1976) and must be prepared to contract efficiently with appropriate voiding characteristics throughout this particular range. During the filling phase the bladder prepares and positions its actomyosin cross-bridges to contract efficiently over this broad length range. Uvelius (B Uvelius, 1976, 2001) and Longhurst (Longhurst, Kang, Wein, & Levin, 1990) showed that detrusor smooth muscle (DSM) produces a nonlinear preload length-tension ($L\text{-}T_p$) curve with greater tension at longer lengths (A. R. Gordon & Siegman, 1971; Herlihy & Murphy, 1973; Siegman et al., 1976). The preload and active L-T relationships for skeletal muscle are considered to be static, with a single preload tension value and a single maximum active tension value for each muscle length (A. M. Gordon et al., 1966). During this time frame, the $L\text{-}T_p$ relationship in smooth muscle similar to $L\text{-}T_a$ was considered to be static. Beginning in the 1990s, several studies challenged the static model by showing that airway and vascular smooth muscles produced different tension during muscle unloading vs. loading and therefore, can adapt to changes in muscle length over time, producing shifts in $L\text{-}T_p$ (Naghshin et al., 2003; Wang et al., 2001) curves (reviewed in (Bai et al., 2004; Bossé et al., 2008; Ford, 2005)). One study showed that the preload stiffness (preload tension) of detrusor smooth muscle can be regained by contraction, and maintained, unless the tissue is stretched (Speich et al., 2007). Furthermore, in practice, smooth muscle tissues are normally preconditioned by cyclic stretching to obtain consistent measurements (Fung, 1993).

Preconditioning is characterized by reductions toward a steady state in stiffness with each subsequent stretching cycle and has been identified in DSM (Minekus & van Mastrigt, 2001). Thus, preload tension is dynamic and can be adapted to different lengths as a function of activation and stretch (Speich et al., 2005). Hence, bladder smooth muscle exhibits activation-history-dependent and muscle-length-dependent adjustable preload tension which has been attributed to actin-myosin cross-links (Speich et al., 2007).

Additionally, bladder smooth muscle can generate low-amplitude spontaneous rhythmic contractile activity (Komari et al., 2013) which is observed to be elevated in patients with overactive bladder (Kinder & Mundy, 1987) and has been shown to regulate subsequent preload tension (A. M. Almasri, Ratz, Bhatia, Klausner, & Speich, 2010a). Bladder muscle can also generate a strong phasic contraction which is responsible for emptying the bladder (Bossé et al., 2008). The main objective of this study was to develop a model with a network of actin and myosin that produces the coupled mechanical behaviors of adjustable preload tension, spontaneous rhythmic contraction and length adaptation exhibited by bladder muscle.

5.2. Conceptual Model

A simple spring-dashpot conceptual mechanical model was developed to simulate some mechanical characteristics of DSM. Two simple mechanical models of smooth muscle are the Kelvin (standard linear) model and the Voigt model. Each of these viscoelastic models contains three elements:

1) A viscoelastic component (VC) that generates active force when the actomyosin cross bridges are attached and cycling (termed a contractile component) which acts as a

dashpot when actomyosin cross bridges do not actively cycle through a power stroke to cause muscle contraction (i.e., when DSM is maintained under preload conditions).

2) A series elastic component (SEC) in series with the contractile component.
3) A parallel elastic component (PEC) in parallel with the contractile component.

In the Kelvin configuration, the nonlinear elastic component (PEC) is in parallel with both series elastic component and viscoelastic component(s) (SEC and VC_K) (Maxwell configuration) (Fung, 1993; R A Murphy, 2011), whereas, in the Voigt configuration (R A Murphy, 2011), the PEC is in parallel only with the VC (Speich et al., 2006).

As discussed in Chapter 1, smooth muscle provides two types of tension, active and preload. The active force is due to the interaction between actin-myosin cross-bridges. The "sliding" action of actin and myosin filaments leads to the shortening of cells and generates force. The level of active tension produced is dependent on the number of active cross-bridges producing positive work, which is dependent on muscle length. Figure 5.1 describes the schematic example of the relationship between actin and myosin overlaps and the smooth muscle active tension parabolic curve.

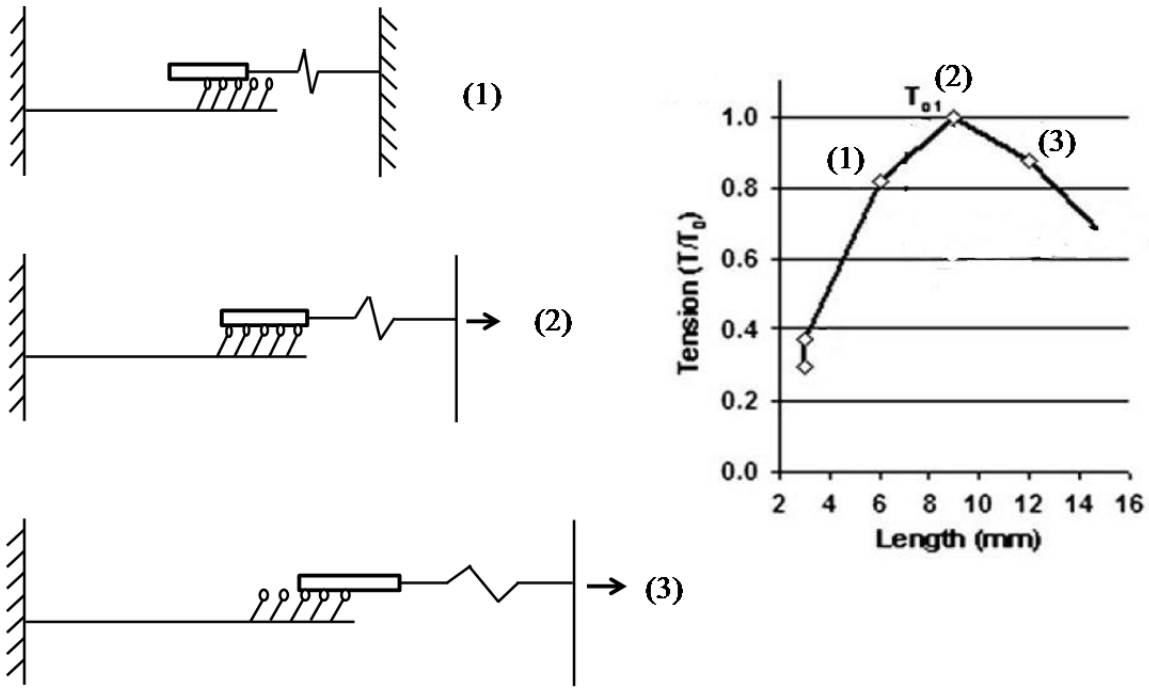

Figure 5.1 An example of a length-active tension curve explained by a simple actin-myosin overlap model (A. M. Almasri, Ratz, & Speich, 2010a).

The model presented in this chapter concentrated on the process of positioning the actin and myosin to regulate the degree of overlap and the strength of the muscle contraction. The model also focuses on the effect of changing the preload stiffness to affect actin myosin overlap and the effects of changing the stiffness on shifting the DSM active and preload length-tension curves. The model focuses on quasi steady state muscle lengths corresponding to very slow bladder filling, so the model was developed to be stress-relaxation and time independent. These simulations were focused on the creation of qualitative dynamic active and preload force-length relationships for the DSM, rather than reproducing exact muscle behavior and experimental data.

A conceptual mechanical model (Figure 5.2) was developed with four main segments:

1) A Kelvin model (Figure 5.2, green) with a viscous component (dashpot, VC_K) and in-series and in-parallel elastic components (springs, SEC_K & PEC_K) was used to represent stretch-dependent DSM preload tension.
2) A population of actin-myosin cross-bridges was modeled to produce SRC (Figure 5.2, purple) transmitted via a series elastic components (XEC).
3) Series and parallel elastic components (XEC, SEC_A, PEC_{CL}) (Figure 5.2, blue) were modeled as springs that produce the preload tension. These XEC elements can be repositioned by SRC and cross-linked by actin-myosin attachments (dashed lines) to provide adjustable stiffness via bypassing one or more of the XEC elements.
4) Another population of actin-myosin cross-bridges (Figure 5.2, red) was modeled to produce the active tension that produces voiding contractions. The overlap of the actin-myosin is regulated by the number of XEC elements that are bypassed.

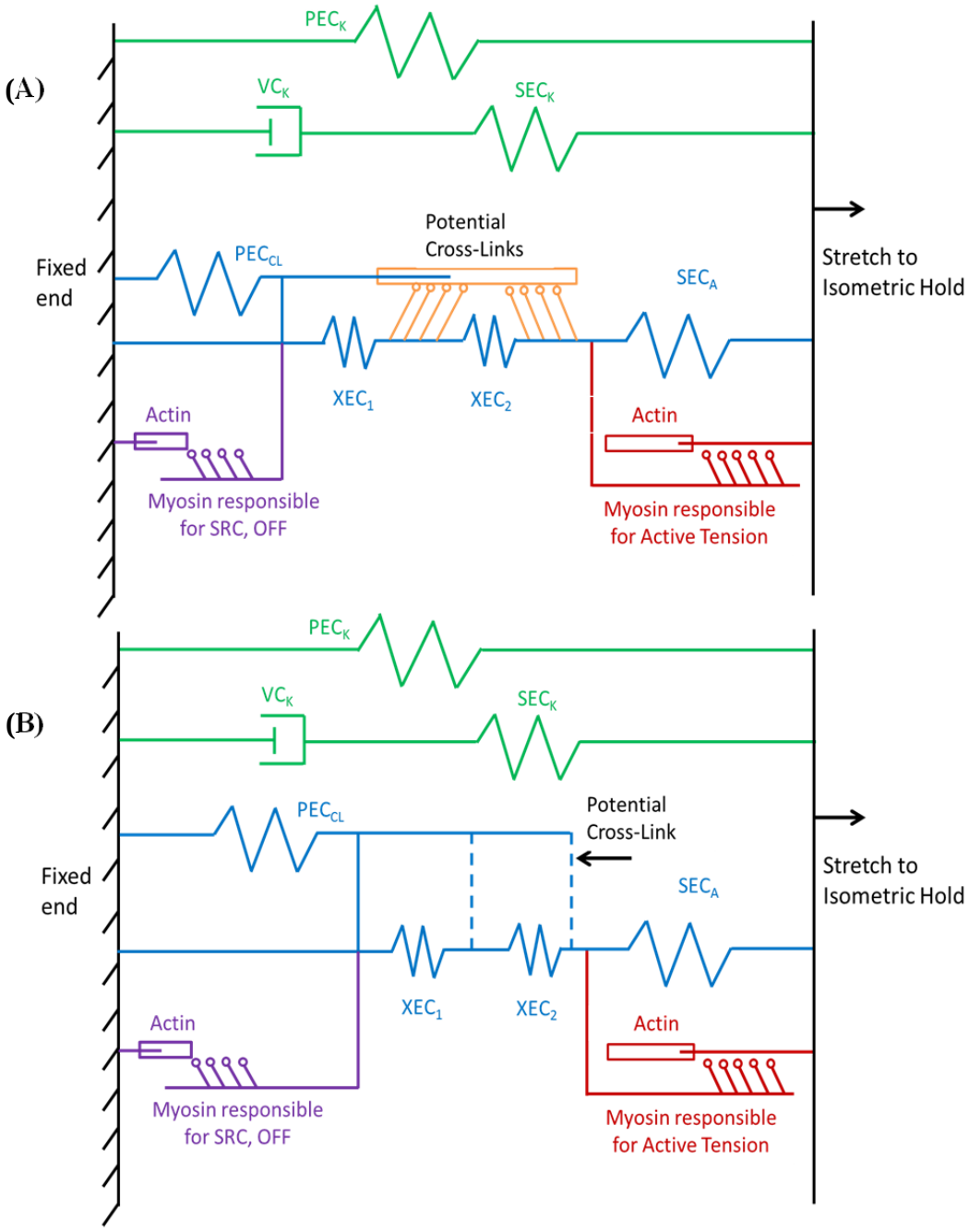

Figure 5.2 Conceptual mechanical model. **(A)** Conceptual model including actin-myosin filaments as potential cross-links**. (B)** Conceptual model including dash lines to show the exact placement of potential cross-links.

The model was simulated using a typical experimental step-length protocol. Figure (5.3A-D) shows the muscle behavior in multiple steps. For the first step, the muscle was relaxed at slack length and no stretch was applied to the model, so the springs were not stretched and the preload tension in the model was zero (Figure 5.3A). As the muscle was stretched in multiple steps (Figure 5.3B-D) the springs exhibited greater tension due to the increased length. This resulted in changes in the number of myosin heads that could reach the thin actin filament in the active tension portion of the model. During the first steps, the overlap increased (ascending length-tension relationship) and during the later steps the overlap decreased (descending length-tension relationship). Thus, the degree of actin-myosin overlap created the active force-length parabolic curve as the preload tension in the springs increased (Figure 5.3 B-D). In a second simulation, the model tissue was returned to the original length and SRC was turned activated. Due to the SRC tension, the cross-linking series elastic components were pulled to the left. At this point, the PEC_{CL} component was cross-linked to bypass the XEC_1 element (Figure 5.4 E) and SRC was deactivated. The preload tension at the original slack length was no longer zero because bypassing the $fXEC_1$ element forced the PEC_{CL}, the XEC_2 element, and the SEC_A element to lengthen. From the original slack length the step-stretch protocol was reapplied to the model. The preload tension in the parallel elastic component was increased, and the preload length-tension curve was shifted to the left (Figure 5.4 G). Additionally, manipulation of preload force relocated the position of actin and myosin filaments and the degree of overlap in the active tension component, shifting the length-active tension curve to the left (Figure 5.4 G). The simulation results were consistent with the experimental studies (Bossé et al., 2008) which show a shift in the active and preload length-tension curves, and the sliding filament theory which predicts that the active length-tension curve is due to the degree of actin-myosin overlap.

(A)

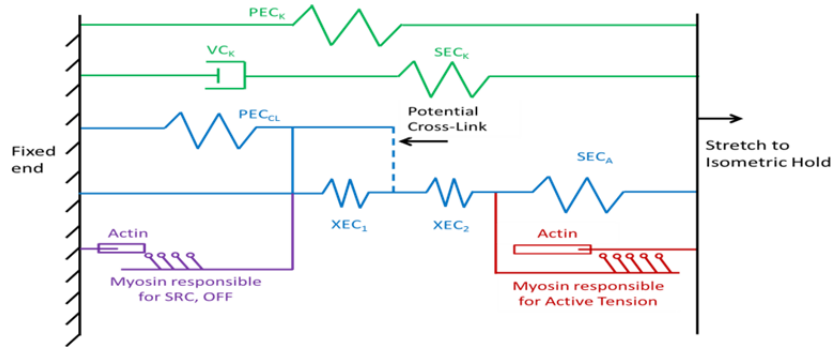
PEC_K
VC_K
SEC_K
PEC_CL
Potential Cross-Link
Fixed end
Stretch to Isometric Hold
SEC_A
XEC_1
XEC_2
Actin
Myosin responsible for SRC, OFF
Actin
Myosin responsible for Active Tension

(B)

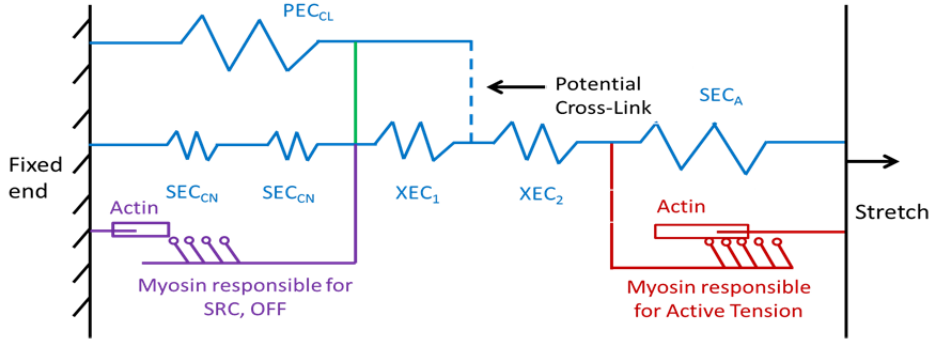
PEC_CL
Potential Cross-Link
SEC_A
Fixed end
SEC_CN
SEC_CN
XEC_1
XEC_2
Actin
Actin
Stretch
Myosin responsible for SRC, OFF
Myosin responsible for Active Tension

(C)

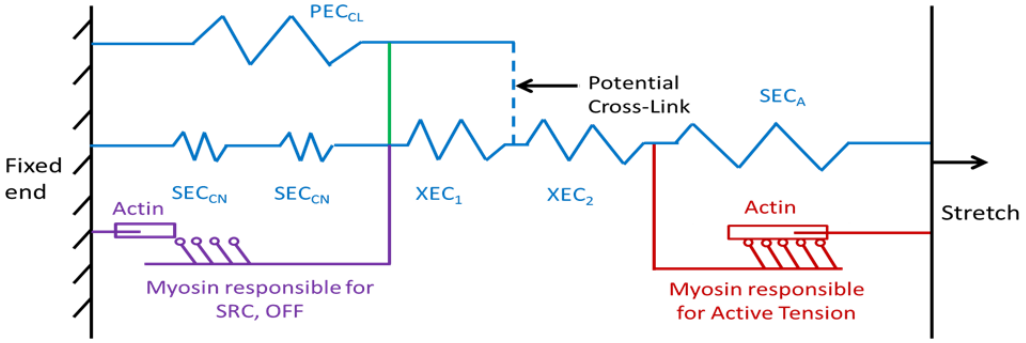
PEC_CL
Potential Cross-Link
SEC_A
Fixed end
SEC_CN
SEC_CN
XEC_1
XEC_2
Actin
Actin
Stretch
Myosin responsible for SRC, OFF
Myosin responsible for Active Tension

(D)

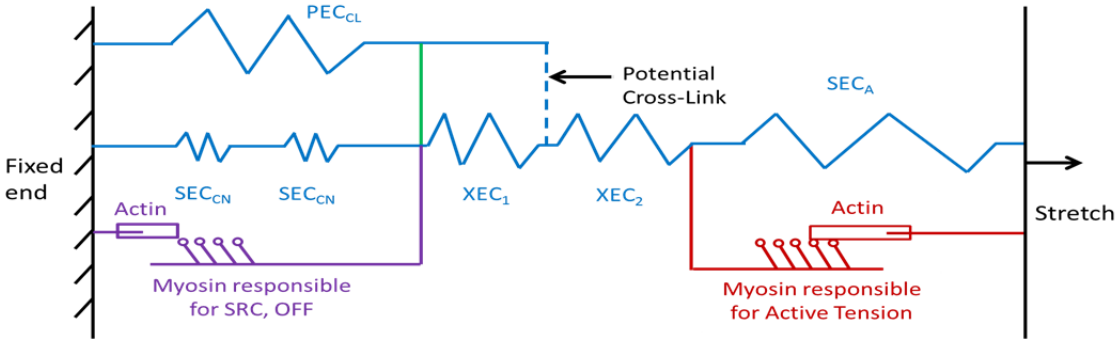
PEC_CL
Potential Cross-Link
SEC_A
Fixed end
SEC_CN
SEC_CN
XEC_1
XEC_2
Actin
Actin
Stretch
Myosin responsible for SRC, OFF
Myosin responsible for Active Tension

(G)

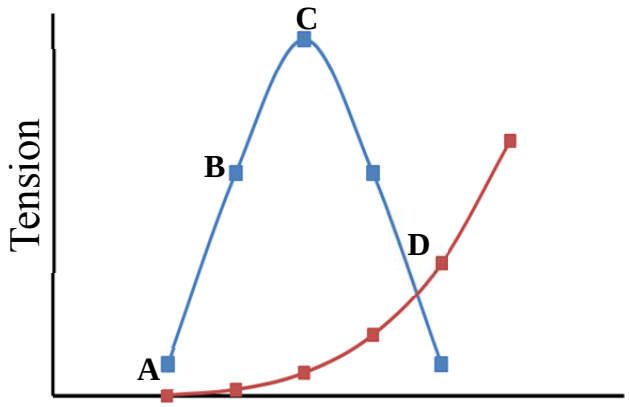
C
B
D
A
Tension
Muscle Length

Figure 5.3 (A-D & G) Conceptual model with multiple length steps. (**A**) The model is not stretched, so preload tension is zero. If the motor is on, active tension equals zero (no overlap). (**B-D**) The model is stretched to different three lengths, and the theoretical output (**G**) is a polynomial curve for active tension (overlap increases and then decreases) and an ascending curve for preload tension.

(B)

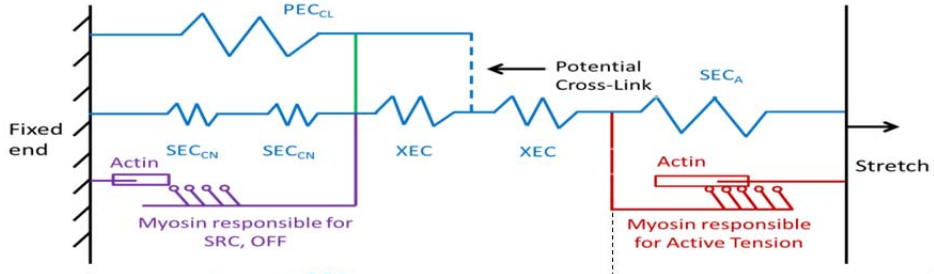
PEC_CL
Potential Cross-Link
SEC_A
Fixed end
SEC_CN
SEC_CN
XEC
XEC
Actin
Actin
Stretch
Myosin responsible for SRC, OFF
Myosin responsible for Active Tension

(C)

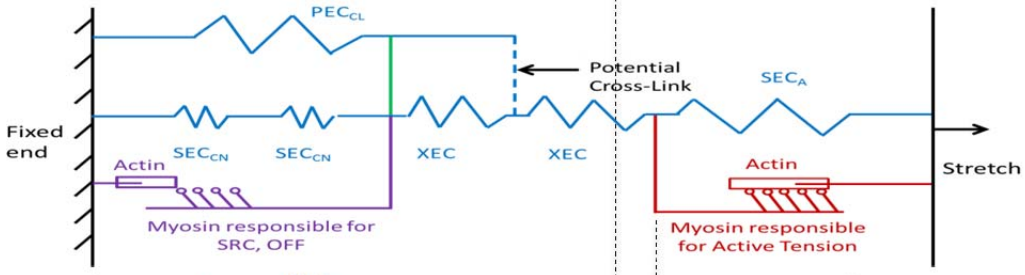
PEC_CL
Potential Cross-Link
SEC_A
Fixed end
SEC_CN
SEC_CN
XEC
XEC
Actin
Actin
Stretch
Myosin responsible for SRC, OFF
Myosin responsible for Active Tension

(E)

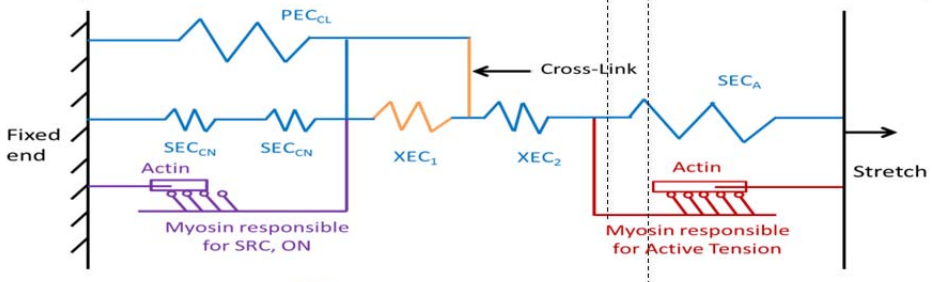
PEC_CL
Cross-Link
SEC_A
Fixed end
SEC_CN
SEC_CN
XEC_1
XEC_2
Actin
Actin
Stretch
Myosin responsible for SRC, ON
Myosin responsible for Active Tension

(F)

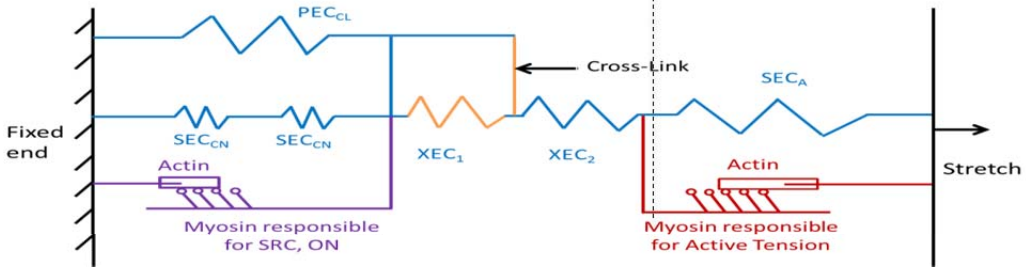
PEC_CL
Cross-Link
SEC_A
Fixed end
SEC_CN
SEC_CN
XEC_1
XEC_2
Actin
Actin
Stretch
Myosin responsible for SRC, ON
Myosin responsible for Active Tension

(G)

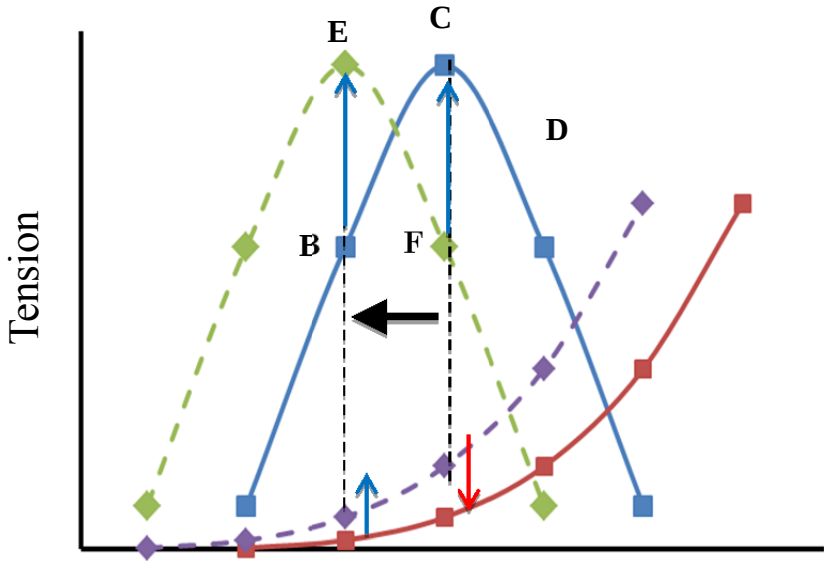
E
C
D
B
F
Tension
Muscle Length

Figure 5.4 Conceptual model without XEC_1 bypassed (**B-C** same as in Figure 5.3B-C) and with XEC_1 bypassed (**E-F**) and the resulting preload and active length-tension curves (**G**).

Relatively compliant series elastic components (SEC_{CN}) (Figure 5.3) were modeled as springs which play a connection role and were modeled contribute negligible force to the system. In future studies the SEC_{CN} elements could be used to study the switching of the XEC elements from series to parallel configurations.

The model was simulated using MATLAB Simulink. The equations used in the simulation are provided in the Appendix B and were solved using the ode45 solver in Simulink 6.0. The parameters are listed in Table B-1 in Appendix B. All of the model elements are nonlinear, including PEC_k, which was assumed to model collagen and elastin resulting in the classic nonlinear preload length-tension curve for smooth muscle.

5.3. Linear Ascending Stretch Protocol

A simple linear ascending stretch protocol (Figure 5.5) was applied to the model. The model produced both a nonlinear length-preload tension curve and polynomial length-active force curve as shown in Figures 512. The model was simulated three times, first low APS, second with XEC_1 bypassed to produce medium APS and third with both XEC_1 and XEC_2 bypassed to produce high APS. The results in Figure 5.66 show the expected dynamic length-tension relationships with both the preload and active length-tension curves shifting to the left as APS increased.

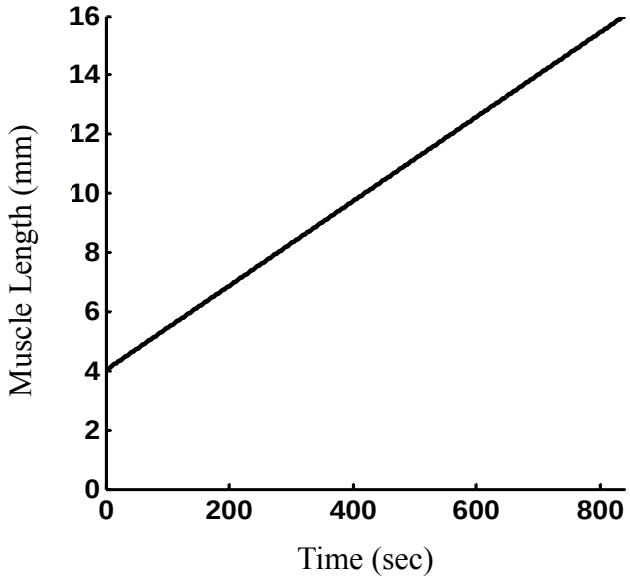

Figure 5.5 Linear stretch simulation protocol.

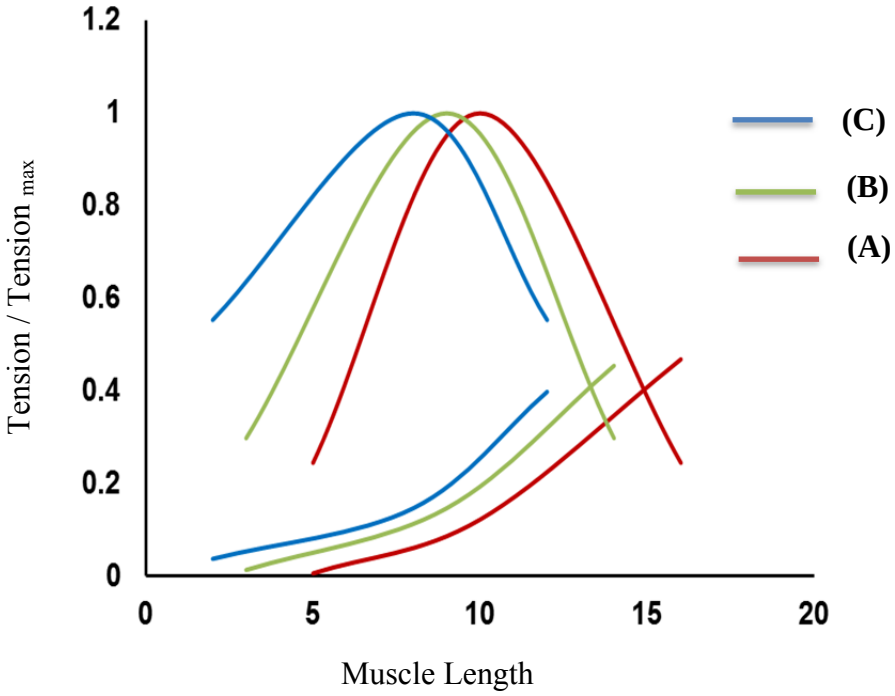

Figure 5.6 Model configurations with low APS (**A**), XEC_1 bypassed to produce medium APS (**B**), and both XEC_1 and XEC_2 bypassed to produce high APS (**C**). Simulation results show that both the preload and active length-tension curves shift to the left as APS increased.

5.4. Step- Stretch Protocol Simulations with Low, Medium, and High APS

To compare model output with experimental results, the model is objected to step-stretch protocol while the active tension producing cross-bridges were turned on and off during and isometric hold between following each stretch. The step-stretch protocol is shown in Figure 5.7. The model simulation results of total tension output are shown in Figures 5.8-5.10). The solid line indicates the preload tension and dash lines indicate the active tension that builds upon the preload tension to yield the total force. For the low APS simulation, the XEC_1 and XEC_2 are in series with the PEC_{CL} and SEC_A in Figure 5.2B. For the medium APS simulation, a crosslink bypasses XEC_1, and the XEC_2 is in series with the PEC_{CL} and SEC_A in Figure 5.2B. For the high APS simulation, the XEC_1 and XEC_2 are bypassed with a crosslink and the PEC_{CL} and SEC_A are in series in Figure 5.2B. The simulation output for the three cases is shown in Figure 5.11. Increasing APS shifts both the active and preload length-tension curves to the left.

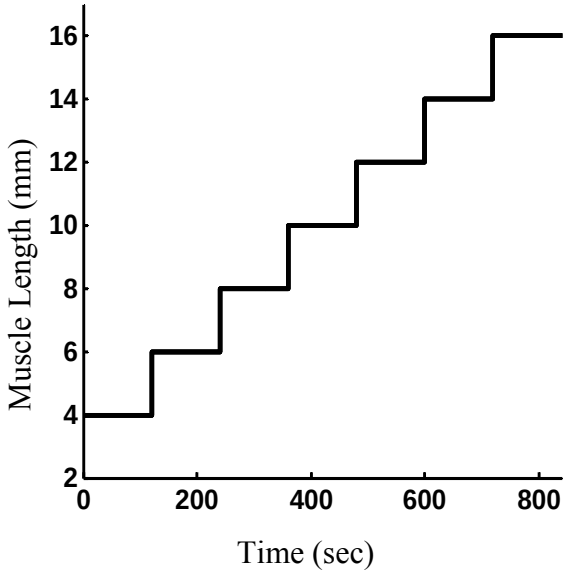

Figure 5.7 Step-stretch simulation protocol with a 120 second isometric hold at each step. The active tension producing crossbridges were activated and deactivated during each hold.

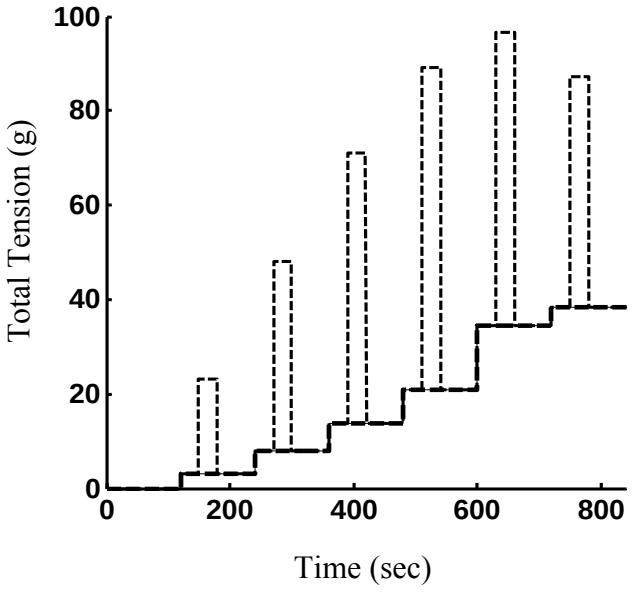

Figure 5.8 Total tension-time curve for the low APS simulation of the step-stretch protocol. The cross-bridges were activated for 30 seconds during each isometric hold. Total tension is the sum of the preload (solid line) and active tension (dashed lines).

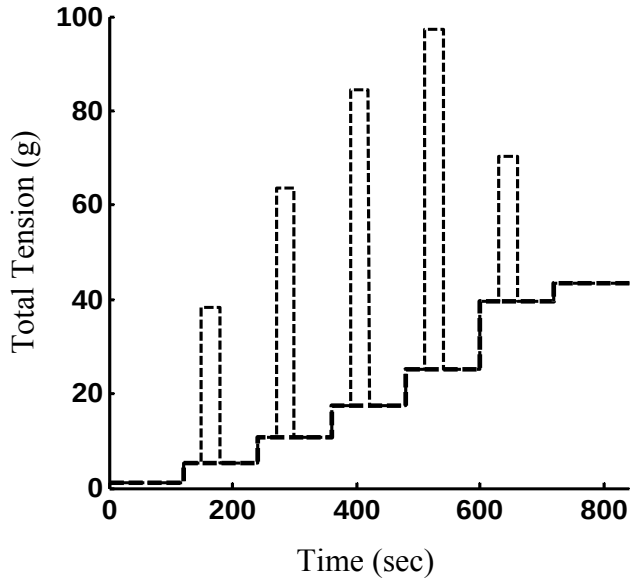

Figure 5.9 Total tension-time curve for the medium APS simulation of the step-stretch protocol. The cross-bridges were activated for 30 seconds during each isometric hold. Total tension is the sum of the preload (solid line) and active tension (dashed lines).

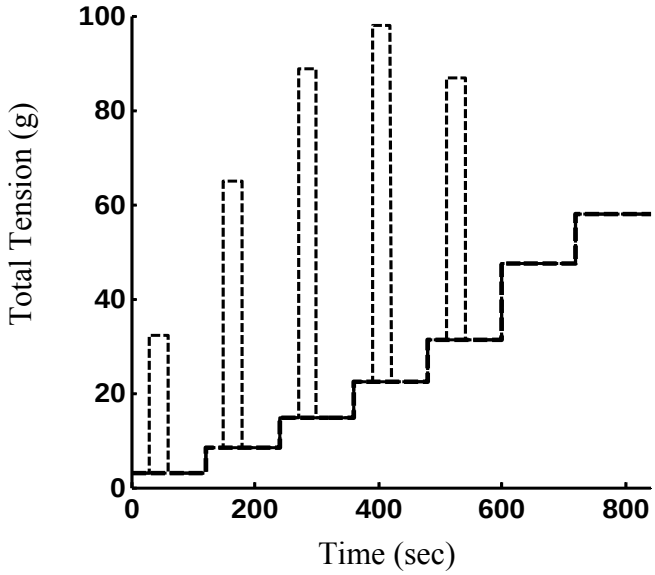

Figure 5.10 Total tension-time curve for the hhigh APS simulation of the step-stretch protocol. The cross-bridges were activated for 30 seconds during each isometric hold. Total tension is the sum of the preload (solid line) and active tension (dashed lines).

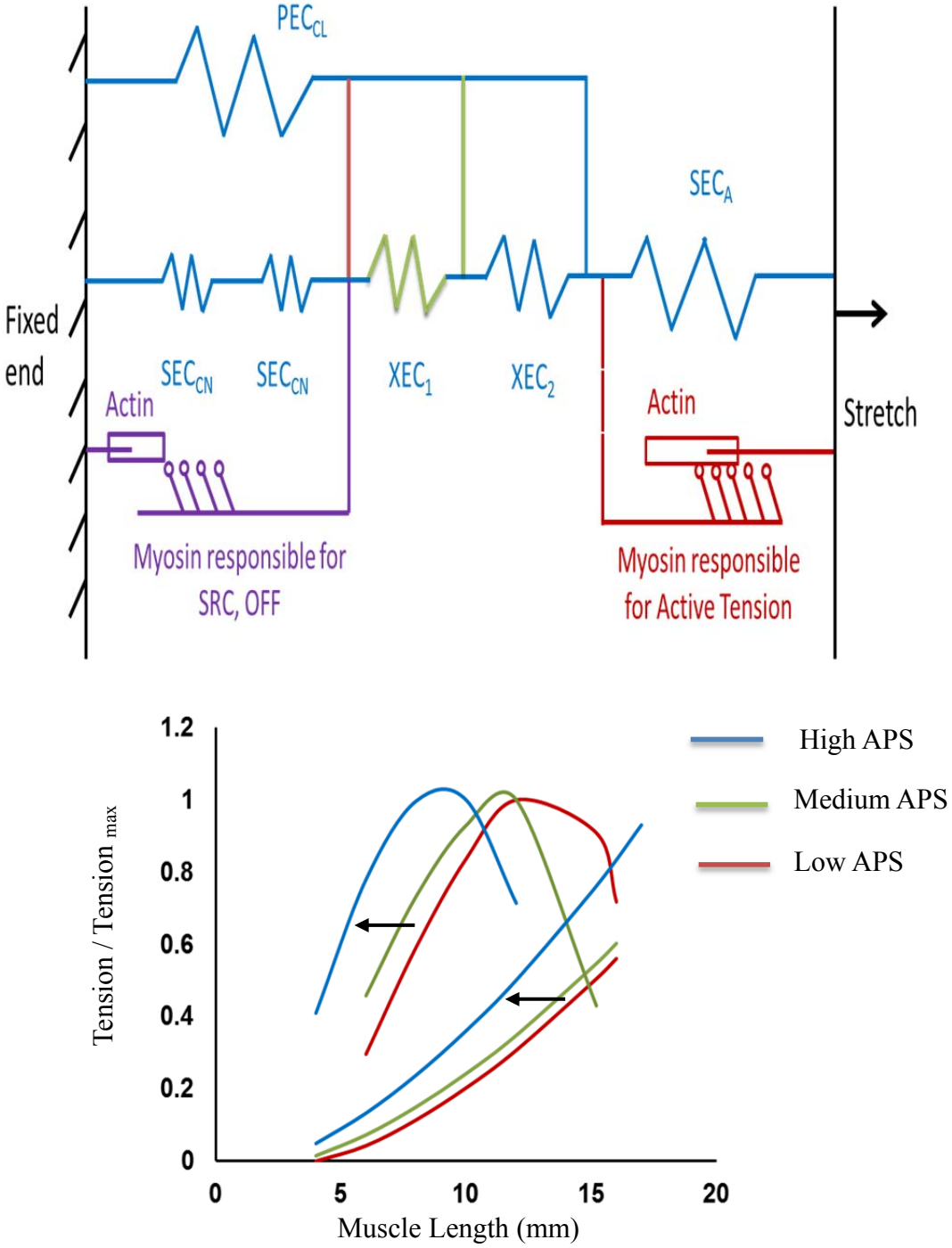

Figure 5.11 A sample of active and preload tension curves for 3 model cases: low APS, medium APS and high APS. Step stretch protocol (Figure 5.6) applied to the model for all cases in this sample. Cross-bridges cwere turned on only during the rest time in between stretches.

CHAPTER 6 DISCUSSION

6.1. Relationship of myogenic contraction to timing of a QS during the SRC cycle

When focusing on a single twitch contraction from a train of RCs, imposing a QS near the trough between two peaks caused a stronger NTP myogenic contraction than when the QS was imposed near the peak (Figures 3.3. and 3.4.). The data from Chapter 3 supports a model in which a single population of actomyosin cross-bridges is responsible for both SRC and stretch-induced myogenic contraction. The NTP tension data suggest that when the mechanism responsible for RC was mostly active (i.e., tension was near a maximum), a smaller proportion of the shared population of cross-bridges was available to produce a myogenic contraction in response to a QS. Likewise, it was proposed that when tension was relatively low (i.e., during the trough between two sequential twitches), the mechanism responsible for inducing RC was largely inactive. Thus, a larger proportion of the shared population of cross-bridges was available to produce a strong contraction in response to a QS.

In contrast, PMR tension values were not different for QSs imposed at different points throughout the SRC cycle (Figure 3.5C) or the TEA-induced RC cycle (Figure 3.5D). These data suggest that PMR tension is a measure of the sum of SRC tension and NTP myogenic tension, and that the result of a QS designed to induce a near maximal myogenic contraction was to activate the remaining cross-bridges that were not already cycling to produce SRC. Thus, these

PMR tension data support the hypothesis that a shared population of cross-bridges is responsible for SRC and QS-induced myogenic contraction.

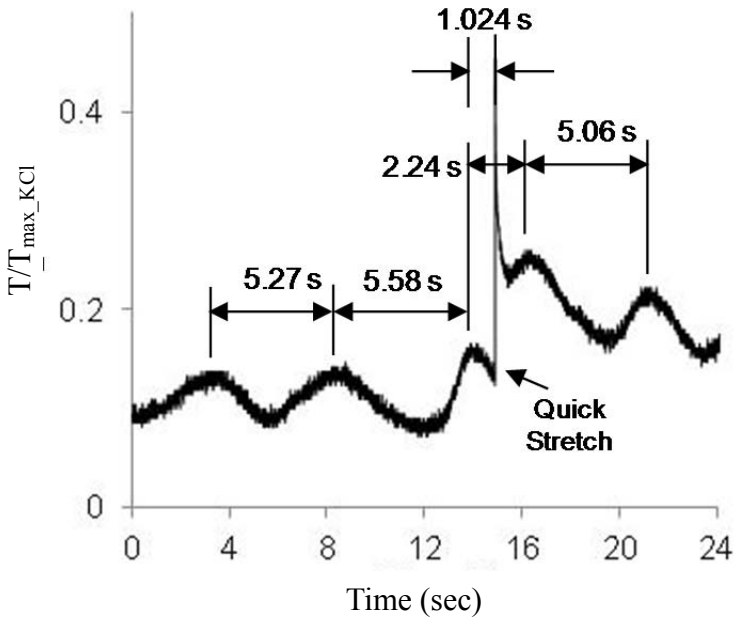

Figure 6.1 Example of a myogenic contraction due to a quick stretch (QS) imposed 1.02 sec after the peak of a spontaneous rhythmic contraction (SRC) cycle with a period of 5.3–5.6 sec. The peak of the myogenic contraction occurred 2.24 sec after the previous rhythmic peak and 5.06 sec before the next peak, suggesting that the QS shifted the timing of the rhythmic contraction (RC) cycle.

Due to the fact that the degree of contractile tension is proportional to the number of active cross-bridges, the maximum number of active cross-bridges during SRC occurs at the peak of each twitch. Likewise, for a given QS stimulus the maximum number of active cross-bridges occurs at the peak of the myogenic contraction. If the proposed hypothesis that SRC and QS-induced contraction are due to the regulation of a shared population of cross-bridges is valid, this leads to a secondary hypothesis that the QS-induced myogenic contraction in detrusor is the first contraction of a shifted SRC cycle. Data demonstrating stretch-induced RC in rat pulmonary

artery (Tanabe et al., 2012) is consistent with this hypothesis. Furthermore, the example in Figure 7.1 shows a myogenic contraction due to a QS imposed an estimated 1 sec after the peak of a SRC cycle with a period of an estimated 5.5 seconds. The peak of the myogenic contraction occurred only an estimated 2.2 seconds after the previous rhythmic peak, but ~5.1 sec before the next peak, suggesting that the QS caused the next peak of the SRC cycle to occur earlier and as a result substantially shifted the timing of the RC cycle with little effect on the SRC frequency. The present study was not designed to specifically test this hypothesis, and data from the present set of experiments was insufficient for statistical analysis since tissues were held at the QS length for only 10 seconds. This did not provide sufficient time for some tissues to complete a full SRC cycle after the QS. Specifically, testing the hypothesis that a QS mechanically resets the SRC cycle in detrusor without altering the frequency will provide additional insight into mechanisms regulating SRC.

In summary, the time within the SRC cycle at which a detrusor strip is subjected to a QS affects the NTP tension (Figures 3.3.-3.4.) but not the PMR tension (Figures 3.3. & 3.5) of the resulting myogenic contraction and appears to reset the timing of the SRC cycle (Figure 7.1.). This supports the hypothesis that SRC and QS-induced contraction are due to a common set of actomyosin cross-bridges.

6.2. Regulation of SRC and QS-induced myogenic contraction

Rho kinase, cyclooxygenase-1, and cyclooxygenase-2 inhibitors affected SRC amplitude and NTP amplitude following a QS to the same degree, providing additional evidence to support the hypothesis that a common regulatory mechanism is responsible for SRC and myogenic contraction due to QS. While the precise mechanism remains to be determined, it was previously shown that attenuation of a QS-induced myogenic contraction by a ROCK inhibitor is due to activation of basal myosin phosphatase rather than to inhibition of stretch-activated myosin phosphorylation (Poley et al., 2008). These studies supported a model in which RCs can be generated by muscle stretch-induced calcium entry that increases myosin phosphorylation "on top of" a basal level of myosin phosphorylation regulated by ROCK. Rabbit detrusor free of mucosa produces prostaglandins basally (Klausner et al., 2011), and both cyclooxygenases 1 and 2 co-localize with interstitial cells surrounding bundles of detrusor smooth muscle in rabbit (Collins et al., 2009). Moreover, after SRC has been abolished, RC of the same magnitude and frequency can be re-established by exogenous addition of prostaglandin E_2 (Collins et al., 2009). Together, these data support a role of prostaglandins in establishing or maintaining rhythmic contractile activity.

As described in Section 1.8, cell-to-cell synchronization is required to produce the uniform contractions seen during SRC or QS-induced contraction, and since detrusor cells are poorly coupled electrically (Bramich & Brading, 1996) and all cells are not innervated (Elbadawi, 1995), mechanical coupling is likely responsible for synchronization. The data in Chapter 3 showing that a QS-induced contraction mimics a single twitch of an SRC train of contractions supports the mechanical coupling model proposed by Elbadawi (Elbadawi, 1995)

and Ji (Ji et al., 2002) in which one cell or group of cells rapidly contracts to stretch and stimulate surrounding cells to propagate a contraction throughout a bundle of cells.

6.3. Relevance of a common mechanism for SRC and QS-induced myogenic contraction

The role of stretch-induced contraction in bladder function remains to be determined. Studies of rabbit detrusor indicate that SRC is responsible for regenerating adjustable preload stiffness (APS) (A. M. Almasri, Ratz, Bhatia, Klausner, & Speich, 2010a) and for length adaptation (Speich et al., 2012). The present data are consistent with a bladder model that includes two contractile systems, one responsible for producing the voiding contraction, and another responsible for SRC, QS-induced myogenic contraction, generation of APS (A. M. Almasri, Ratz, Bhatia, et al., 2010a; Ratz & Speich, 2010; Southern et al., 2012; Speich et al., 2006, 2012)and length adaptation (A. M. Almasri, Ratz, & Speich, 2010a; Speich et al., 2012, 2009) during filling. These roles are consistent with Gillespie's conclusion that pre-micturition activity during filling and micturation activity in the bladder are regulated by distinct systems (Gillespie, 2004).

Elevated levels of RC have been shown in patients with overactive bladder disorder (M. Drake & Harvey, 2005; Kinder & Mundy, 1987); however, a pathological link between RC and overactive bladder has not yet been determined. Furthermore, SRC in human and rabbit bladder often has an inconsistent amplitude and/or frequency (Byrne et al., 2013; Sibley, 1984) and requires complex analysis to quantify (Byrne et al., 2013; Klausner et al., 2013). If SRC and QS-induced myogenic contraction are due to a common population of actomyosin cross-bridges and are regulated by a common mechanism, then QS is a potential mechanical probe to study SRC

regulation and its alteration in overactive bladder. More specifically, it was proposed that a QS protocol could be used to temporally isolate a single SRC twitch or reset the SRC cycle. Thus, QS could be used as a simple alternative or complement to SRC analysis for the comparison of tissues from individuals with and without overactive bladder and during animal testing of agents to specifically target contractile activity during the filling phase.

6.4. Sensor-based model supports a common mechanism for SRC and QS-induced contraction

Chapter 4 describes the design of a simple mechanical sensor to trigger and regulate QS-induced contraction amplitude based on stretch magnitude, stretch rate, and the delay between QSs. Model simulations qualitatively produced these experimentally observed tissue behaviors (Poley et al., 2008). Furthermore, model simulation results were consistent with the experimental data presented in Chapter 3 showing that QSs imposed throughout the SRC cycle produced a myogenic contraction with greater (less) nadir-to-peak tension when the QS was imposed near the trough (peak) of the cycle, suggesting more (fewer) cross-bridges were available to be activated (Komari et al., 2013). These results suggested that a common mechanism is responsible for these two types of contraction.

The sensor-based mechanical contraction model developed in Chapter 4 was expanded to study the concept of mechanical coupling and contraction prorogation through bundles of muscle cells. The model simulations support Elbadawi's (Elbadawi, 1995) hypothesis that rapid contraction of innervated DSM cells can lead through mechanical coupling to myogenic activation and contraction of many non-innervated muscle cells. This process could be used to

produce a synchronized uniform contraction. Additionally, since SRC can have an amplitude of approximately 20% of a maximum contraction (Collins et al., 2009) the question has never been answered whether SRC is due to all cell contacting with 20% of their maximum force, or 20% of cells contracting maximally. Based on the propagation model (Figure 4.13), the more efficient alternative would be for all of the cells to each produce 20% of their maximal force. In this case, the PEC_k in each cell would be stretched a relatively small amount. If only 20% of the cells contracted, these cells would likely stretch the PEC_k elements in the other cells to relatively longer lengths, which would require more energy.

6.5. Potential roles for actin and myosin in APS and length adaptation

A conceptual mechanical model was developed using springs and actin-myosin cross bridges and cross-links to produce several mechanical behaviors of smooth muscle. As described in Chapter 5, the output of the model was length-tension curves that exhibit adjustable preload stiffness and length adaptation. The purpose of the study was to provide a conceptual explanation of the mechanical relationship between length adaptation and adjustable preload stiffness in DSM and the role of SRC in regulating these dynamic tension-length relationships. The model simulations were consistent with the previous length adaptation experimental results (A. M. Almasri, Ratz, & Speich, 2010a) that indicated that DSM exhibits dynamic active and preload length-tension as shown in Figure 6.2. Tissues contracted multiple times on the ascending limb of the length-active tension curve exhibited increases in both preload and active tension, while tissues contracted on the multiple times on the descending limb of the length-active tension curve exhibited an increases in active tension, but a decrease in preload tension. This model supports

the hypothesis that the role of APS is to position actin and myosin such that they are prepared to produce a strong contraction.

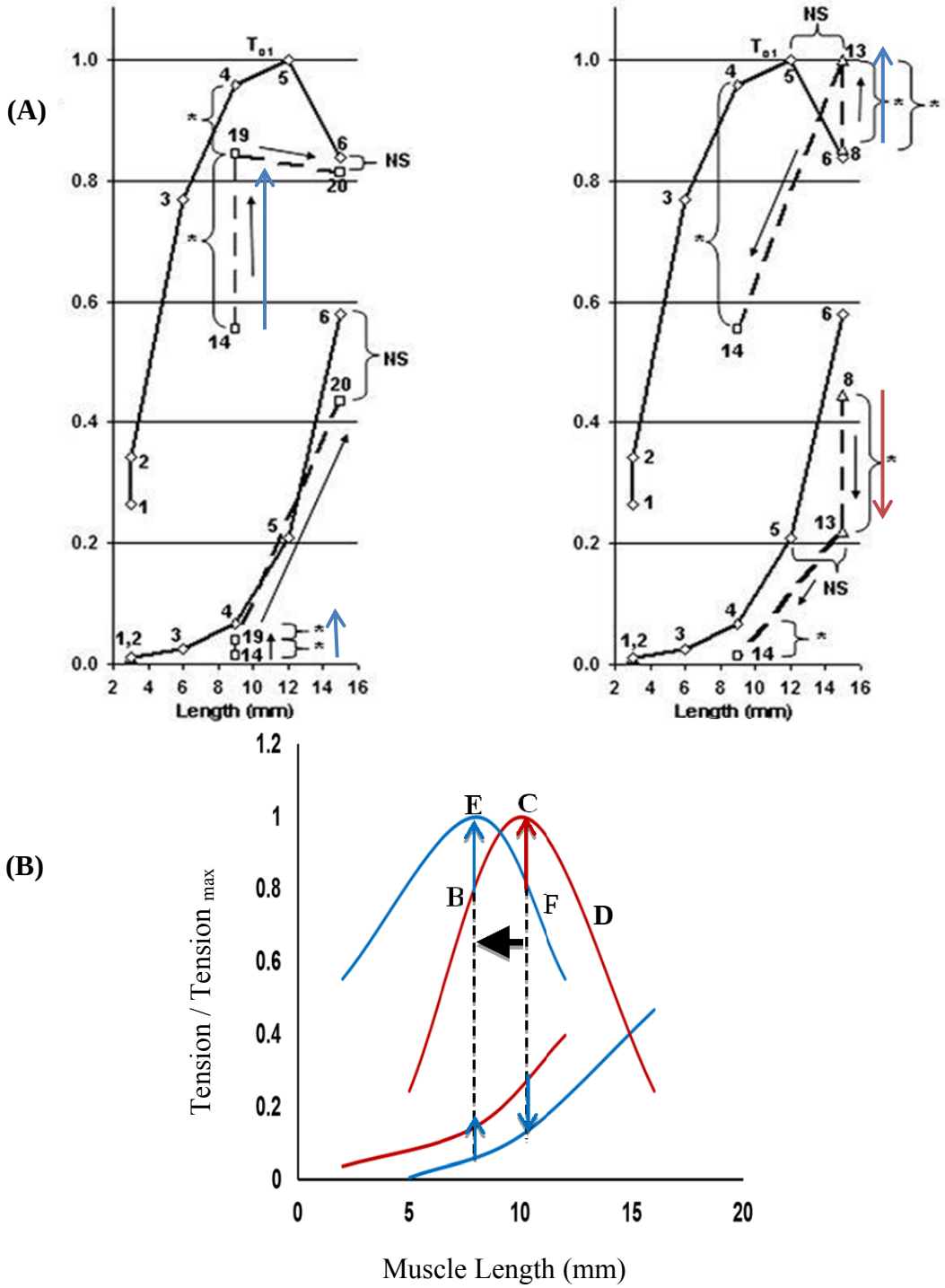

Figure 6.2 Dynamic length-active/preload tension from model output (**A**) in compassion with experimental results (**B**)

6.6. Role of SRC on APS and shifting the active/preload length-tension relationship

The model developed in Chapter 5 uses SRC to regulate APS as determined in a previous study (A. M. Almasri, Ratz, Bhatia, et al., 2010a)The model supports the hypothesis that a role of SRC is to stretch elastic elements to pull them into position to be cross-linked to generate APS and to pull the elements to relieve strain on crosslinks so that they can be released to decrease APS. The model uses APS to regulated length adaptation. Thus, by regulating APS, SRC is indirectly regulating length adaptation in the model, which is consistent with a previous experimental study (A. M. Almasri, Ratz, & Speich, 2010a). Overall this dissertation supports the hypothesis that actin-myosin interactions produce the interrelated behaviors of SRC, APS and length adaptation observed in DSM.

CHAPTER 7 CONCLUSIONS AND FUTURE WORK

7.1. Conclusion

This dissertation focused on the role of actin-myosin interactions in the multiple interrelated functions of spontaneous rhythmic contraction, quick-stretch myogenic response, adjustable preload stiffness and length adaptation in detrusor smooth muscle. The first objective was to test the hypothesis that a common mechanism is responsible for SRC and quick-stretch-induced contraction. The results illustrated the following:

1) The myogenic response was relatively large when tension in the rhythm cycle was small, suggesting that the common mechanism was primarily "off" at that point in the rhythm cycle, leaving a substantial fraction that was "turned on" by the QS

2) The myogenic response was relatively small at a point when tension in the rhythm cycle was large, suggesting that the common mechanism was mostly "on" and only a small fraction remained to be "turned on" by the QS.

Together these results support the hypothesis that a common mechanism is responsible for SRC and quick-stretch-induced contraction.

The second objective of this dissertation was to develop a sensor-based mechanical model that exhibits several characteristics of the myogenic response and SRC in DSM and use the model to test the hypothesis that the myogenic response can propagation a contraction through a series of cells. The following results were obtained:

1) A simple mechanical sensor that regulates QS-induced contractions with amplitudes that are dependent on stretch magnitude, refractory periods between stretches and stretch rate was developed (Poley et al., 2008).
2) Simulation results qualitatively reproduced the characteristics of QS-induced myogenic contraction observed in experimental studies (Poley et al., 2008).
3) A network model was developed to test the hypothesis that rapidly stretching DSM cells could trigger a myogenic response in other cells to propagate the contraction throughout a bundle of cells. Model simulation results supported this hypothesis.

The third objective of this dissertation was to develop a model with a network of actin and myosin that produces the coupled mechanical behaviors of adjustable preload tension, spontaneous rhythmic contraction, and length adaptation exhibited by the bladder muscle. Model simulations produced active and preload length-tension curves that were a function of length and SRC history, which qualitatively matched data from previous experimental studies (Bossé et al., 2008). The results illustrate a potentially important role for actin-myosin cross-bridge overlap and cross-links in the dynamic active and preload length-tension relationships in DSM, as well as a potential role of SRC in regulation of APS and length adaptation as suggested by previous experimental studies (A. M. Almasri, Ratz, & Speich, 2010a).

This study explained the role of actin-myosin cross-bridges in multiple interrelated mechanical behaviors of detrusor smooth muscle by expanding biomechanical models and analyzing experimental data with a main focus of spontaneous rhythmic contraction. Ultimately, these results may be helpful in understanding DSM mechanical behavior, which could be important for the identification of treatments for OAB and UAB. Since low-grade rhythmic contractions occur in human bladder and since elevated levels of SRC have been shown in

patients with OAB disorder (Kinder & Mundy, 1987), understanding the role of SRC in both APS and length adaptation may be essential to understanding a potential mechanism for OAB.

7.2. Future Studies

Potential next steps of this study can be developed in four categories. First, based on the evidence for a common mechanism for SRC and the QS-induced myogenic contraction described in Chapter 3, it was proposed that the QS-induced myogenic contraction in detrusor is the first contraction of a shifted SRC cycle. More specifically, the example in Figure 8.1 shows a myogenic contraction due to a QS imposed ~1 sec after the peak of a SRC cycle with a period of ~5.5 sec. The peak of the myogenic contraction occurred only ~2.2 sec after the previous rhythmic peak, but ~5.1 sec before the next peak, suggesting that the QS caused the next peak of the SRC cycle to occur earlier and as a result substantially shifted the timing of the RC cycle with little effect on the SRC frequency. Our previous experiments did not provide enough data to support this hypothesis. As a result, one important next step will be to validate the hypothesis that QS resets the rhythm cycle. This would provide further evidence that they share a common mechanism.

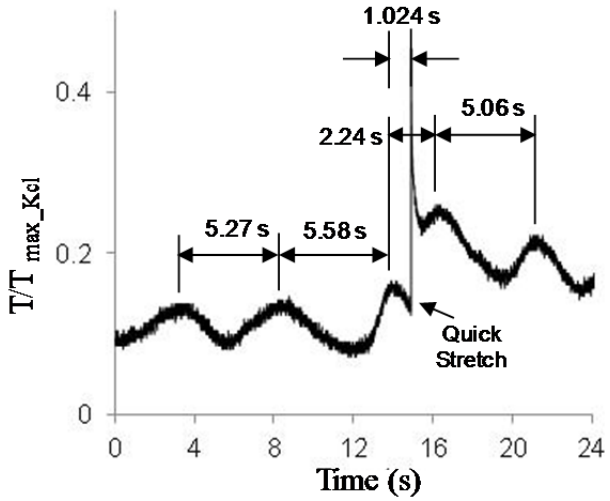

Figure 7.1 Example of a myogenic contraction due to a quick stretch (QS) imposed 1.02 sec after the peak of a spontaneous rhythmic contraction (SRC) cycle with a period of 5.3–5.6 sec.

Second, based on a review of the literature, spontaneous rhythmic contractions have not been a main focus of study underactive bladder (UAB) and spinal cord injury urodynamic studies. Smith and his colleagues (ref) stated that due to lack of appropriate animal models the current understanding of the UAB pathophysiology is limited, and although animal modelsfor UAB have limitations they could be useful tools to improve the understanding of UAB and potentially develop medical interventions. Also, it can be argued that although most of the animal models do not essentially mimic UAB, they may bear enough similarities to make them relevant for a limited number of aspects of the human condition. Therefore, SRC studies in an animal model for UAB could lead to a greater understanding of the potential role of SRC in mechanical characteristics such as adjustable preload stiffness or length adaptation and their potential role in UAB.

Third, development of more detailed biomechanical models that can quantitatively reproduce or predict DSM behavior could be another step in future studies. For instance, Hill's (Hill, 1938) force-velocity equation was been used in our propagation model developed in

Chapter 4. Van Mastrigt (R. van Mastrigt, 1979) expanded the force-velocity relationship into a pressure-flow rate relationship which is the relationship observed during clinical urodynamics studies. The tissue-level models developed in this dissertation could be expanded to organ-level models to study clinically observed behaviors.

Fourth, the effects, if any of age on the mechanical behaviors of APS and length adaptation in DSM have not been studied. Previous research (PAGALA, TETSOTI, NAGPAL, & WISE, 2001) showed that in the circular detrusor of rats collagen membranes increased with age. In contrast, the results from another study (Sjuve, Uvelius, & Arner, 1997) suggest that aging is not associated with pronounced changes in the cellular contractile and cytoskeletal proteins or in the mechanical properties of the contractile machinery. They proposed that this change may be due to alterations in the activation systems and urinary bladder smooth muscle Ca^{2+} sensitivity. Other studies associated with the male rat suggest that age related differences may be due to neuronal innervations and central control of micturition rather than alteration in muscle contractility system. I proposed that the contribution of APS may increase with age and understanding APS and its relationship with the age may be essential to understanding a potential mechanism for OAB in the elderly. Future experimental studies could be developed to test this hypothesis regarding the effects of age on bladder smooth muscle.

Literature Cited

Almasri, A. M.-. (2009). *Mechanical behavior and length adaptation of rabbit bladder smooth muscle*. (J. E. Speich, Ed.)*ProQuest Dissertations and Theses*. Virginia Commonwealth University, United States -- Virginia.

Almasri, A. M., Ratz, P. H., Bhatia, H., Klausner, A. P., & Speich, J. E. (2010a). Rhythmic contraction generates adjustable passive stiffness in rabbit detrusor. *Journal of Applied Physiology (Bethesda, Md.: 1985)*, *108*(3), 544–553.

Almasri, A. M., Ratz, P. H., & Speich, J. E. (2010a). Length adaptation of the passive-to-active tension ratio in rabbit detrusor. *Annals of Biomedical Engineering*, *38*(8), 2594–2605.

Andersson, & Arner, A. (2004). Urinary bladder contraction and relaxation: physiology and pathophysiology. *Physiological Reviews*, *84*(3), 935–986.

Andersson, K.-E., Nomiya, M., Sawada, N., & Yamaguchi, O. (2014). Pharmacological treatment of chronic pelvic ischemia. *Therapeutic Advances in Urology*, *6*(3), 105–14. doi:10.1177/1756287214526768

Andersson, S., Kronström, A., & Teien, D. (1988). Wall mechanics of the rat bladder. I. Hydrodynamic studies in the time domain. *Acta Physiologica Scandinavica*, *134*(4), 457–461.

Battistella-Patterson, A. S., Wang, S., & Wright, G. L. (1997). Effect of disruption of the cytoskeleton on smooth muscle contraction. *Canadian Journal of Physiology and Pharmacology*, *75*(12), 1287–1299.

Biers, S. M., Reynard, J. M., Doore, T., & Brading, A. F. (2006). The functional effects of a c-kit tyrosine inhibitor on guinea-pig and human detrusor. *BJU International*, *97*(3), 612–6. doi:10.1111/j.1464-410X.2005.05988.x

Bossé, Y., Sobieszek, A., Paré, P. D., & Seow, C. Y. (2008). Length adaptation of airway smooth muscle. *Proceedings of the American Thoracic Society*, *5*(1), 62–67. doi:10.1513/pats.200705-056VS

Brading, A. F. (1997). A myogenic basis for the overactive bladder. *Urology*, *50*(6A Suppl), 57–67; discussion 68–73.

Bramich, N. J., & Brading, A. F. (1996). Electrical properties of smooth muscle in the guinea-pig urinary bladder. *The Journal of Physiology*, *492 (Pt 1*, 185–98.

BURNSTOCK, G., & PROSSER, C. L. (1960). Responses of smooth muscles to quick stretch: relation of stretch to conduction. *The American Journal of Physiology*, *198*, 921–5.

Byrne, M. D., Klausner, A. P., Speich, J. E., Southern, J. B., Habibi, J. R., & Ratz, P. H. (2013). Fourier Transform Analysis of Rabbit Detrusor Autonomous Contractions Reveals Length Dependent Increases in Tone and Slow Wave Development at Long Lengths. *The Journal of Urology*, *190*(1), 334–340.

Collins, C., Klausner, A. P., Herrick, B., Koo, H. P., Miner, A. S., Henderson, S. C., & Ratz, P. H. (2009). Potential for control of detrusor smooth muscle spontaneous rhythmic contraction by cyclooxygenase products released by interstitial cells of Cajal. *Journal of Cellular and Molecular Medicine*, *13*(9b), 3236–3250.

Costanzo, L. S. (2002). Acid-base physiology. *Costanzo LS.Physiology.2nd ed.Philadelphia, Pa: Saunders*, 275–299.

Davis, M. J., & Hill, M. a. (1999). Signaling Mechanisms Underlying the Vascular Myogenic Response\r. *Physiol. Rev.*, *79*(2), 387–423.

Drake, M., & Harvey, I. (2005). Localized contractions in the normal human bladder and in urinary urgency. *BJU …*.

Drake, M. J., Harvey, I. J., & Gillespie, J. I. (2014). Autonomous activity in the isolated guinea pig bladder Experimental Physiology : Experimental Physiology :

Dulin, N. O., Fernandes, D. J., Dowell, M., Mcconville, J., Lakser, O., Mitchell, R., … Solway, J. (2003). Smooth Muscle in the Cause of BHR ? Index Entries :, *24*.

Elbadawi, A. (1995). Pathology and pathophysiology of detrusor in incontinence. *The Urologic Clinics of North America*, *22*(3), 499–512.

Ford, L. E. (2005). Plasticity in airway smooth muscle: an update. *Canadian Journal of Physiology and Pharmacology*, *83*(10), 841–50. doi:10.1139/y05-089

Ford, L. E., Seow, C. Y., & Pratusevich, V. R. (1994). Plasticity in smooth muscle, a hypothesis. *Canadian Journal of Physiology and Pharmacology*, *72*(11), 1320–1324.

Fung, Y. C. (Yuan-cheng) [1919-]. (1993). *Biomechanics : mechanical properties of living tissues / Y.C. Fung. New York: Springer-Verlag, 1993. xviii, 568 pp.* (Vol. 2nd ed., pp. 2–xviii, 568). Springer-Verlag.

Fust, A., & Stephens, N. L. (2005). Mechanical plasticity and contractile properties of airway smooth muscle. *Canadian Journal of Physiology and Pharmacology*, *83*(10), 865–868.

Geeves, M. A., & Holmes, K. C. (1999). Structural mechanism of muscle contraction. *Annual Review of Biochemistry*, *68*, 687–728. doi:10.1146/annurev.biochem.68.1.687

Gillespie, J. I. (2004). The autonomous bladder: a view of the origin of bladder overactivity and sensory urge. *BJU International*, *93*(4), 478–483.

Golenhofen, K. (1970). Slow rhythms in smooth muscle (minute-rhythm). *Smooth Muscle*.

Gordon, A. M., Huxley, A. F., & Julian, F. J. (1966). The variation in isometric tension with sarcomere length in vertebrate muscle fibres. *The Journal of Physiology*, *184*(1), 170–92.

Griffith, T. M. (1996). Temporal chaos in the microcirculation. *Cardiovascular Research*, *31*(3), 342–58.

Gunst, Meiss, R. A., Wu, M.-F., & Rowe, M. (1995). Mechanisms for the mechanical plasticity of tracheal smooth muscle. *American Journal of Physiology-Cell Physiology*, *268*(5), C1267–C1276.

Gunst, S. J., & Zhang, W. (2008). Actin cytoskeletal dynamics in smooth muscle: a new paradigm for the regulation of smooth muscle contraction. *American Journal of Physiology. Cell Physiology*, *295*(3), C576–87.

Guyton, A. C., & Hall, J. E. (1961). *Medical physiology*. Saunders.

Guyton, Hall. (2000). Textbook of Medical Physiology.

Herlihy, J. T., & Murphy, R. A. (1973). Length-tension relationship of smooth muscle of the hog carotid artery. *Circulation Research*, *33*(3), 275–83.

Hill, A. V. (1938). The Heat of Shortening and the Dynamic Constants of Muscle. *Proceedings of the Royal Society of London.Series B, Biological Sciences*, *126*(843), 136–195.

Huizinga, J. D., Robinson, T. L., & Thomsen, L. (2000). The search for the origin of rhythmicity in intestinal contraction; from tissue to single cells. *Neurogastroenterology and Motility : The Official Journal of the European Gastrointestinal Motility Society*, *12*(1), 3–9.

Ji, G., Barsotti, R. J., Feldman, M. E., & Kotlikoff, M. I. (2002). Stretch-induced calcium release in smooth muscle. *The Journal of General Physiology*, *119*(6), 533–44.

Kanai, A., Roppolo, J., Ikeda, Y., Zabbarova, I., Tai, C., Birder, L., … Fry, C. (2007). Origin of spontaneous activity in neonatal and adult rat bladders and its enhancement by stretch and muscarinic agonists. *American Journal of Physiology. Renal Physiology*, *292*(3), F1065–72. doi:10.1152/ajprenal.00229.2006

Kim, K., & Keller, T. C. S. (2002). Smitin, a novel smooth muscle titin-like protein, interacts with myosin filaments in vivo and in vitro. *The Journal of Cell Biology*, *156*(1), 101–11. doi:10.1083/jcb.200107037

Kinder, R. B., & Mundy, A. R. (1987). Pathophysiology of idiopathic detrusor instability and detrusor hyper-reflexia. An in vitro study of human detrusor muscle. *British Journal of Urology*, *60*(6), 509–15.

King, G. G., Paré, P. D., & Seow, C. Y. (1999). The mechanics of exaggerated airway narrowing in asthma: the role of smooth muscle. *Respiration Physiology*, *118*(1), 1–13.

Klausner, A. P., Johnson, C. M., Stike, A. B., Speich, J. E., Sabarwal, V., Miner, A. S., … Ratz, P. H. (2011). Prostaglandin E_2mediates spontaneous rhythmic contraction in rabbit detrusor muscle. *The Canadian Journal of Urology*, *18*(2), 5608–14.

Klausner, A. P., King, A. B., Byrne, M. D., Habibi, J. R., Li, K., Sabarwal, V., … Ratz, P. H. (2013). A new and automated method for objective analysis of detrusor rhythm during the filling phase. *World Journal of Urology*, 1–6.

Komari, S. O., Headley, P. C., Klausner, A. P., Ratz, P. H., & Speich, J. E. (2013). Evidence for a common mechanism for spontaneous rhythmic contraction and myogenic contraction induced by quick stretch in detrusor smooth muscle. *Physiological Reports*, *1*(6), e00168. doi:10.1002/phy2.168

Masters, J. G., Neal, D. E., & Gillespie, J. I. (1999). Contractions in human detrusor smooth muscle induced by hypo-osmolar solutions. *The Journal of Urology*, *162*(2), 581–9.

Mullins, C. D. (2009). New perspectives on overactive bladder and its treatment. Introduction. *The American Journal of Managed Care*, *15*(4 Suppl), S88–S89.

Mulvany, M. J., & Warshaw, D. M. (1979). The active tension-length curve of vascular smooth muscle related to its cellular components. *The Journal of General Physiology*, *74*(1), 85–104.

Murphy, R. A. (2011). Mechanics of Vascular Smooth Muscle. John Wiley & Sons, Inc.

Murphy, R. A., & Rembold, C. M. (2005). The latch-bridge hypothesis of smooth muscle contraction. *Canadian Journal of Physiology and Pharmacology*, *83*(10), 857–864.

Poley, R. N., Dosier, C. R., Speich, J. E., Miner, A. S., & Ratz, P. H. (2008). Stimulated calcium entry and constitutive RhoA kinase activity cause stretch-induced detrusor contraction. *European Journal of Pharmacology*, *599*(1-3), 137–145.

Pollard, T. D., Earnshaw, W. C., & Lippincott-Schwartz, J. (2007). *Cell biology*. Elsevier Health Sciences.

Pratusevich, V. R., Seow, C. Y., & Ford, L. E. (1995). Plasticity in canine airway smooth muscle. *The Journal of General Physiology*, *105*(1), 73–94.

R. van Mastrigt, D. J. G. (1979). Contractility of the Urinary Bladder, (804).

Ratz, P. H., & Miner, A. S. (2003). Length-dependent regulation of basal myosin phosphorylation and force in detrusor smooth muscle. *American Journal of Physiology. Regulatory, Integrative and Comparative Physiology*, *284*(4), R1063–70.

Ratz, P. H., & Speich, J. E. (2010). Evidence that actomyosin cross bridges contribute to "passive" tension in detrusor smooth muscle. *American Journal of Physiology. Renal Physiology*, *298*(6), F1424–35.

ROACH, M. R., & BURTON, A. C. (1957). The reason for the shape of the distensibility curves of arteries. *Canadian Journal of Biochemistry and Physiology*, *35*(8), 681–90.

Seow, C. Y., Pratusevich, V. R., & Ford, L. E. (2000). Series-to-parallel transition in the filament lattice of airway smooth muscle. *Journal of Applied Physiology*, *89*(3), 869–876.

Seow, C. Y., Pratusevich, V. R., Ford, L. E., Chun, Y., & Lincoln, E. (2000). Series-to-parallel transition in the filament lattice of airway smooth muscle, *3*, 869–876.

Shenfeld, O. Z., McCammon, K. A., Blackmore, P. F., & Ratz, P. H. (1999). Rapid effects of estrogen and progesterone on tone and spontaneous rhythmic contractions of the rabbit bladder. *Urological Research*, *27*(5), 386–92.

Sibley, G. N. (1984). A comparison of spontaneous and nerve-mediated activity in bladder muscle from man, pig and rabbit. *The Journal of Physiology*, *354*, 431–43.

Siegman, M. J., Butler, T. M., Mooers, S. U., & Davies, R. E. (1976). Calcium-dependent resistance to stretch and stress relaxation in resting smooth muscles. *The American Journal of Physiology*, *231*(5 Pt. 1), 1501–8.

Silveira, P. S. P., Butler, J. P., & Fredberg, J. J. (2005). Length adaptation of airway smooth muscle: a stochastic model of cytoskeletal dynamics. *Journal of Applied Physiology (Bethesda, Md. : 1985)*, *99*(6), 2087–2098. doi:10.1152/japplphysiol.00159.2005

Southern, J. B., Frazier, J. R., Miner, a. S., Speich, J. E., Klausner, a. P., & Ratz, P. H. (2012). Elevated steady-state bladder preload activates myosin phosphorylation: Detrusor smooth muscle is a preload tension sensor. *AJP: Renal Physiology*, *303*(11), F1517–26.

Spassova, M. A., Hewavitharana, T., Xu, W., Soboloff, J., & Gill, D. L. (2006). A common mechanism underlies stretch activation and receptor activation of TRPC6 channels. *Proceedings of the National Academy of Sciences of the United States of America*, *103*(44), 16586–91.

Speich, J. E., Almasri, A. M., Bhatia, H., Klausner, A. P., & Ratz, P. H. (2009). Adaptation of the length-active tension relationship in rabbit detrusor. *American Journal of Physiology-Renal Physiology*, *297*(4), F1119–F1128.

Speich, J. E., Borgsmiller, L., Call, C., Mohr, R., & Ratz, P. H. (2005). ROK-induced cross-link formation stiffens passive muscle: reversible strain-induced stress softening in rabbit detrusor. *American Journal of Physiology. Cell Physiology*, *289*(1), C12–C21.

Speich, J. E., Dosier, C., Borgsmiller, L., Quintero, K., Koo, H. P., & Ratz, P. H. (2007). Adjustable passive length-tension curve in rabbit detrusor smooth muscle. *Journal of Applied Physiology (Bethesda, Md. : 1985)*, *102*(5), 1746–1755.

Speich, J. E., Quintero, K., Dosier, C., Borgsmiller, L., Koo, H. P., & Ratz, P. H. (2006). A mechanical model for adjustable passive stiffness in rabbit detrusor. *Journal of Applied Physiology (Bethesda, Md. : 1985)*, *101*(4), 1189–1198.

Speich, J. E., Wilson, C. W., Almasri, A. M., Southern, J. B., Klausner, A. P., & Ratz, P. H. (2012). Carbachol-induced volume adaptation in mouse bladder and length adaptation via rhythmic contraction in rabbit detrusor. *Annals of Biomedical Engineering*, *40*(10), 2266–2276.

Stephens, N. L., Kroeger, E., & Mehta, J. A. (1969). Force-velocity characteristics of respiratory airway smooth muscle. *Journal of Applied Physiology*, *26*(6), 685–692.

Tanabe, Y., Saito-Tanji, M., Morikawa, Y., Kamataki, A., Sawai, T., & Nakayama, K. (2012). Role of secretory phospholipase A(2) in rhythmic contraction of pulmonary arteries of rats with monocrotaline-induced pulmonary arterial hypertension. *Journal of Pharmacological Sciences*, *119*(3), 271–81.

Teixeira, C. E., Jin, L., Priviero, F. B. M., Ying, Z., & Webb, R. C. (2007). Comparative pharmacological analysis of Rho-kinase inhibitors and identification of molecular components of Ca2+ sensitization in the rat lower urinary tract. *Biochemical Pharmacology*, *74*(4), 647–58. doi:10.1016/j.bcp.2007.06.004

Uvelius, B. (1976). Isometric and Isotonic Length-Tension Relations and Variations in Cell Length in Longitudinal Smooth Muscle from Rabbit Urinary Bladder. *Acta Physiologica Scandinavica*, *97*(1), 1–12.

Wang, L., Paré, P. D., & Seow, C. Y. (2001). Selected contribution: effect of chronic passive length change on airway smooth muscle length-tension relationship. *Journal of Applied Physiology*, *90*(2), 734–740.

Webb, R. C. (2003). Smooth muscle contraction and relaxation. *Advances in Physiology Education*, *27*(4), 201–206.

Wein, A. J. (2007). *Campbell-walsh urology*. Saunders Elsevier.

Wellner, M. C., & Isenberg, G. (1994). Stretch effects on whole-cell currents of guinea-pig urinary bladder myocytes. *The Journal of Physiology*, *480 (Pt 3*, 439–48.

Whitney, G., Throckmorton, D., Isales, C., Takuwa, Y., Yeh, J., Rasmussen, H., & Brophy, C. (1995). Kinase activation and smooth muscle contraction in the presence and absence of calcium. *Journal of Vascular Surgery*, *22*(1), 37–44.

XU, J.-Q., GILLIS, J.-M., & CRAIG, R. (1997). Polymerization of myosin on activation of rat anococcygeus smooth muscle. *Journal of Muscle Research & Cell Motility*, *18*(3), 381–393.

Appendices

Appendix A

This appendix presents the equations for the SRC-Myogenic model (Figure 4.1). In these equations, F and L represent force and length, respectively, and subscripts on the variables correspond to the labels on the model elements defined in Figure 4.1. F_{total} is the total force in the model, L_{PEC} is the total length of both the tissue and the PEC element, and ΔL is the change in length of the tissue. Parameter values and initial lengths are provided in Table A1.

The model calculated the total force in the tissue using the equation:

$$F_{total} = F_{PECk} + F_{SECk} + F_{SECm}$$

For Kelvin part of the model (Fig4.1), the force in PEC element governed by the equations:

$$F_{PECk}\,(mN) = (\Delta L_{PECk} \times PEC_k)^4$$

$$\Delta L_{PECk} = L_{PECk} - L_{PECk\ initial}$$

$$L_{total}=L_{PECk}=\text{Input (mm)}$$

The initial lengths of the model components are governed by the following relationships. Also length extension is considered as a positive value.

$$L_{PECk} = L_{SECk} + L_{VCk} = L_{SECm}+L_{PECs}(mm)$$

$$L_{PECs} = L_{SECs +} L_{VCs}\,(mm)$$

Force in the other parts elements of Kelvin model are calculated using these equations:

$$F_{SECk}=F_{VCk}\,(mN)$$

$$F_{SECk} = \Delta L_{SECk} \times SEC_k$$

$$\Delta L_{SECk} = L_{PECk} - L_{VCk} - L_{SECk\ initial}$$

$$L_{VCk}\,(mm) = \int_0^t \left(\frac{F_{SECk}}{VCk}\right) dt + L_{VCk\ initial}$$

A single population of cross-bridges was modeled as a linear motor with the equation:

$$F_M\,(mN) = (R \times A)^n \left(\sin\left(\omega(t - B) + \frac{\pi}{2}\right)\right) + \beta$$

ω = Frequency of the sine wave (constant, Hz)

β = Offset value is used to shift the sine wave above zero (constant, mN)

A = Amplitude of the force in the SEC_s used to determine the amplitude of the sine wave (F_{SECs}, mN)

$$F_{SECs} = \Delta L_{SECs} \times SEC_s$$

$$\Delta L_{SECs} = L_{SECs} - L_{SECs\ initial}$$

R = Scaling factor for the sine wave amplitude

Stiffness, damping and initial length values were used from the previous adjustable preload stiffness model (Speich et al., 2006). The following methodology was used to determine the remaining model parameters. By applying a stretch to 115% of Lref to the adjustable preload stiffness (Speich et al., 2006) and Kelvin sections of the model, the maximum steady-state preload force for that stretch was calculated as 35.316 mN. Based on Almasri's study (A. M. Almasri, Ratz, & Speich, 2010a), a ratio of $T_p/T_a = 0.208$ was used. Therefore, $T_{a\_max} = 169.79$ mN. Previous experimental data (Klausner et al., 2013) (Komari et al., 2013) shows that the amplitude of SRC approximately equals 12% of maximum isometric active tension. Therefore, $(R \times A)^n \cong 12\%$ of T_{a_max} which was equal to 20.375 mN. Since a linear sensor was used to trigger SRC and myogenic contractions, which are nonlinear phenomena, the value of n was selected as n=3.33 to reasonably reproduce the observed NTP variation. As a result, $(R \times A) = 2.4724$. Finally, the corresponding peak force in the SEC_s for the simulation was calculated as A= 1.4553 mN; therefore, a scaling factor of R=0.59 was used so that the model

simulation produced a myogenic contraction with a normalized NTP amplitude similar to the experimental results (Poley et al., 2008).

B = Delay between the stretch and the myogenic contraction (constant, sec). There is a time delay for the myogenic QS-induced contractions to chemical reaction times within. This delay is included inside the sine wave equation.

The force in series elastic component that connects the motor to the system was calculated using this equation:

$$F_{SECm}\ (mN) = \Delta L_{SECm} \times SEC_m$$

$$\Delta L_{SECm} = L_{SECm} - L_{SECm\ initial}$$

$$L_{SECm}\ (mm) = L_{total} - L_{PECs}$$

Also from the model configuration,

$$L_{PECs}\ (mm) = L_{VCs} + L_{SECs}$$

The length of the VC_s and SEC_s was calculated using the following equations:

$$L_{VCs} = \int_0^t \left(\frac{F_{SECs}}{VCs}\right) dt + L_{VCs\ initial}$$

$$L_{SECs} = F_{SECs} / SEC_s + L_{SECs\ initial}$$

The force in parallel elastic element of the sensor (F_{PECs}) was calculated using the equation:

$$F_{PECs} = \Delta L_{PECs} \times PEC_s$$

$$\Delta L_{PECs} = L_{PECs} - L_{PECs\ initial}$$

The force in the viscoelastic component and series elastic component of the sensor were calculated using the equation:

$$F_{VCs} = F_{SECs} = F_{SECm} - F_{PECs} - F_M$$

In order to simulate propagation of a contraction, one cell was shortened at the maximum velocity, which varied (decreased) as the load changed (increased) during the simulation according to Hill's equation (Hill, 1938):

$$(F+a) \times (V+b) = (F_o+a) \times b,$$

Where "a" and "b" are constants, F is force, V is velocity of shortening and F_o is maximum isometric force.

Because F_o and "a" both are cross-sectional area dependent, Hill's equation was normalized as:

$$(\frac{F}{Fo} + \frac{a}{Fo}) \times (V+b) = (\frac{a}{Fo} +1) \times b,$$

where $a/F_o = 0.27$ and b=12 mm/s based on van Mastrigt's (R. van Mastrigt, 1979) experimental study of bladder smooth muscle. Force from this equation was used as the force in the motor, F_M.

Table A.1. Sensor-based mechanical model parameters

Model Element	Value	Initial (Slack)length, mm
PEC_K	0.44 $mN^{0.25}$/mm	5
SEC_K	9.81 mN/mm	3
VC_K	75.43 mN-s/mm	2
SEC_M	245.25 mN/mm	3
PEC_S	0.05 mN/mm	2
SEC_S	0.981 mN/mm	1
VC_S	0.088 mN-s/mm	1
PEC_{APS}	4.91 mN/mm	1
SEC_{APS}	19.62 mN/mm	4/11
VC_{APS}	19620 mN-s/mm	1
K_{eq} (attached)	981 mN/mm	4/11
K_{eq} (detached)	9.81 mN/mm	4/11
Minimum QS amplitude to trigger the sensor for the length dependency curve fit (figure 4.5 A)	3.1% L_{ref}	N/A
Approximate slowest QS rate to trigger the sensor for the rate dependency curve fit (figure 4.5 B)	1 sec	N/A

B	0.35 sec	N/A
T_p/T_a	0.208	N/A
A	1.4553	N/A
β	$-\pi/2$	N/A
ω	1 rad/sec	N/A
a/F_o	0.27	N/A
b	12 mm/s	N/A

Appendix B

This appendix presents the equations for the dynamic length-tension model (Figures B.1-3). In these equations, F and L represent force and length, respectively, and subscripts on the variables correspond to the labels on the model elements defined in Figure 5.1. F_{total} is the total force in the model, L_{PEC} is the total length of both the tissue and the PEC element, and ΔL is the change in length of the tissue. Parameter values and initial lengths are provided in Table 5.1.The SEC_{CN} elements are only connecting elements that were considered to be very weak structures that did not apply any stiffness to the system; therefore; they were not included in the calculations.

Three sets of equations were used, one for the system with PEC_{CL}, XEC_1, XEC_2, and SEC_A in series; one with a crosslink to bypass XEC_1, and one with a crosslink to bypass XEC_1 and XEC_2.

The system with PEC_{CL}, XEC_1, XEC_2, and SEC_A in series is shown in Figure B1. When the cross-bridges were not cycling the set of equations were as follows:

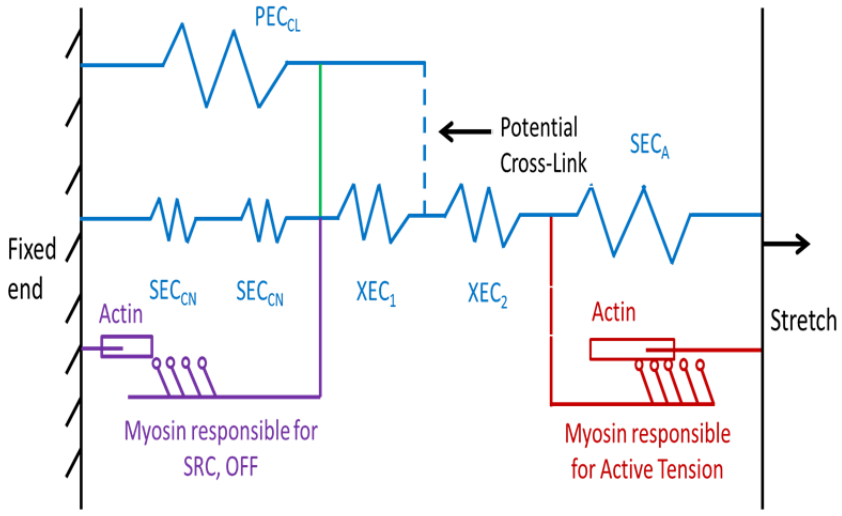

Figure B.1 Conceptual model with the PEC_{CL}, XEC_1, XEC_2, and SEC_A in series.

1) $\Delta L_{total} = \Delta L_{PECk} = \Delta L_{PECcl} + \Delta L_{XEC1} + \Delta L_{XEC2} + \Delta L_{SECA}$

$\Delta L_{PECk} = L_{PECk} - L_{PECk\ initial}$

$\Delta L_{PECcl} = L_{PECcl} - L_{PECcl\ initial}$

$\Delta L_{XEC1} = L_{XEC1} - L_{XEC1\ initial}$

$\Delta L_{XEC2} = L_{XEC2} - L_{XEC2\ initial}$

$\Delta L_{SECA} = L_{SECA} - L_{SECA\ initial}$

$F_{PECk} = (\Delta L_{PECk} \times PEC_k)^4$

2) $F_{PECcl} = (\Delta L_{PECcl} \times PEC_{cl})^{1.5}$

3) $F_{XEC1} = (\Delta L_{XEC1} \times XEC_1)^{1.5}$

4) $F_{XEC2} = (\Delta L_{XEC2} \times XEC_2)^{1.5}$

5) $F_{SECA} = (\Delta L_{SECA} \times SEC_A)^{1.5}$

6) $F_{PECcl} = F_{XEC1}$

7) $F_{XEC1} = F_{XEC2}$

8) $F_{XEC2} = F_{SECA}$

The eight numbered equations above were solved for the eight unknown parameters, the forces and lengths of the four elements in series.

$F_{PECcl} = F_{XEC1} = F_{XEC2} = F_{SECA}$ since all PEC_{CL}, XEC_1, XEC_2 and SEC_A are in-series.

When the myosin responsible for active tension are cycling, Equation 9 below is added for the motor force and Equation 8 is modified so that the equations become:

1) $\Delta L_{total} = \Delta L_{PECk} = \Delta L_{PECcl} + \Delta L_{XEC1} + \Delta L_{XEC2} + \Delta L_{SECA}$

$\Delta L_{PECk} = L_{PECk} - L_{PECk\ initial}$

$\Delta L_{PECcl} = L_{PECcl} - L_{PECcl\ initial}$

$\Delta L_{XEC1} = L_{XEC1} - L_{XEC1\ initial}$

$\Delta L_{XEC2} = L_{XEC2} - L_{XEC2\ initial}$

$\Delta L_{SECA} = L_{SECA} - L_{SECA\ initial}$

$F_{PECk} = (\Delta L_{PECk} \times PEC_k)^4$

2) $F_{PECcl} = (\Delta L_{PECcl} \times PEC_{cl})^{1.5}$

3) $F_{XEC1} = (\Delta L_{XEC1} \times XEC_1)^{1.5}$

4) $F_{XEC2} = (\Delta L_{XEC2} \times XEC_2)^{1.5}$

5) $F_{SECA} = (\Delta L_{SECA} \times SEC_A)^{1.5}$

6) $F_{PECcl} = F_{XEC1}$

7) $F_{XEC1} = F_{XEC2}$

8) $F_{XEC2} = F_{SECA} + F_M$

9) $F_M = (A-(B-\Delta L_{SECA})\ ^C)*D$

A, B, C, and D are constants and the values are provided in Table B-1.

The nine numbered equations above were solved for the nine unknown parameters, the forces and lengths of the four elastic elements and the motor force. The preload tension was the sum of F_{PECk} and F_{SECA} and the active force was F_M.

SRC was used to adjust APS. When SRC was turned on, it pulled the XEC_1 to the left and the PEC_{CL} was linked to XEC_2 through a cross-link to bypass XEC_1 and SRC was simultaneously turned off.

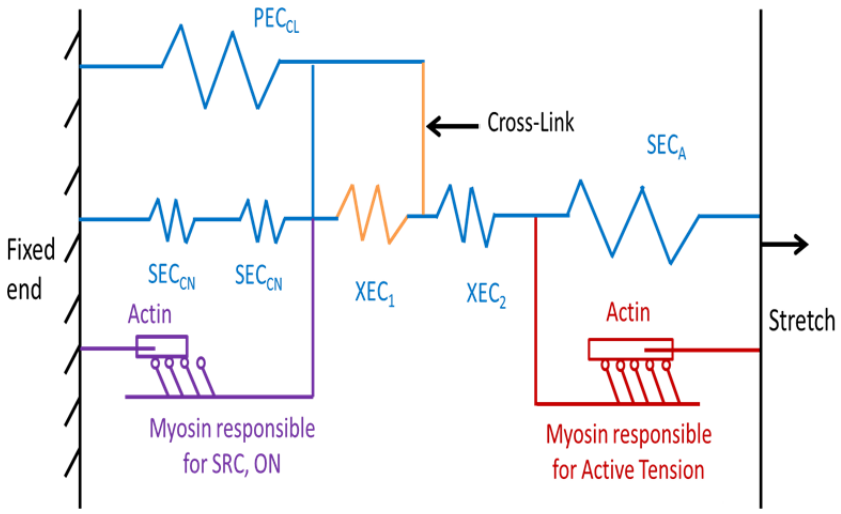

Figure B.2 Conceptual model with the PEC_{CL}, XEC_2, and SEC_A in series and XEC_1 bypassed.

The APS was increased in the model due to SRC. With XEC_1 bypassed the model equations become:

1) $\Delta L_{total} = \Delta L_{PECk} = \Delta L_{PECcl} + \Delta L_{XEC2} + \Delta L_{SECA}$

$$\Delta L_{PECk} = L_{PECk} - L_{PECk\ initial}$$

$$\Delta L_{PECcl} = L_{PECcl} - L_{PECcl\ initial}$$

$$\Delta L_{XEC2} = L_{XEC2} - L_{XEC2\ initial}$$

$$\Delta L_{SECA} = L_{SECA} - L_{SECA\ initial}$$

$F_{PECk} = (\Delta L_{PECk} \times PEC_k)^4$

2) $F_{PECcl} = (\Delta L_{PECcl} \times PEC_{cl})^{1.5}$

3) $F_{XEC2} = (\Delta L_{XEC2} \times XEC_2)^{1.5}$

4) $F_{SECA} = (\Delta L_{SECA} \times SEC_A)^{1.5}$

5) $F_{PECcl} = F_{XEC2}$

6) $F_{XEC2} = F_{SECA}$

The six numbered equations above were solved for the six unknown parameters, the forces and lengths of the three elements in series.

$F_{PECcl} = F_{XEC2} = F_{SECA}$ since PEC_{CL}, XEC_2 and SEC_A are in-series.

When myosins responsible for active tension are cycling, Equation 7 below is added for the motor force and Equation 6 is modified so that the equations become:

1) $\Delta L_{total} = \Delta L_{PECk} = \Delta L_{PECcl} + \Delta L_{XEC2} + \Delta L_{SECA}$

$\Delta L_{PECk} = L_{PECk} - L_{PECk\ initial}$

$\Delta L_{PECcl} = L_{PECcl} - L_{PECcl\ initial}$

$\Delta L_{XEC2} = L_{XEC2} - L_{XEC2\ initial}$

$\Delta L_{SECA} = L_{SECA} - L_{SECA\ initial}$

$F_{PECk} = (\Delta L_{PECk} \times PEC_k)^4$

2) $F_{PECcl} = (\Delta L_{PECcl} \times PEC_{cl})^{1.5}$

3) $F_{XEC2} = (\Delta L_{XEC2} \times XEC_2)^{1.5}$

4) $F_{SECA} = (\Delta L_{SECA} \times SEC_A)^{1.5}$

5) $F_{PECcl} = F_{XEC2}$

6) $F_{XEC2} = F_{SECA} + F_M$

7) $F_M = (A-(B-\Delta L_{SECA})\ ^C)*D$

The seven numbered equations above were solved for the seven unknown parameters, the forces and lengths of the three elastic elements and the motor force. The preload tension was the sum of F_{PECk} and F_{SECA} and the active force was F_M.

For the second time SRC was turned on and it pulled the XEC_1 and XEC_2 to the left and the PEC_{CL} was linked to SEC_A through a cross-link to bypass XEC_1 and XEC_2 and SRC was simultaneously turned off.

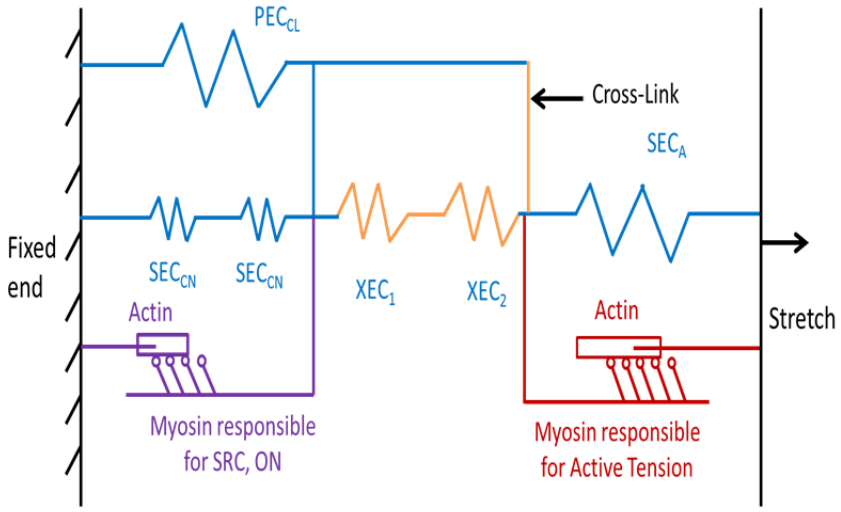

Figure B.3 Conceptual model with the PEC_{CL}, and SEC_A in series and XEC_1 and XEC_2 bypassed.

When both XEC_1 and XEC_2 are bypassed, the model equations become:

1) $\Delta L_{total} = \Delta L_{PECk} = \Delta L_{PECcl} + \Delta L_{SECA}$

$\Delta L_{PECk} = L_{PECk} - L_{PECk\ initial}$

$\Delta L_{PECcl} = L_{PECcl} - L_{PECcl\ initial}$

$\Delta L_{SECA} = L_{SECA} - L_{SECA\ initial}$

$F_{PECk} = (\Delta L_{PECk} \times PEC_k)^4$

2) $F_{PECcl} = (\Delta L_{PECcl} \times PEC_{cl})^{1.5}$

3) $F_{SECA} = (\Delta L_{SECA} \times SEC_A)^{1.5}$

4) $F_{PECcl} = F_{SECA}$

The four numbered equations above were solved for the four unknown parameters, the forces and lengths of the two elements in series.

$F_{PECcl} = F_{SECA}$ since PEC_{CL} and SEC_A are in-series.

When myosins responsible for active tension are cycling, Equation 5 below is added for the motor force and Equation 4 is modified so that the equations become:

1) $\Delta L_{total} = \Delta L_{PECk} = \Delta L_{PECcl} + \Delta L_{SECA}$

$\Delta L_{PECk} = L_{PECk} - L_{PECk\ initial}$

$\Delta L_{PECcl} = L_{PECcl} - L_{PECcl\ initial}$

$\Delta L_{SECA} = L_{SECA} - L_{SECA\ initial}$

$F_{PECk} = (\Delta L_{PECk} \times PEC_k)^4$

2) $F_{PECcl} = (\Delta L_{PECcl} \times PEC_{cl})^{1.5}$

3) $F_{SECA} = (\Delta L_{SECA} \times SEC_A)^{1.5}$

4) $F_{PECcl} = F_{SECA} + F_M$

5) $F_M = (A-(B-\Delta L_{SECA})\ ^C)*D$

The five numbered equations above were solved for the five unknown parameters, the forces and lengths of the two elastic elements and the motor force. The preload tension was the sum of F_{PECk} and F_{SECA} and the active force was F_M.

Table B.1. Dynamic Length- tension relationship mechanical model parameters

Model Element	Value	Initial (Slack) Length, mm
PEC_k	0.44 $mN^{0.25}$/mm	4
PEC_{CL}	24.06 $mN^{0.667}$/mm	1
XEC_1	33.82 $mN^{0.667}$/mm	1
XEC_2	33.82 $mN^{0.667}$/mm	1
SEC_A	5.18 $mN^{0.667}$ /mm	1
SEC_{CN}	1 mN/mm	0.5
A	30.25 mm^2	N/A
B	5.5 mm	N/A
C	2	N/A
D	1.5 mN/mm^2	N/A

VITA

Seyed Omid Komari zadeh
DOB: 02/07/1983
518 N 2nd Street, Richmond, VA, 23219
(619) 888-9211
omid.komari@gmail.com

EDUCATION

Doctor of Philosophy in Engineering, Major: Mechanical and Nuclear Engineering
Virginia Commonwealth University, Richmond, VA
Expected 12/2014
GPA: 3.8

Master of Science, Major: Mechanical Engineering
California State University (CSUS), Sacramento, CA
09/2008—05/2011
GPA: 3.97

COMPUTATIONAL AND TECHNICAL SKILLS

Software: ANSYS Fluent, Mathematica, MatLab, SolidWorks, Microsoft Office Suites (Excel, Power Point, Word), Sigma Plot, Prism, LabVIEW, Nastran, Patran, Hysis, Aspen B-jack.
Programs: C++, Fortran
Technical: Writing proposals, developing programs, collecting, analyzing and reporting data, excellent oral and writing skills and strong leadership and teaming skills

PROFESSIONAL EXPERIENCE

Graduate Research Assistant
Biomechanics of Smooth Muscle 08/2011—Present
VCU Medical Center Biochemistry and Molecular Biology Lab, VA
Study muscle behaviors and molecular biology in Detrusor smooth muscle of urinary bladder on macro and micro scopes.
Macro scope:

- Study the pressure/volume relationship in Detrusor and the effect of surface area on stress and muscle walls sensitivity.
- Expand the FEA model to study the effect of surface area on stress for simulate muscle strips and compare the results with experimental data.

Micro scope:

- Develop conceptual biomechanical models of Detrusor to characterize and describe the mechanical behaviors of the muscle using analytical concepts and Matlab coding.
- Design experimental hypothesis and protocols to test the mechanical characteristics of Detrusor in mice, rats and rabbits.
- Analyze the experimental data from muscle behavior observations and drug studies on contraction of Detrusor

Graduate Teaching Assistant
08/2011—Present
Department of Mechanical and Nuclear Engineering
Virginia Commonwealth University, Richmond, VA

- Assist department faculty members with lecturing for courses such as Heat Transfer, Mechanical System Design, Robotics, Mechanics of Deformables and etc.
- Assist department faculty members with teaching-related duties such as preparing and giving examinations and grading assignments for courses like Heat Transfer, Mechanical System Design, Robotics and etc.

Graduate Teaching Assistant

01/2009—01/2011

Department of Mechanical Engineering

California State University (CSUS), Sacramento, CA

- Assist department faculty members with lecturing for courses such as Advanced Heat Transfer, Engineering Advanced Mathematics, and Thermodynamics.
- Assist department faculty members with teaching-related duties such as preparing and giving examinations and grading assignments for courses like Advanced Heat Transfer, Engineering Advanced Mathematics, Thermodynamics and etc.

Technical Internship

Energy Service Company, Smartwatt Energy, Roseville, CA 6/2010-11/2010

- Project engineer and head of energy auditing team in both electrical and mechanical sections. Audit, design and propose the FedEx national lighting projects in West Coast.
- Audit the sites and measure the critical parameters, analyze the data and calculate the energy consumption to generate the optimum design based on the standards, the economic costs and return of investment.

Private Tutor

- *Huntington Learning Center, Sacramento, CA*
  01/2011-06/2011
- *Physics and Astronomy Department, California State University (CSUS), Sacramento, CA*
  01/2009-12/2009

RESEARCH AND PROJECTS

Dissertation: Analysis and Modeling of the Roles of Actin-Myosin Cross-Bridges in Bladder Smooth Muscle Biomechanics

Master Thesis: Advanced Modeling of Vertical Ground Source Heat Pump Systems Using Finite Element Techniques

Studied the previous designs which were focused on horizontal ground source heat pump. Developed and designed the vertical configuration of ground source heat pump model and studied the stress, strain and thermal distribution using FEA techniques.

Computational Fluid Dynamics Project: Design and layout the combination of forced and free convection effects in two dimensional rectangular enclosure by using Gambit and Fluent computer software.

Finite Model Computer-Aid Project: Stress and thermal analysis of International Space Station's solar panels using finite element method in Patran and Solid Works software.

Senior Project: Design and simulate HVAC (Heating, Ventilation, Air condition and Cooling) system of a 20 floors tower including piping, types and sizes of heating and cooling equipment using computer software.

JOURNAL PUBLICATIONS

1. **Omid Komari**, Headley, P. C., Klausner, A. P., Ratz, P. H., & Speich, J. E. (2013). Evidence for a Common Mechanism for Spontaneous Rhythmic Contraction and Myogenic Contraction Induced by Quick Stretch in Detrusor Smooth Muscle. Physiological reports, 1(6).
2. **Omid Komari**, Adam P. Klausner, Paul H. Ratz, John E. Speich,2014, Modeling Stretch-Induced Myogenic Detrusor Smooth Muscle Contraction and Spontaneous Rhythmic Contraction Based on the Feedback of a Mechanical Sensor, under preparation
3. **Omid Komari**, John E. Speich,2014, A Model for the Roles of Actin and Myosin in Adjustable Preload Tension and Acute Mechanical Adaptation in Bladder Smooth Muscle, under preparation
4. Firdaweke G. Habteyes, **Omid Komari,** R. Wayne Barbee, Adam P. Klausner, Paul H. Ratz and John E. Speich, 2014, Modeling the Influence of Acute Changes in Bladder Compliance and Shape on Wall Tension During Filling, under review

5. Firdaweke G. Habteyes, **Omid Komari,** R. Wayne Barbee, Adam P. Klausner, Paul H. Ratz and John E. Speich, 2014, Does Change of Bladder Shape Matter on Wall Tension During Filling?, under preparation

CONFERENCE PUBLICATIONS (Peer Reviewed)

1. **Omid Komari**, J, Speich, P,H Ratz, 2013, Amplitude of Myogenic Detrusor Contraction Due to Quick Stretch Is One Half Period Out of Phase with the Amplitude of Spontaneous Rhythmic Contraction, Indicating a Common Mechanism, SUFU conference, Feb 2013
2. **Omid Komari**, Adam P. Klausner, Paul H. Ratz, John E. Speich,2013, Modeling Stretch-Induced Myogenic Detrusor Contraction as a Single Twitch of Spontaneous Rhythmic Contraction, MAAUA conference, Oct 2013
3. **Omid Komari**, Adam P. Klausner, Paul H. Ratz, John E. Speich,2014, Modeling Stretch-Induced Myogenic Detrusor Smooth Muscle Contraction and Spontaneous Rhythmic Contraction Based on the Feedback of a Mechanical Sensor, W&M College Symposium, March 2014
4. Firdaweke G. Habteyes, **Omid Komari**, R. Wayne Barbee, Adam P. Klausner, Paul H. Ratz and John E. Speich, 2014, Modeling the Influence of Acute Changes in Bladder Compliance and Shape on Wall Tension During Filling, W&M College Symposium, March 2014
5. **Omid Komari**, John E. Speich,2014, A Model for the Roles of Actin and Myosin in Adjustable Preload Tension and Acute Mechanical Adaptation in Bladder Smooth Muscle, 17th Annual Research Symposium and Exhibit, VCU, March 2014
6. Firdaweke G. Habteyes, **Omid Komari**, R. Wayne Barbee, Adam P. Klausner, Paul H. Ratz and John E. Speich, 2014, Modeling the Influence of Acute Changes in Bladder Compliance and Shape on Wall Tension During Filling,17th Annual Research Symposium and Exhibit, VCU, March 2014
7. **Omid Komari**, Adam P. Klausner, Paul H. Ratz, John E. Speich,2013, The Effects of Age on Adjustable Preload Stiffness and Adaption of Bladder Smooth Muscle, under preparation, Spring 2014

Accomplishment and Activities:

- Member of university team in MCAA (Mechanical Contractors Association of America) group and participated in 2008 MCAA conference in Omaha, Nebraska – CSUS, Sacramento, CA (2008-2009)
- Teacher Assistant and Research Assistant fellowship award – VCU, Richmond, VA (2011-2014)
- Nominated for outstanding teacher assistant, School of Engineering – VCU, Richmond, VA (2013-2014)